2001-73

HIGH RESOLUTION P- AND S-WAVE STUDY TO DETECT A SHALLOW GAS SAND IN SOUTHEASTERN KANSAS

by

Deidra K. Begay
B.S., University of New Mexico, 1998

Submitted to the Department of
Geology and the Faculty of
the Graduate School of the University
of Kansas in partial fulfillment of
the requirements for the degree of
Master of Science

Advisory Committee:

Chairperson

Department Chairperson

Date submitted

Abstract

High-resolution P- and S-wave seismic data collected near Independence, Kansas defined the presence and extent of a shallow (150 m) gas sand. This area is characterized by cyclic sequences of limestone and shale with intervening sandstones deposited throughout the Upper Pennsylvanian (Missourian). The purpose of this study was to define the shallow (upper 300 m) stratigraphy of this region using high resolution P-wave seismic data. After initial analysis of the P-wave data, an amplitude anomaly at the southern portion of the seismic line was confirmed by drilling to be a result of gas saturation. Shear-wave data collected in response to that analysis, as expected, does not exhibit an amplitude anomaly in the area where P-wave data defined the extent of the gas. This provides more confirmation that this amplitude anomaly is likely a result of gas saturation. Using amplitude versus offset (AVO) analysis, it is determined that this sand is a class 2 gas sand. Evidence for this is provided by the presence of a "bright spot" on P-wave stacked sections and an increase in amplitude with offset on pre-stacked data. Based on the general geologic setting, this is opposite what is expected. In addition to the seismic data, core and well log information collected encountered free gas at a depth equivalent to the amplitude anomaly on the P-wave stacked section. A VSP survey was conducted to provide time-depth conversions for the P- and S-wave data sets. The use of the seismic data, VSP data, and well information showed that this anomaly is caused by the presence of gas within the pore space of the Cottage Grove Sandstone.

Deidra K. Begay, M. S.
Department of Geology, May 2001
University of Kansas

ACKNOWLEDGEMENTS

I would like to thank my advisor, Rick Miller, and the Kansas Geological Survey for providing the funding and equipment for this project. An appreciation also goes out to the field crew who were available to collect the data presented here. The field crew consisted of Rick Miller, Dave Laflen, Chad Gratton, Lynn Watney, John Davis, and John Siceloff. An extended appreciation goes out to Lynn Watney of the Kansas Geological Survey. I appreciate the time that Lynn took to talk to me about the geology of the area. I would also like to thank Jianghia Xia for taking time to explain more than a few things. Last, but not the least, I would like to thank my officemate, Chris Tapie for providing time and ideas during our lunch discussions.

A great amount of thanks and appreciation goes out to my family, Frank, Bettie, Mike, and Tamera. Without their support, this struggle would have been a lot more difficult to overcome. I would also like to thank my companion, Bernell, for allowing me to vent my frustration during the writing phase of this project.

I dedicate this thesis to the memory of
my grandfather, Tom Largo.
Through his spirit,
he has inspired me to
continue my education.

Table of Contents

Abstract..... ii

Acknowledgements..... iii

Dedication..... iv

Table of Contents..... v

List of Figures..... vii

List of Tables..... ix

List of Plates..... x

Introduction..... 1

Gas Sand Classification..... 4

Research Objectives and Observations..... 7

Geologic Background..... 9

Existing Gas Reservoirs..... 16

Seismic Acquisition..... 23

P-wave data..... 28

Shear-wave data..... 30

Vertical Seismic Profile data..... 33

Seismic Processing..... 34

P-wave data..... 38

P-wave data (non-AGC)..... 47

Shear-wave data..... 55

Vertical Seismic Profile data..... 61

Seismic Data Analysis..... 66

Conclusions..... 73

References..... 75

List of Figures

1. Modeled CMP gathers showing the seismic response of gas sand classifications..... 5

2. Pennsylvanian tectonic features in Kansas and Oklahoma..... 11

3. Idealized "Kansas" Cyclothem..... 13

4. Generalized stratigraphy of the Chanute Shale and adjacent units..... 14

5. Oil and gas fields in Kansas..... 17

6. Kansas cumulative gas production in percent by formation during the years 1987-1998..... 18

7. Map of oil and gas fields in Chautauqua County, Kansas..... 20

8. Map of oil and gas fields in Montgomery County, Kansas..... 21

9. Site map..... 24

10. A shotgather from the 240-channel data set showing an asymmetrical split-spread..... 26

11. Dominant frequencies of the 96- and 240-channel P-wave data sets..... 27

12. Seismographs are linked together to acquire both the P- and S-wave data sets..... 29

13. IVI Minvib, used as the source, is designed in a buggy-style configuration..... 29

14. An example of a shotgather with an asymmetrical split-spread..... 31

15. Source motions and receiver sensitivity directions for P-P and SH-SH wave surveys..... 32

16. General processing flow used in processing the P-wave data sets..... 35

17. General processing flow used in processing the S-wave data set..... 36

18. General processing flow used in processing the VSP data set..... 37

19. 96-channel P-wave shotgathers showing the results of correlation tests 39

20. Results of processing the 96-channel P-wave data set 43

21. General processing flow used in processing the non-AGC P-wave data set 48

22. Results of processing the non-AGC P-wave data set 50

23. CMP time stacked section with geometric spreading correction applied, P-wave Trip1 (96-channels) 53

24. CMP time stacked section with geometric spreading correction applied, P-wave Trip2 (240-channels) 54

25. Results of processing the S-wave data set 57

26. P-wave uphole survey for the various offsets recorded at the Pitts #1 well near station 1130 63

27. VSP processing steps used to produce a P-wave stacked trace in the Pitts well for the 60.1 offset 64

28. Interpreted Pitts #1 edited well data 67

List of Tables

1. P-wave data processing information..... 42

2. True amplitude P-wave data processing information..... 49

3. S-wave data processing information..... 56

4. VSP data processing information for both P- and S-components..... 62

List of Plates

1. CMP time stacked section, P-wave Trip1 (96-channels)
2. CMP time stacked section, P-wave Trip2 (240-channels)
3. CMP depth stacked section, P-wave Trip1 (96-channels)
4. CMP depth stacked section, P-wave Trip2 (240-channels)
5. CMP time stacked section, S-wave
6. CMP depth stacked section, S-wave
7. P-wave Trip1 (96-channels) Stacking Velocity Field
8. P-wave Trip2 (240-channels) Stacking Velocity Field
9. S-wave Stacking Velocity Field
10. P-wave Trip1 (96-channels) True Fold Map
11. P-wave Trip2 (240-channels) True Fold Map
12. S-wave True Fold Map
13. Interpreted CMP depth stacked section, P-wave Trip1 (96-channels)
14. Interpreted CMP depth stacked section, P-wave Trip2 (240-channels)
15. Interpreted CMP depth stacked section, S-wave
16. CMP time stacked section with corridor VSP stack, P-wave Trip1 (96-channels)
17. CMP time stacked section with corridor VSP stack, P-wave Trip2 (240-channels)
18. CMP time stacked section with corridor VSP stack, S-wave

Introduction

Coincident compressional (P) - and shear (S) -wave, high resolution, shallow seismic reflection techniques have proven effective at imaging shallow and relatively small targets in a variety of geologic settings (Pullan and Hunter, 1990; Jongerius and Helbig, 1988; Miller et al., 1989; Miller et al., 1995; Shtivelman et al., 1998). Laterally extensive shallow gas zones have been easy targets to detect but an obstacle to many shallow compressional wave high-resolution seismic reflection surveys (Pullan et al., 1998).

High amplitude P-wave reflections associated with the boundary between gas-bearing zones (sands) and cap rocks (shale) are routinely referred to as "bright spots" (Khattri et al., 1979). Offset dependent reflection amplitude (Amplitude Versus Offset [AVO]) characteristics for gas rich sediments can vary significantly with geologic setting, gas concentrations, and lithology (Ostrander, 1982). Three unique types of reservoirs or classes of gas deposits have been described that incorporate geology setting and lithology with seismic attributes (Rutherford and Williams, 1989). Lithologically, the encasing medium and reservoir rock distinguish these classes, while seismically a distinct impedance range aids in classifying each type of gas sand.

P- and S-wave velocities are important for determining rock properties such as lithology, porosity, and pore fluid content. The speed at which a compressional wave will propagate through a medium is

$$V_p = \sqrt{(k + 4/3\mu)/\rho}\,,$$

where k = bulk modulus or rock incompressibility, μ = shear modulus, and ρ = bulk density of the material. If the interstitial fluid within the pores is replaced by gas, ρ and k will change. As a result, the P-wave velocity and reflection coefficient will be affected. The P-wave velocity will decrease significantly. This change in the reflection coefficient will result in either a "dim spot" or in this case, a "bright spot" (Sheriff and Geldart, 1982).

S-wave velocities are useful when combined with P-wave velocities because Vs provides additional information about the pore fluid. Shear-wave velocity is independent of the pore fluid type and this is defined by the absence of the bulk modulus variable in the velocity equation (Domencio and Danbom, 1987).

$$V_s = \sqrt{(\mu/\rho)}\,.$$

As the S-wave passes through the material, the rock changes shape but the volume does not. Thus, there is no distinct change in shear-wave velocity as it passes through the gas-saturated medium (Domencio and Danbom, 1987). Therefore, the presence of gas within the pores of the sand layer will result in the lack of an amplitude anomaly on the shear-wave stacked section (McCormack and Tatham, 1986).

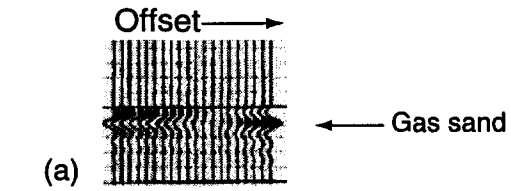
There are many advantages for using P-waves as opposed to S-waves. First of all, P-wave energy is easier to generate and the data are easier to interpret. Another advantage of using P-wave energy is that there is only one direction or mode that exists. On the other hand, the S-wave energy has two modes, the SV- and SH-modes. This can either be considered a complication or an advantage depending on the objective of the study. In this case, the SH-direction is the mode that is used to aid in confirming the presence of gas. Together, V_p and V_s are useful in providing information about the interstitial fluid and lithology of a potential gas reservoir (Sheriff and Geldart, 1982).

Gas Sand Classification

High impedance contacts between encasement material and sand, termed class 1, are caused by mature sands that have been exposed to moderate to high compaction (Rutherford and Williams, 1989). Seismically, reflection amplitudes decrease with offset and may result in a polarity reversal if sufficient offsets are recorded (Figure 1a) (Rutherford and Williams, 1989; Peddy, et. al., 1995). As a result, on stacked sections amplitude dimming (dim outs) is apparent due to the cancellation of amplitudes caused by the polarity reversal. At first glance, logs and continuous core samples from the study site suggest a geologic setting consistent with a class 1 sand reservoir.

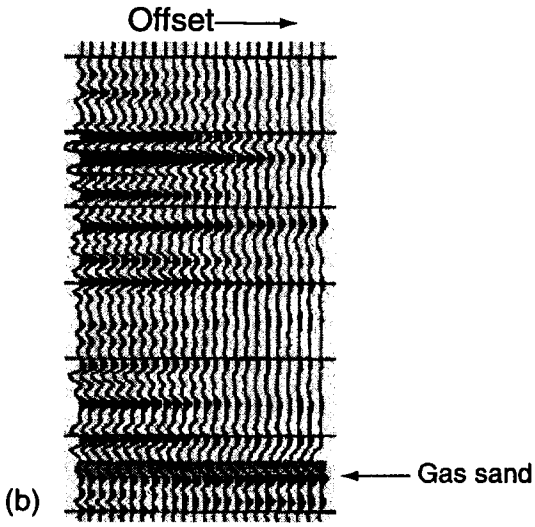
Class 2 sand reservoirs possess near-zero impedance contrast between the sand and encasing materials and are moderately compacted sands (Rutherford and Williams, 1989). This type of gas sand has very low amplitude reflections at near offsets and significantly higher amplitude reflections at far offsets; if sufficient offsets are recorded (Figure 1b). This offset-dependent seismic response is opposite from a "normal" seismic response. Processing flows designed for average earth materials are rarely effective in detecting the unique characteristics of these class 2 gas reservoirs.

The third class of gas sands has a lower impedance than the encasing medium, is usually unconsolidated, and can be found in mostly marine depositional environments (Rutherford and Williams, 1989). Seismically, reflections appear at all



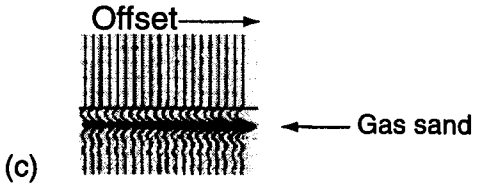
Class 1 response

Decrease in amplitude with offset with a polarity reversal at the far offsets. Often associated with "dim outs" on stacked data



Class 2 response

Increase in amplitude with offset. May or may not be associated with amplitude anomalies on stacked sections.



Class 3 response

Large reflectivities at all offsets. Polarity changes are not characteristic of this type of sand. Classic "bright spot" of the Gulf of Mexico Plio-Pleistocene sands.

Figure 1. Modeled CMP gathers showing the seismic response of gas sand classifications (data from Peddy and Sengupta, 1995; Ross and Kinman, 1995).

offset ranges and without polarity changes (Figure 1c). In some cases, deeper layers are not imaged due to limited or no transmission of energy through the base of the confining layer (Pullan et al., 1998).

This classification scheme for distinguishing gas sands is useful in providing an understanding of basic characteristics of possible amplitude anomalies and whether any preliminary expectations of the general geology can be inferred. For example, the Plio-Pleistocene sands of the Gulf of Mexico are typically classified as a class 3 sand based on the sand being undercompacted and unconsolidated.

Based on the compacted and mature geologic setting, a gas sand in the present study area is expected to have a class 1 amplitude response, a "dim out" on the CMP stacked section. This study of a gas sand uses the above classification scheme, P-wave, S-wave, and Vertical Seismic Profile (VSP) data to support the presence of shallow gas. Although conventional AVO analysis was not conducted here, coincident seismic data and drilling information acquired were used to support the presence of gas.

Research Objectives and Observations

High-resolution seismic reflection data collected over a cyclic sequence of limestones, shales, and sandstone provided an opportunity to observe the presence of a small, shallow gas deposit trapped in a consolidated sand with a gradational upper boundary. The original objective for this study was to delineate the geometries of clastic-dominated strata in relationship to adjoining carbonate buildups believed to be present to the north. This dramatic change in strata extends across five miles in this otherwise uniform geologic setting. The seismic line was designed in a north-south orientation to image the transition between the clastic succession and the carbonate bank. An amplitude anomaly apparent on the CMP stacked section resulted in an extension of the overall program objective to address the seismic imaging of this anomaly. A P- and S-wave survey were planned to study this gas anomaly, further complemented by Vertical Seismic Profile (VSP) data for true depth information and amplitude of reflections. Along with these data, well log and core data were collected in a borehole that penetrated the anomaly.

Preliminary observations of the P-wave stacked section exhibit an amplitude anomaly at shallow depths of around 150 m. This anomaly extends from stations 1050 to 1250 with the Pitts well drilled 100 m offline near station 1130. Confirmation that this anomaly is associated with gas lies in the CMP gathers. These gathers show an increase in amplitude with offset. This amplitude increase supports a class 2 gas sand interpretation. In addition to the presence of a "bright spot" on the

CMP stacked section, a well drilled 100 m offline of the seismic line encountered free gas at a depth of around 150 m. On the stacked section, the anomaly appears to have a concave up geometry with the highest point at about station 1105. This sand is encased in a low reflectivity medium identified within the core as shale.

Considering the geologic setting alone, this site would support a class 1 sand reservoir. Given the high impedance contrast between the shale and limestone intervals, "dim outs" should be observed on CMP stacked sections. However, the seismic P-wave reflection data possess high amplitude "bright spots" on CMP stacked data, which is opposite to what was expected. To further support the presence of this gas, the S-wave stacked section does not exhibit this amplitude anomaly. These high amplitude reflections on the P-wave CMP stacked section have been confirmed by drilling to correlate them with a shallow gas zone within a consolidated sandstone, shale, and limestone sequence.

Geologic Background

The general geologic setting in this Midcontinent region consists of cyclic limestone and shale sequences (termed cyclothems) interbedded with sandstone. These units are widespread, specifically in eastern Kansas, and are Middle to Upper Pennsylvanian in age (Watney, et al., 1989). The stratigraphic units that are seismically imaged and interpreted belong to the Cherokee Group (Desmoinesian), the Marmaton Group (Desmoinesian), the Pleasanton Group (Missourian), the Kansas City Group (Missourian), and the Lansing Group (Missourian). The unit that contains the gas sand is part of the Upper Pennsylvanian Chanute Shale, a formation in the Kansas City Group.

The Cherokee Group consists of shale layers with thin beds of alternating lenses of sandstone and thin limestone beds. The reflections from the Cherokee Group do not appear to be strong (Watney, pers. comm.). The more continuous Marmaton Group is composed of an equal percentage of alternating shale and limestone. Above the Marmaton Group lies the Pleasanton Group. This unit, unusually thin at this location, contains mostly shale beds that were deposited on a sediment-starved lower shelf. The younger unit above is defined as the Kansas City Group. This group consists of limestone and shale beds with interbedded lenticular sandstones. This is the stratigraphic position of the Chanute Shale, the location of the gas sand in this study area.

The unit above the Kansas City Group is the Lansing Group. It consists of alternating limestone, shale, and some siltstone and sandstone beds (Jewett, et. al, 1968). The youngest unit that is seen seismically is the Captain Creek Limestone member of the Stanton Formation. This unit is part of the Lansing Group, Missourian in age.

The study area is located within the Cherokee basin between the Bourbon arch to the north, the Nemeha uplift to the west, and the Arkoma basin to the south. The source of sediments within the unit of interest, the Chanute Shale, is primarily from the Ouachita Mountains, a topographic high to the south and southeast of the study area (Figure 2). The Ouachita Mountains of southeastern Oklahoma formed as a result of a late Early Pennsylvanian orogeny. Previously deposited sediments in this region were subjected to folding and thrusting during the formation of the Ouachitas. Due to the widespread lateral continuity of the Upper Pennsylvanian cyclothems, it is interpreted that the study area during this time was more tectonically stable than the basin and mountain area to the south (Fernandez, 1993).

Transgressive and regressive sea level in this region were influenced by glaciation in Gondwana from the late Mississippian through the middle of the Permian (Heckel, 1980, Fernandez, 1993). The cyclic sequences in the study area were deposited as a response to these sea level changes (Mitchell, 1981; Watney, et al., 1989; Fernandez, 1993). An idealized cyclothem used to describe the

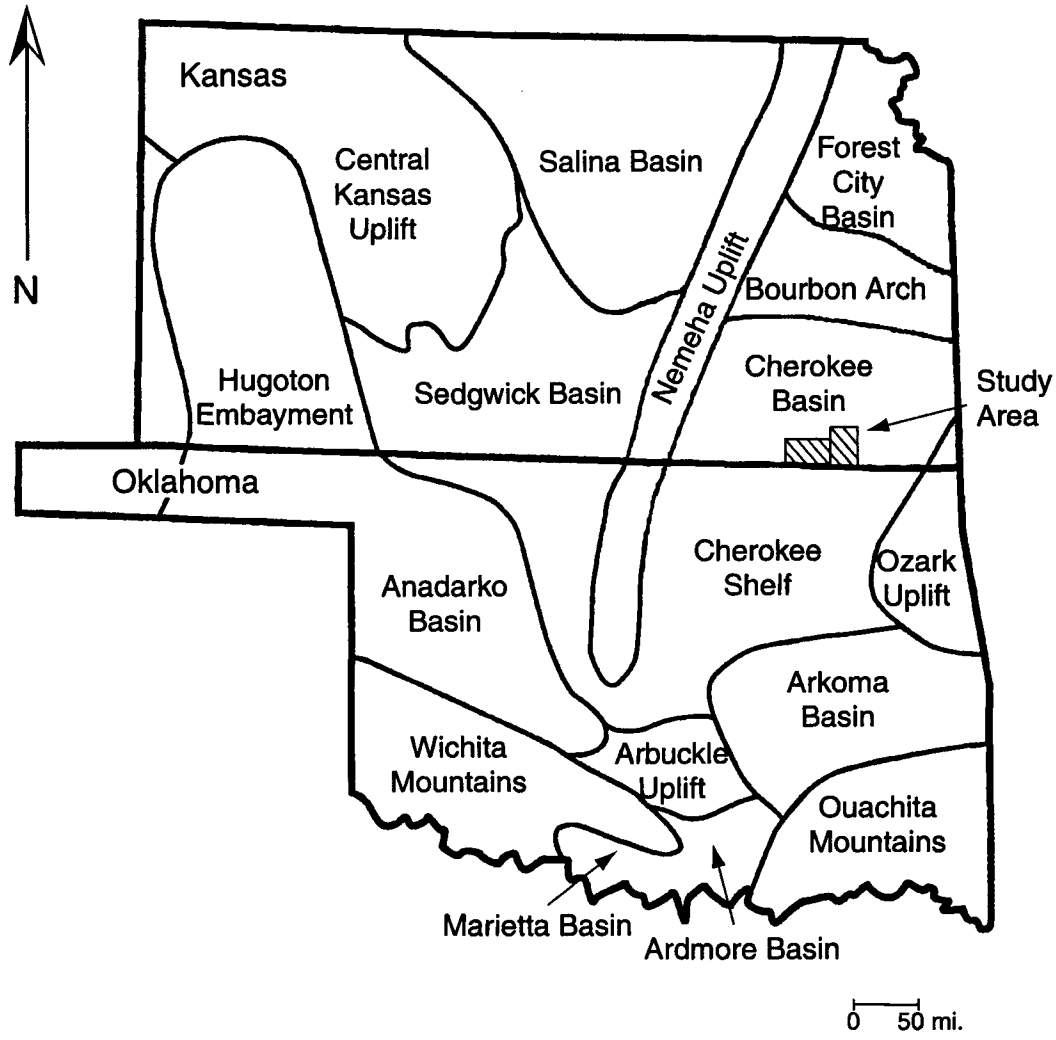


Figure 2. Pennsylvanian tectonic features in Kansas and Oklahoma (modified from Fernandez, 1993).

limestone/shale cyclic sequences of the region are shown in figure 3. In this figure, a complete cycle is defined by a middle transgression limestone, a core offshore shale, an upper regressive limestone, and an outside nearshore shale (Heckel, 1979). The Chanute Shale, a formation of the Kansas City Group, is classified as an outside, nearshore shale of the cyclothem. The Chanute Shale contains the gas sand that is interpreted on the seismic data. Fluvially-derived sandstones, shales, and a thin coal layer comprise the Chanute Shale in this area (Fernandez, 1993).

The Chanute Shale overlies the transgressive-regressive Dewey Limestone and is overlain by the transgressive-regressive Iola Limestone (Figure 4). The Chanute Shale represents maximum regression of the cyclothem and the initial transgression of the overlying cyclothem (Figure 3). Although this unit is termed the Chanute Shale, it contains a considerable amount of sandstone in this area. This Upper Pennsylvanian (Missourian) aged unit is subdivided into a lower Chanute, the Thayer coal bed, and an upper Chanute (Figure 4). The lithofacies of the lower Chanute consist of interbedded fine sandstone and silty clayey shale, massive channeled sandstones, gray, fissile clayey shale, and silty shale. Channel sandstones, termed the Noxie sandstone, at the base of the unit characterize the lower Chanute. It grades into a silty shale, a shale, and occasionally an underclay just below the extensive, but relatively thin, Thayer coal bed (Fernandez, 1993). The lower Chanute is deposited in deltaic, estuarine, to fluvial environments during the waning staages of regression and marine transgression (Watney, pers. comm.).

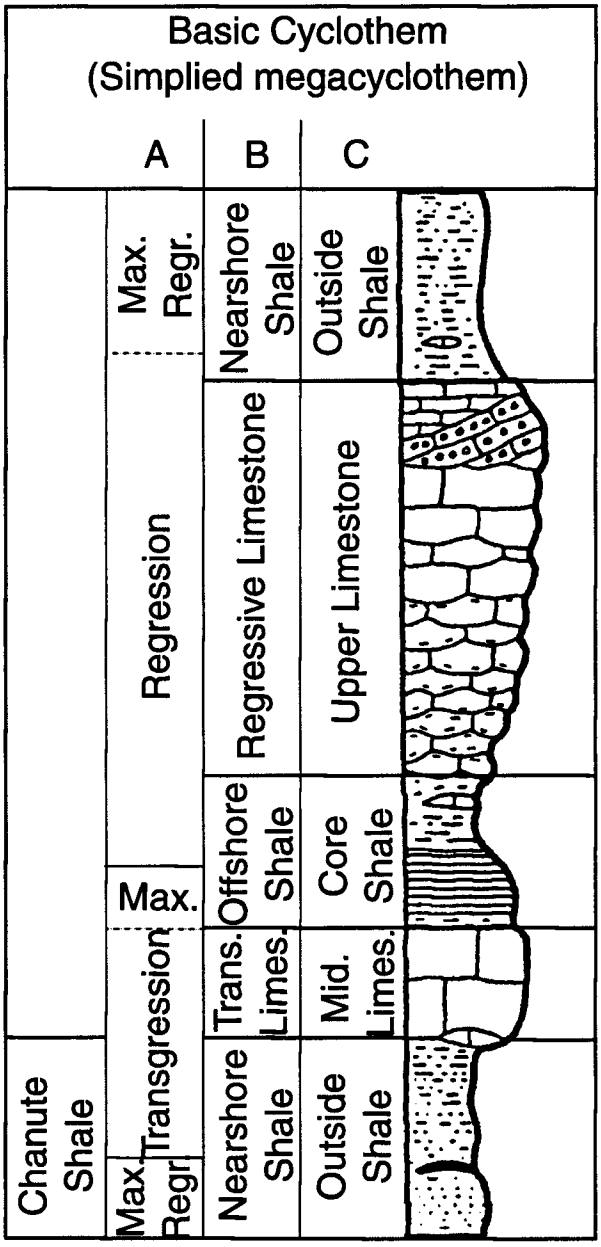


Figure 3. Idealized "Kansas" Cyclothem. A. direction of sea-level change; B. Depositional member; C. Positional member. The nearshore shale characterizes the Chanute Shale, the host rock for the gas (modified from Heckel, 1979).

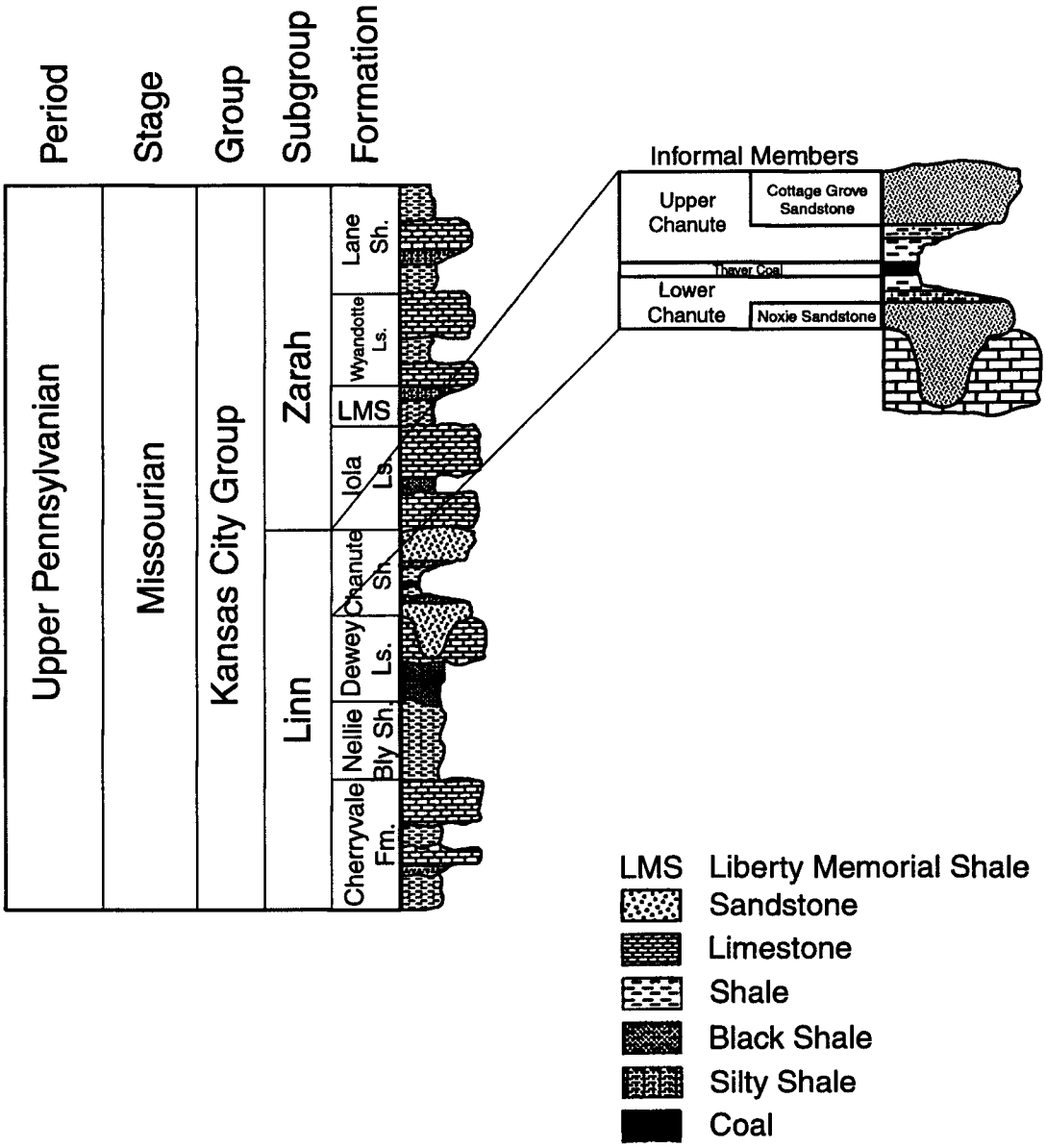


Figure 4. Generalized stratigraphic column of the Chanute Shale and adjacent units (modified from Fernanadez, 1993).

This was followed by the formation of an extensive soil during subaerial exposure of this lower shelf setting followed by the initial transgression delimited by the Thayer coal bed. Above the coal layer is the upper Chanute (Figure 4). The lithofacies of the upper Chanute consist of thinly-bedded, thinly-laminated micaceous sandstone, carbonate-cemented, contorted fine micaceous sandstone, and interlaminated siltstone and shale. The upper Chanute contains the Cottage Grove sandstone, a widespread fluvial to estuarine sandstone, locally filling incised valleys that were cut into underlying strata (Fernandez, 1993).

Existing Gas Reservoirs

In the state of Kansas, cumulative gas production is 35 Tcf. Permian aged reservoirs of southwest Kansas serve as the dominant provider of gas particularly from the Hugoton Gas Field of the Chase Group (Figure 5 and 6) (Gerlach, 1999). In Eastern Kansas, hydrocarbon production is principally oil from the Pennsylvanian Cherokee channel sandstones (Newell, 1995). These shallow, discontinuous sandstones are lenticular in shape and interpreted to be deposited in incised valleys (Jenden, et. al., 1988; Knapp, et. al., 1995). As a result, these channel sandstones are routinely referred to as "shoestring sandstones" (Bass, 1936). The Upper Bartlesville Sandstone, specifically the Bluejacket, is an example of these lenticular sandstones in eastern Kansas. Shales, the probable source rocks, stratigraphically trap the hydrocarbons in this sandstone (Jenden, et. al., 1988; Knapp, et. al, 1995).

Closer to the study area, gas production from Chautauqua and Montgomery Counties have provided only 0.1% of gas in Kansas in the past five years (from Kansas Geological Survey website, 2001). For comparison, in the past five years Stevens and Grant Counties within the Hugoton Gas field produce 40% of gas in Kansas (from Kansas Geological Survey website, 2001). The Hugoton Field has an estimated reserve of about 75 Bcf. (Jenden, et. al., 1988). The gas trap for the Hugoton carbonate reservoirs is a combination of a stratigraphic trap and a facies change (Parham, 1993).

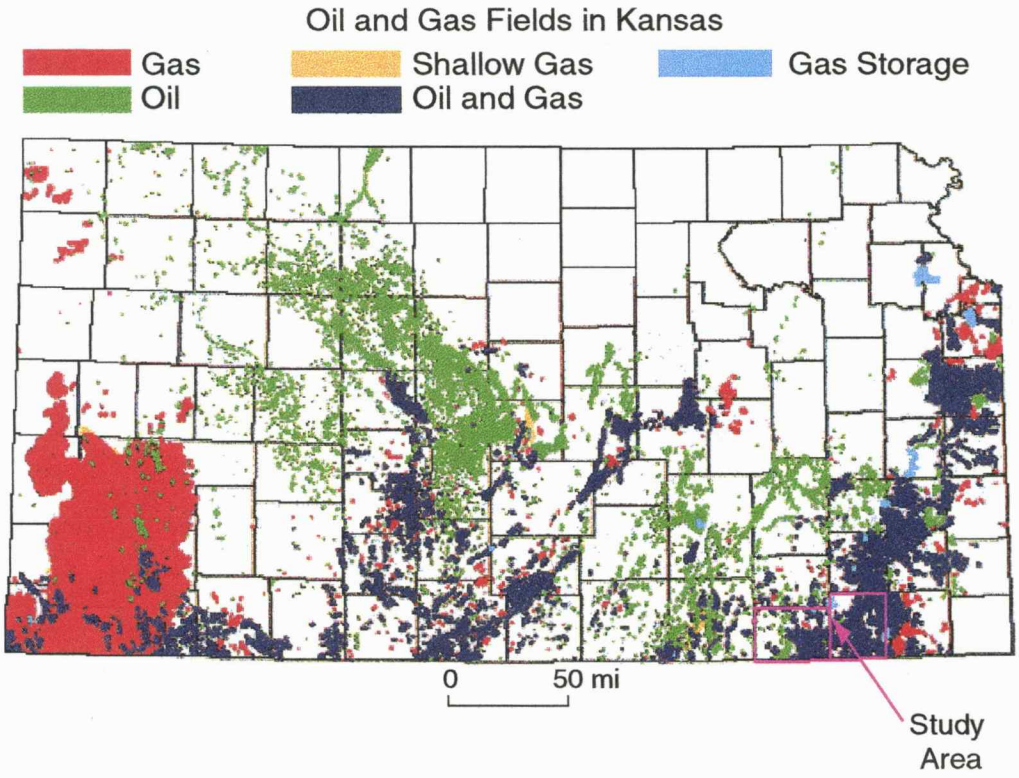


Figure 5. Oil and gas fields in Kansas (modified from Baars et. al., 1989). The red in the lower left corner is the Hugoton Gas Field. The study area in the lower right corner is indicated by the arrow.

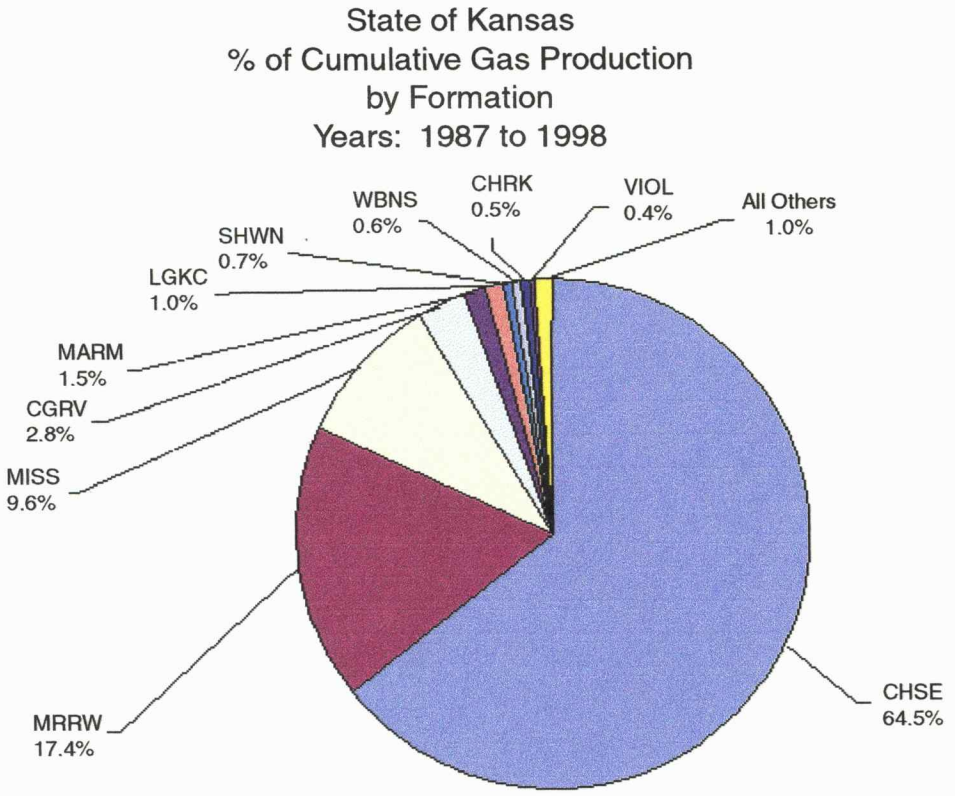


Figure 6. Kansas cumulative gas production in percent by formation during the years 1987-1998. CHSE=Chase (Permian); MRRW=Morrowan (Pennsylvanian); MISS=Mississippian; CGRV=Council Grove (Permian); MARM=Marmaton (Pennsylvanian); LGKC=Lansing-Kansas City (Pennsylvanian); SHWN=Shawnee (Pennsylvanian); WBNS=Wabaunsee (Pennsylvanian); CHRK=Cherokee (Pennsylvanian); VIOL=Viola (Ordovician). (from Kansas Geological Survey website, 2001).

As of 2000, cumulative gas production in Chautauqua County was 10 Bcf. Currently, there are 54 active oil and gas fields in the county (Figure 7). Near the study site, Elk City (the field lies within Chautauqua, Montgomery, and Elk counties), Elk City South, and Hoover fields have produced 2.8 Bcf of gas cumulatively (from Kansas Geological Survey website, 2001). Oil and gas production in the Wayside-Havana field of eastern Chautauqua and western Montgomery counties occurs in Pennsylvanian sandstones, particularly from the "Wayside sand" of the Nowata Shale (Marmaton). Depth to the producing zones, "Wayside," "Weiser," and "Bartlesville," in this field is 175-365 m (Jewett, 1954).

The Peru-Sedan field of south-central Chautauqua produces from the "Peru sand" of the Labette Shale (Marmaton). Other producing sands in this county are found in the Little Osage Shale, member of the Fort Scott Limestone (Marmaton), the "Bartlesville sand" of the Cherokee shale, from the upper Mississippian limestones, and the upper Cotter dolomite (Arbuckle) (Jewett, 1954).

In Montgomery County, there are 17 active gas fields (Figure 8). Fields in this county have produced a cumulative 26.5 Bcf of gas (from Kansas Geological Survey website, 2001). Elk City is the closest field to the study area in this county. This field has produced a cumulative 2 Bcf of gas within Montgomery, Chautauqua, and Elk counties (from Kansas Geological Survey website, 2001). Gas production in Montgomery County is from the Lane-Vilas (Kansas City-Lansing), Bandera

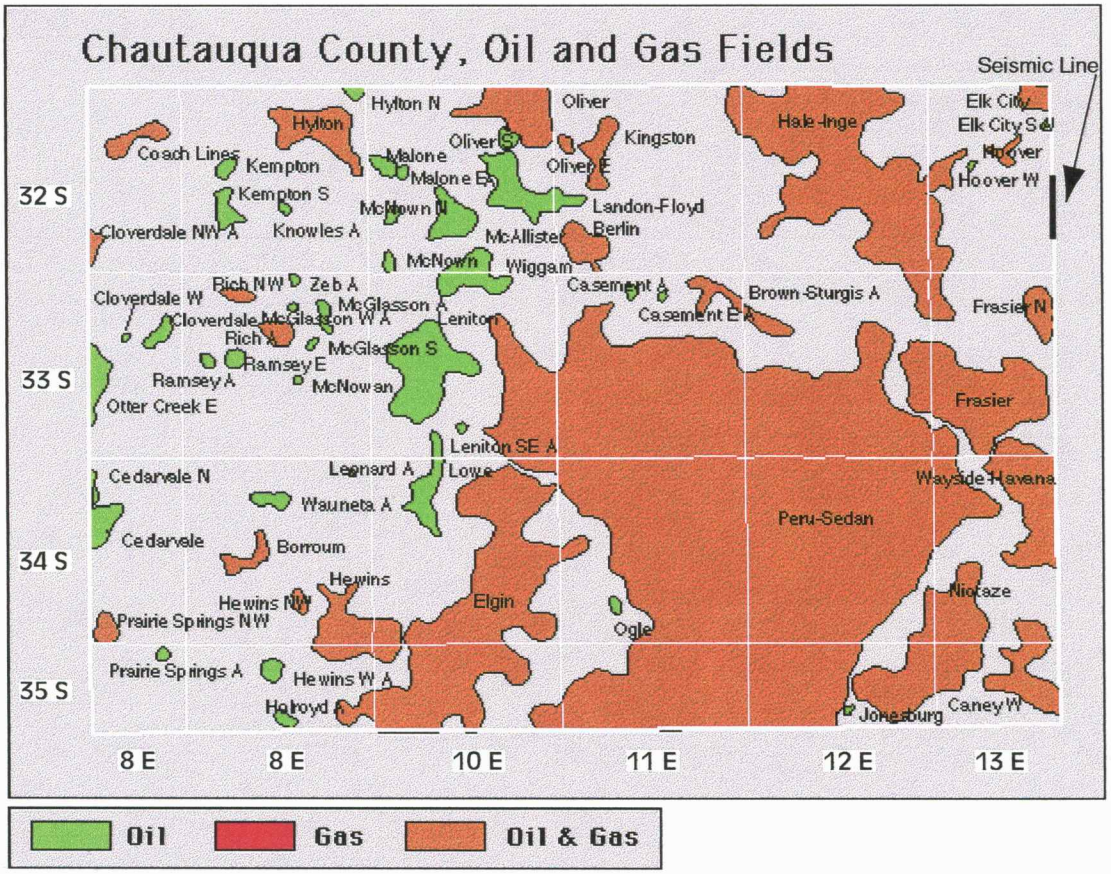


Figure 7. Map of oil and gas fields in Chautauqua County, Kansas. Site of seismic line is along eastern margin of county line in T32S, R13E (from Kansas Geological Survey website, 2001).

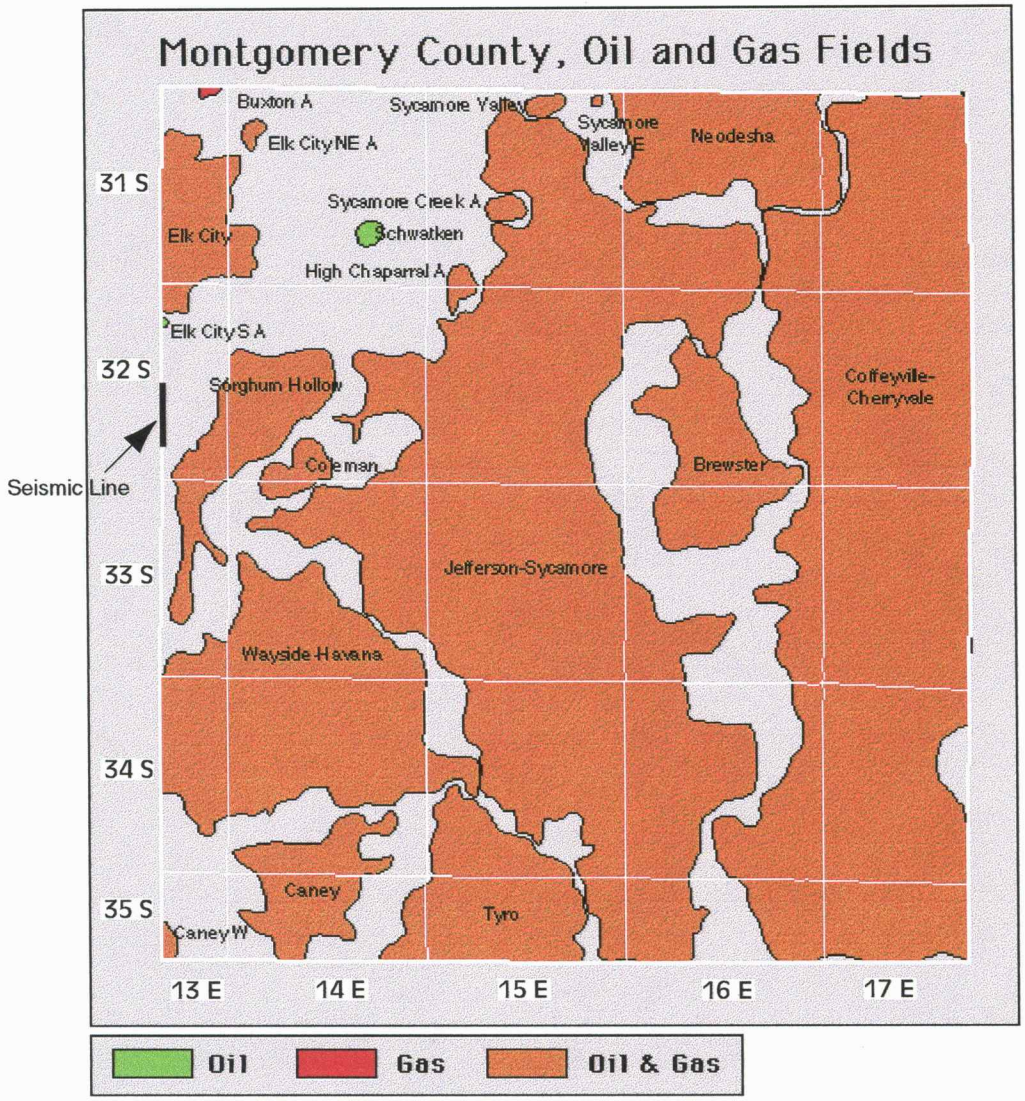


Figure 8. Map of oil and gas fields in Montgomery County, Kansas. Site of seismic line is along western margin of county line in T32S, R13E (from Kansas Geological Survey website, 2001).

(Marmaton), Labette (Marmaton), and Cherokee (Marmaton) shales with production chiefly from the "Bartlesville sand" of the Cherokee shale. Gas is also produced from the Fort Scott, Mississippian, and Arbuckle limestones. Close to the study area in the northwestern part of the county, gas has been found within the Lane-Vilas shale in at least three sandstones, "Bush-Denton," "Webb," and the "Encill" (Jewett, 1954).

Gas reservoirs in Chautauqua and Montgomery counties have trapping mechanisms that include both stratigraphic and structural traps. The structural traps are due to local and regional structural folds in the area. One major fold in Chautauqua County is the subsurface Longton anticline in the central part of the county. Gas accumulations are generally up-dip along the flanks of these folds with or without closure. In portions of the gas fields that do not exhibit structural closure, up-dip stratigraphic terminations serve as the dominant trap (Jewett, 1954).

Seismic Data Acquisition

P- wave, S-wave, and Vertical Seismic Profile (VSP) data were acquired as part of this study. Preliminary feasibility studies include collecting 96-channel P-wave data along an approximately two mile north-south seismic line on the Chautauqua-Montgomery county line (Figure 9). A 0.6 mi-long amplitude anomaly was discovered on the CMP stacked section which was used as the basis for planning subsequent research.

Core and wireline log data were collected in the Pitts well 100 m offline near CMP station 1130. The initial well was only drilled to 122 m before encountering mechanical problems. As a result, another well (Pitts #1twin) was drilled 10 m to the southwest. In this well, a sonic log was acquired only in the lower 150 m of the well before problems occurred in recording that were attributed to a malfunction of the instrument. A day after logging, the well flowed gas and had to be plugged. This prompted a more detailed study of the well logs and core information. It was determined that gas was detected at about a depth of 134 m. The entrained gas in the mud has apparently led to the loss of the acoustic signal of the sonic log from the gas-bearing zone to the surface.

After identifying the seismic anomaly corresponding to the gas-bearing zone, another P-wave survey was designed and conducted using revised acquisition

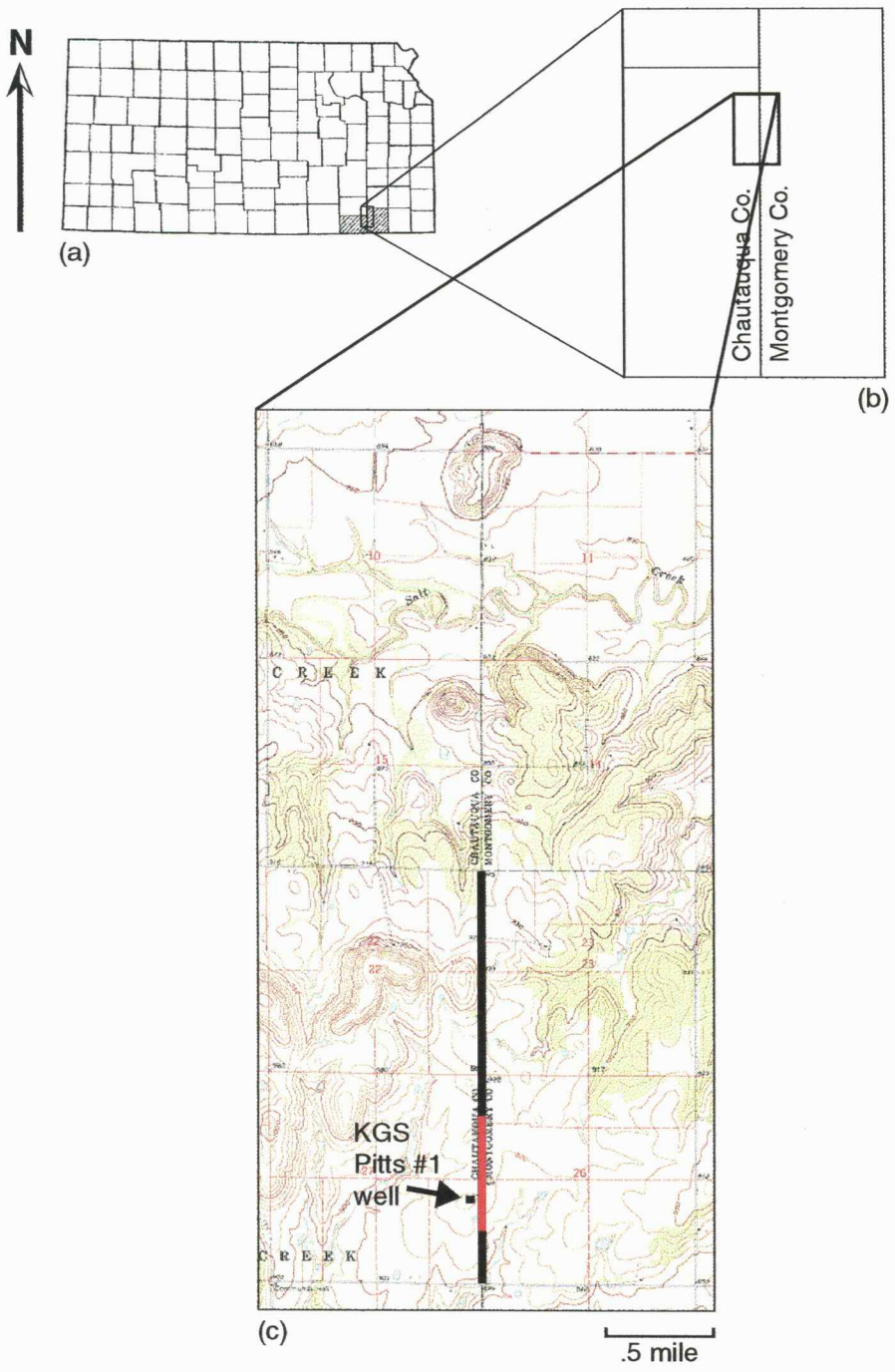


Figure 9. Site map of (a) Kansas counties with Chautauqua and Montgomery counties indicated by hatched lines. (b) Location of seismic line in relation to county line. (c) A detailed map of the study site with black line indicating the 2-mile P-wave seismic line. The .6-mile Shear-wave line is indicated by the red line. The location of the Pitts well is specified by the black square.

parameters. Changes in parameters included increasing the number of recording channels, revising the sweep frequency of the vibrator, and increasing the listening time of the sweep. The number of recording channels was increased from 96 to 240. The 240 channels provided an opportunity to expand the long offset distance and maintain the minimum number of channels at the near offsets at 60 channels using an asymmetrical split-spread (Figure 10). The input sweep frequency was changed from 30-300 Hz to 25-225 Hz. For this data set, the dominant frequencies for the 96-channel and 240-channel data set are 110 Hz and 100 Hz, respectively (Figure 11). The last parameter that was modified was the listening time which was increased from 8 s to 12 s.

To further study this amplitude anomaly detected on the P-wave stacked section, a 0.6 mi-long shear wave data set was collected over the area of the amplitude anomaly. A vertical seismic profile (VSP) data set was collected at three surface offsets and throughout the upper 65m of the Pitts #1 well. This VSP data set provides time-depth measurements as a basis for correlation of reflecting events on both P- and S-wave stacked sections.

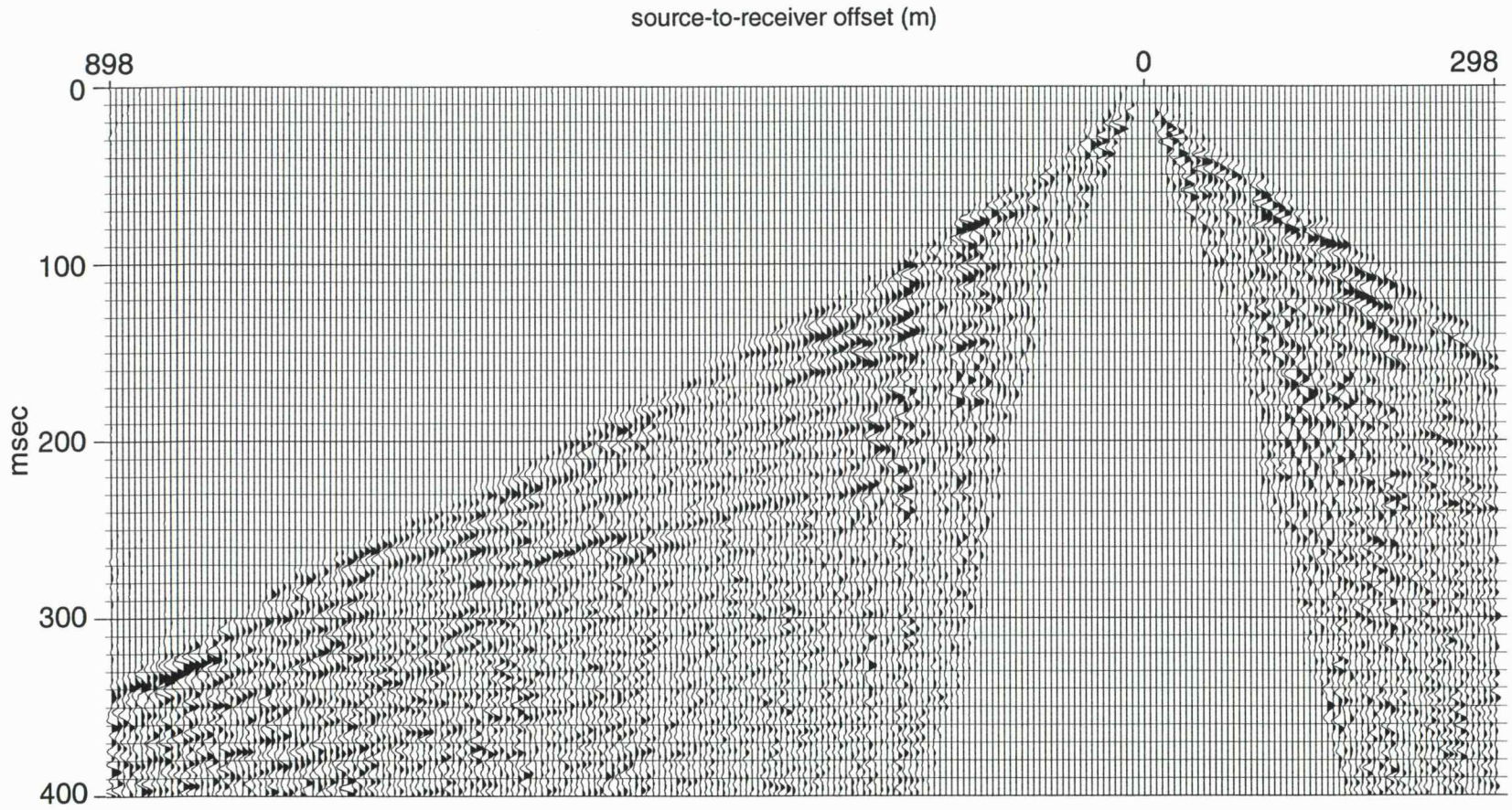


Figure 10. A shotgather from the 240-channel data set showing an asymmetrical split-spread. The minimum number of channels on the right and left ends are maintained at 60 channels as the source moves throughout the survey.

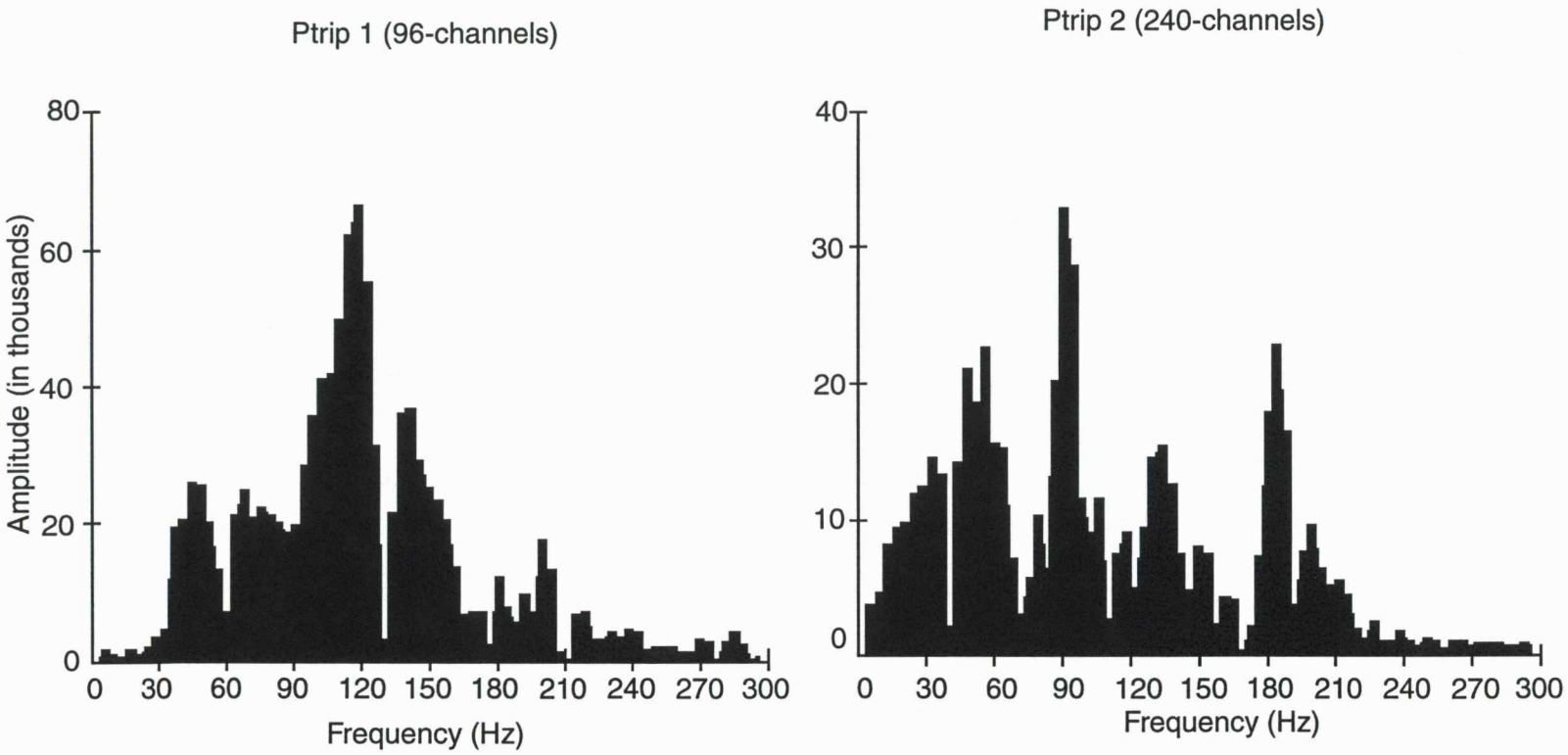


Figure 11. Dominant frequencies for the 96- and 240-channel P-wave data sets.

P-wave data

The seismic data were acquired using equipment and parameters selected based on a series of walkaway tests. The uncorrelated vibroseis data were recorded using networked Geometrics Strataview seismographs (Figure 12). High output, Mark Products 40 Hz geophones attached to 14 cm spikes with three geophones per string were deployed in 1 m arrays every 5 m along the line.

Considering the target objectives, required resolution, near-surface conditions, and economics, the P-wave source selected for this study was an Industrial Vehicles Inc. (IVI) Minivib in a buggy style configuration (Figure 13). Three sweeps were recorded individually at each shot station. The 96-channel data set was recorded with a frequency range of 30-300 Hz, whereas, a frequency range of 25-225 Hz was used in acquiring the 240-channel data set. Shot locations on 10 m intervals were assigned an inline offset ranging 2 to 2.5 and an offline offset ranging 6 to 7 m. The data were saved uncorrelated and unstacked to permit post acquisition evaluation of correlation techniques.



Figure 12. Seismographs are networked together to acquire both the P- and S-wave data sets.



Figure 13. IVI Minivib, used as the source, is designed in a buggy-style configuration.

A split-spread geometry provided reasonable velocity and dip control for deeper reflecting events while increasing near-offset redundancy and minimizing longer offset NMO-stretch effects. With the 96-channel data set, a roll-along symmetrical split-spread geometry was used half way through the acquisition process. At this point, the geometry was changed to an asymmetrical split-spread due to near-surface velocity changes, to extend the maximum offset, and to maintain the redundancy for near offsets (Figure 14). For the 240-channel data set, a split-spread geometry was maintained throughout the survey (Figure 10). This geometry was used to maintain the recurrence of the number of near offsets. Given the number of channels, minimum offsets were retained throughout the survey.

Shear wave data

The shear wave data were recorded uncorrelated using the same networked Geometrics Strataview seismographs as with the P-wave data set (Figure 12). There were 140 channels used to record the S-wave data set. The data acquired during this study used the horizontal vibratory configuration of the IVI Minivib as the source (Figure 13). Four 15–150 Hz upsweeps were recorded at each station with the first sweep used to seat the base plate. The mass on the Minivib was oriented perpendicular to the survey line providing a polarized SH-wave (Figure 15). Single 14 Hz geophones oriented in an SH configuration were deployed along the survey line in 5 m intervals. The shot stations were at a 2.5 m inline offset and a 1.52 m offline offset.

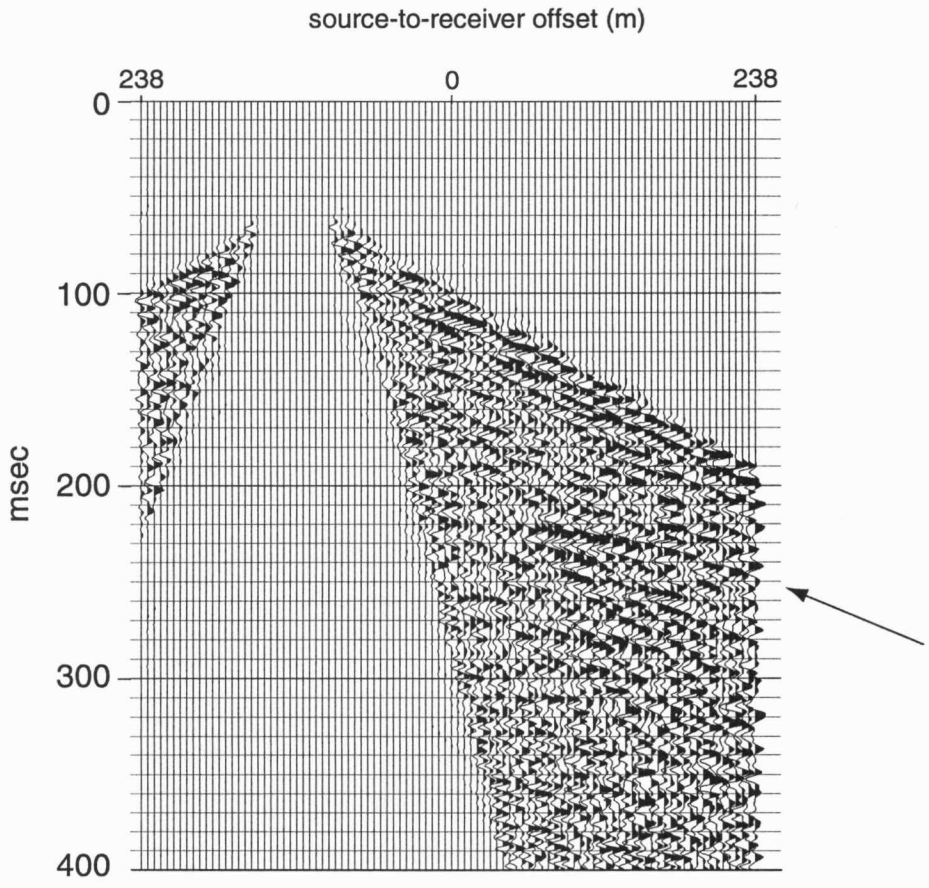


Figure 14. An example of a shotgather with an asymmetrical split-spread. Data is from the 96-channel P-wave data set. A reflection can be seen with a close offset reflection time at 220 msec.

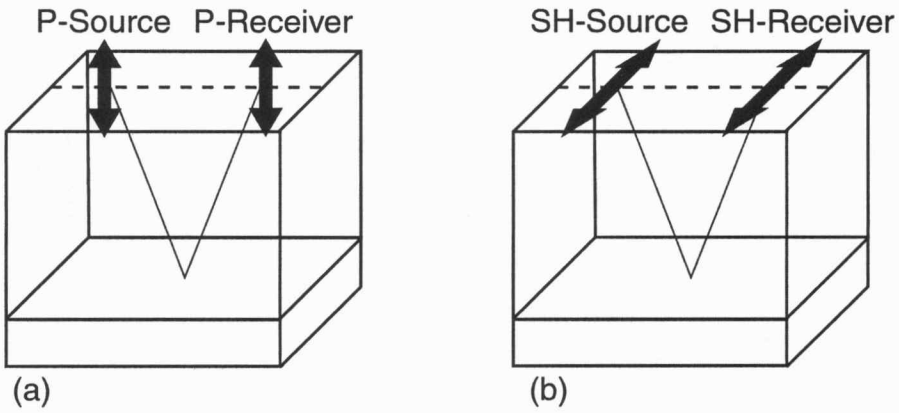


Figure 15. Source motions and receiver sensitivity directions for (a) P-P and (b) SH-SH wave surveys. The SH-source motion and SH-receiver direction used for the shear-wave data set is illustrated by (b). (Modified from McCormack and Tatham, 1986).

Vertical Seismic Profile (VSP)

The Geometrics Strataview seismograph system recorded the VSP data using the IVI Minivib to produce three 20-500 Hz sweeps at each geophone depth interval in the borehole. The borehole spatial sampling interval used in collecting the data was 1.52 m. A 3-component downhole geophone recorded the data at the Pitts #1 well adjacent to station 1130. The source-to-borehole offsets used to record the data were 6.1 m, 30.5 m , and 60.1 m. In this well, maximum penetration of the downhole geophone was 65.5 m. It was feared that if the geophone was forced past this sticky swollen clay/shale interval, the tool might become stuck in the hole.

Seismic Data Processing

The P-wave, S- wave, and VSP data were processed using WinSeis, a commercial processing software package designed at the Kansas Geological Survey for shallow seismic data processing. The processing flow used for the P- and S-wave data was consistent with acceptable shallow, high-resolution processing practices (Steeples and Miller, 1990) as well as all aspects of conventional processing approaches (Yilmaz, 1987). The VSP data were susceptible to basic steps in VSP processing that included wave separation, static correction, filtering, and stacking (Yilmaz, 1987).

P-wave data were processed using a processing sequence designed for signal and high frequency enhancement (Figure 16). The S-wave data were processed similarly with a focus on removing surface waves that contaminate the data (Figure 17). The processing flow for the VSP data set involved steps that include filtering, static corrections, muting, and stacking (Figure 18). The P-wave, S-wave, and VSP data were recorded and saved uncorrelated.

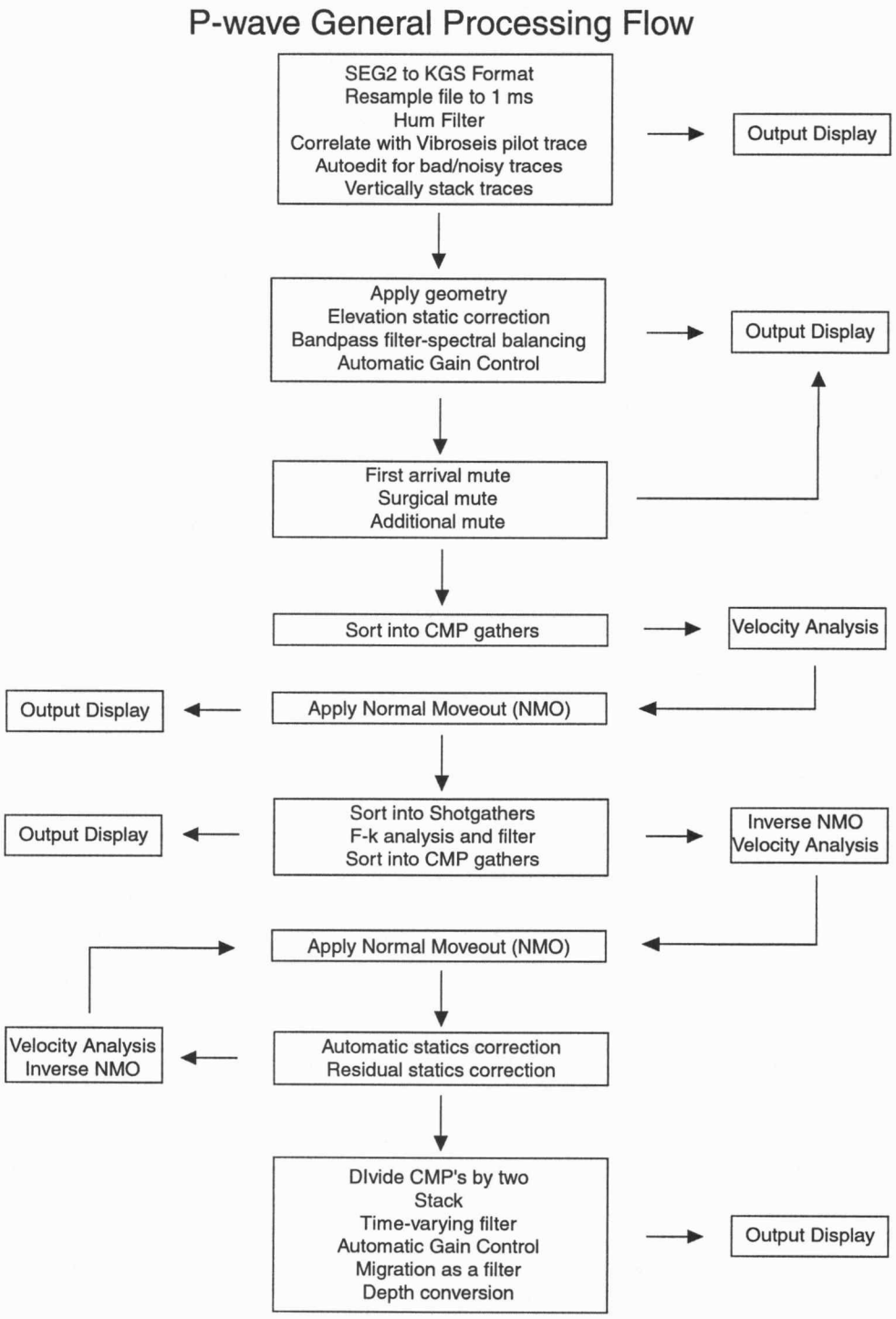


Figure 16. General processing flow used in processing the P- wave data sets. Proper care was taken to maintain the presence of interpretable reflection events throughout the processing sequence.

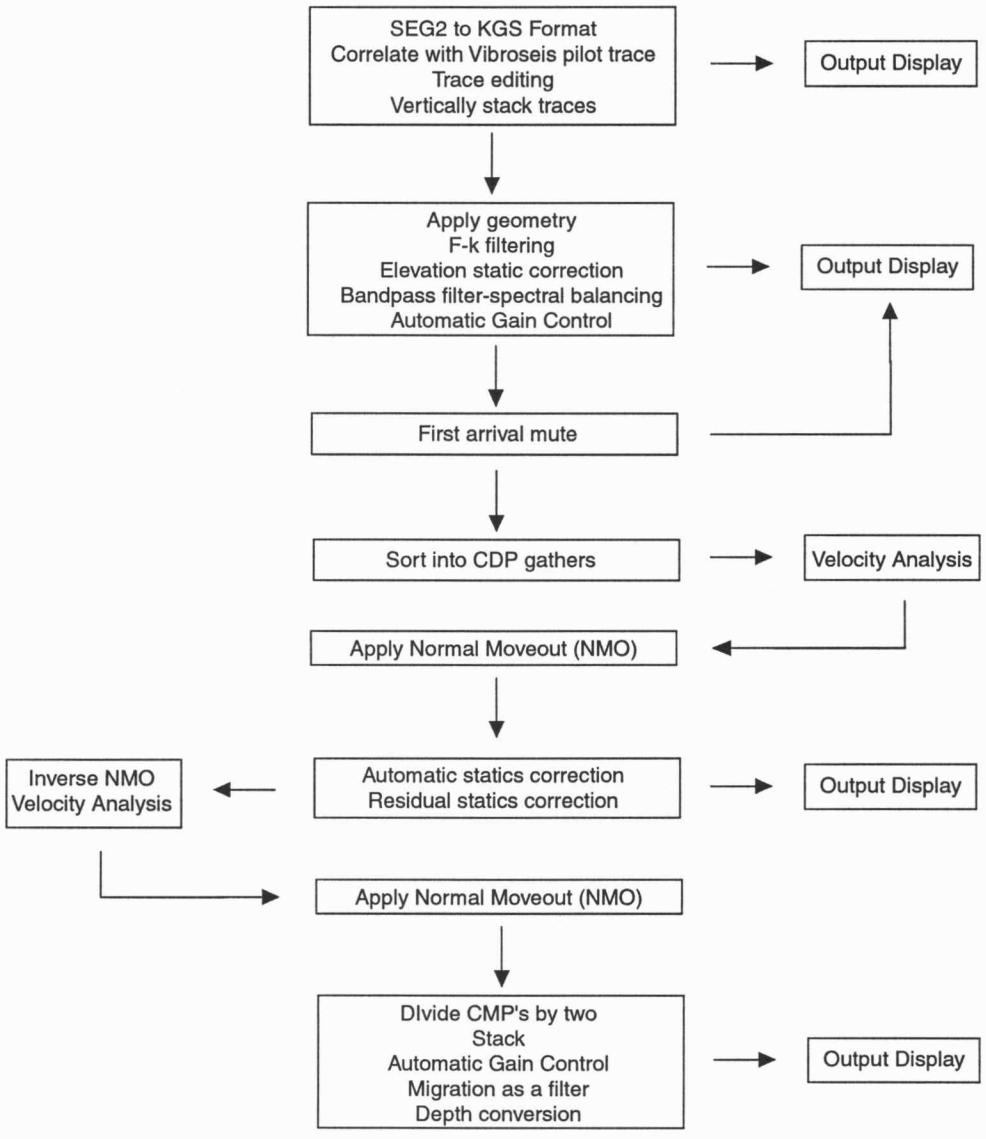


Figure 17. General processing flow used in processing the S- wave data set. Time was taken to remove the surface waves as much as possible. Again, proper care was taken to maintain the presence of interpretable reflection events throughout the processing sequence.

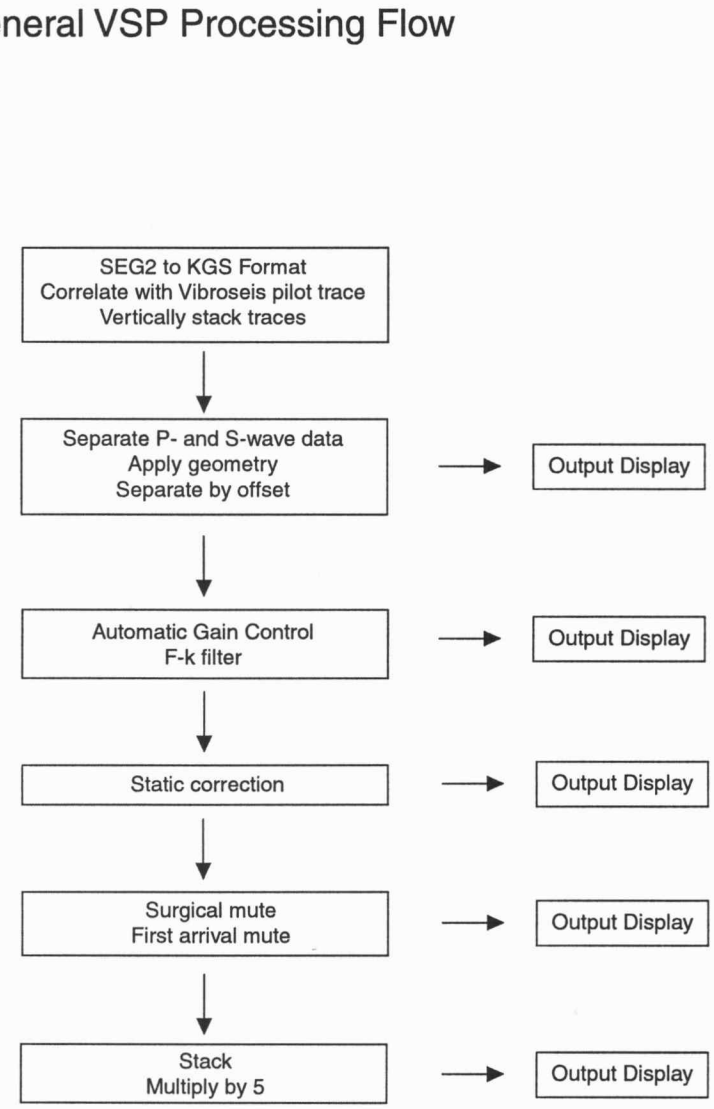


Figure 18. General processing flow used in processing the VSP data set.

P-wave data

After formatting the data, a power-line noise filter was applied to frequencies 60 Hz, 120 Hz, and 180 Hz (Xia and Miller, 1998). Once this was completed, the data were tested using the correlation method and deconvolution method with the recorded ground force. According to the convolution model, the vibroseis seismogram is,

$$x(t) = s(t) * w(t) * e(t),$$

where x(t) is the recorded seismogram, s(t) is the sweep signal, w(t) is the seismic wavelet, e(t) is the earth's impulse response, and * denotes the convolution operator (Yilmaz, 1987). Cross-correlation involves mathematically multiplying the sweep signal to both sides of the equations in the frequency domain,

$$S(\omega)\ X(\omega) = S^2(\omega)W(\omega)E(\omega).$$

The autocorrelation function of $S^2(\omega)$ gives the Klauder wavelet k(t) in the time domain. This zero-phase wavelet does not aid in recovering the earth's seismic response when using vibroseis data (Yilmaz, 1987). Deconvolving the data involves dividing the sweep signal in the frequency domain,

$$X(\omega) / S(\omega) = S(\omega)W(\omega)E(\omega) / S(\omega) = W(\omega)E(\omega).$$

This results in the cancellation of the sweep signal. Therefore, the Klauder wavelet does not become an issue. In theory, the deconvolution method will produce data the same as implusive data would. After testing these two methods, it was determined that deconvolving the data with the recorded ground force provided the better results (Figure 19).

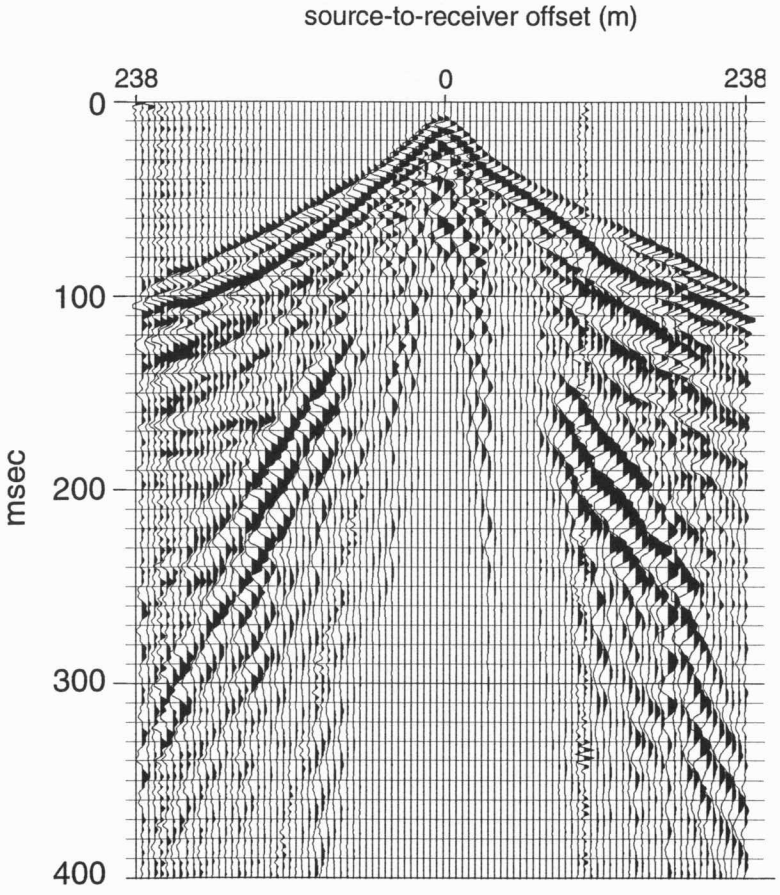


Figure 19a. 96-channel shotgather. The ground force has been deconvolved with the data. Deconvolving the data here proved to provide better results.

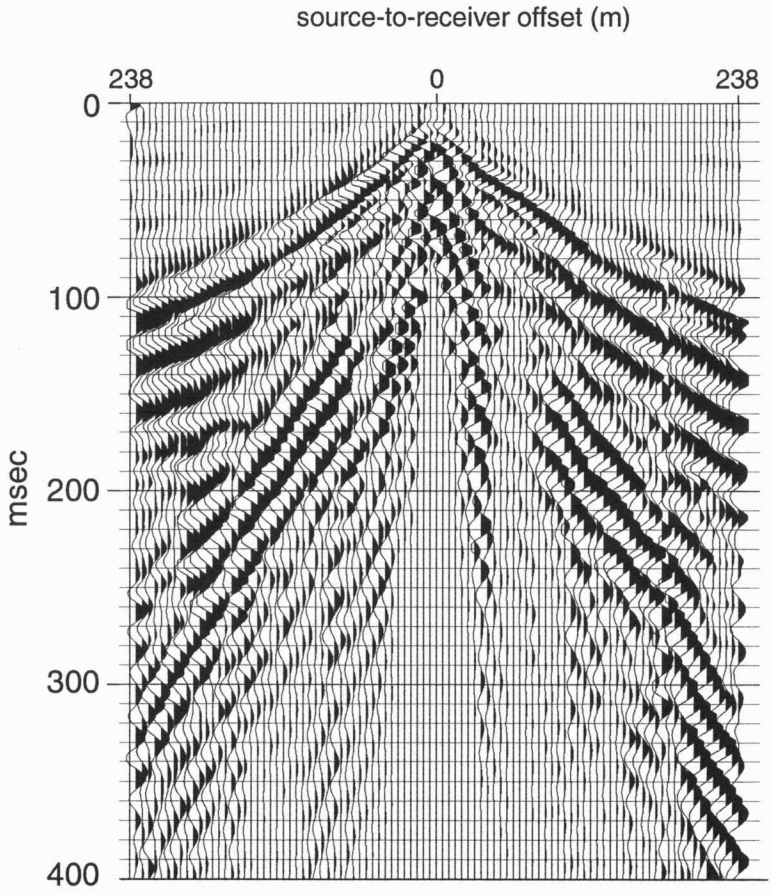


Figure 19b. 96-channel shotgather. The ground force has been cross-correlated with the data.

Once the data were correlated, the data were subjected to a processing flow that is outlined in Table 1 and Figures 20a, b, c, d, e, f, and g. Muting and filtering of noise (i.e. groundroll, refractions, air wave) was conducted while care was taken to maintain the presence of identifiable reflections throughout the processing flow (Figure 20c and d). An iterative velocity analysis was conducted using constant-velocity stacks before and after automatic and residual static corrections were applied. After the velocity model was applied, the data were sorted into shotgathers (Figure 20e). An f-k filter was applied to normally moved out data to ensure that the filter is applied to linear events only (Figure 20e and f).

After the data were filtered, muted, and normally moved out, the data were resorted into CMP gathers and divided by two to create 5 m CMP trace intervals (Figure 20g). The gas sand can be seen at 90 msec. This reflection increases in amplitude with increasing offset, supporting the interpretation that this amplitude anomaly is a class 2 gas sand. After the 96-channel data were stacked, a time-varying bandpass filter was applied at 100 ms and at 500 ms while interpolating between the two times. The 240-channel data set did not have a time-varying filter applied.

A post-stack AGC window was applied to the data sets to image deeper events. This was followed by the application of a migration filter (Plate 1 and 2). This migration filter aids in attenuating higher frequency noise in the stacked section. A 10 m trace interval was used as a parameter in the migration filter. This is twice

the actual interval (5m) used in the data acquisition. This doubling of the trace interval serves as the parameter that causes the data to be severely undermigrated. As a result, the data are migrated to a small degree that does not critically affect the two-way travel times of the reflective events. After the post-stack processing, the data were subject to depth conversion to aid in correlating with the well log data (Plate 3 and 4).

Processing Steps	Purpose	Figure	Additional information
Resampled the data	different sampling rates		mid acquisition, sampling rate was changed (96-channel only)
Power line noise filter			at frequencies 60, 120, 180 Hz
Deconvolve data with ground force	correlate data with vibroseis		
Trace editing	kill noise/dead traces		
Vertical stacking	enhance S/N	20a	stacked three files at each shotpoint
Geometry			
Elevation static correction	correct data for changes in elevation	20b	
Bandpass filter		20b	BP filter 30 60 225 275 (96-channel); 30 60 150 225 (240-channel)
Automatic Gain Control	enhance deep reflections	20b	150 msec scaling window for P-wave data
First arrival mute	mute noise	20c/d	mute direct arrivals, refractions, correlation noise
Surgical mute	mute within the air wave cone incl. ground roll	20c 20d	
Velocity analysis	determine stacking vel.		used constant velocity scans at every 100 CDPs
Normal Moveout (NMO)	produce normal incident data	20e	
F-k filter	filter linear events	20f	conducted in the shot domain
Inverse NMO	subtract stacking vel.		conduct another vel analy to refine vel mod and apply NMO again
Automatic and Residual static corrections	correct for slight diff. In arrival times		7 ms static limit; 320 ms window centered at 240 ms; 21 CDP's x-cor 3 ms static limit; 300 ms window centered at 240 ms; 9 CDP x-cor.
Divide CMP's by 2	equal trace spacing	20g	amplitude increase with offset at 90 msec (class 2 gas sand)
Time-varying filter	bandpass filter at varying times		for 96-ch. only: bp filt at 100 ms 30 60 150 225 and at 500 ms 20 40 100 150
Stack and apply AGC	enhance deep reflections		for 96-ch. scaling window of 100 ms and 240-ch. window of 150 ms
Migration filter	attenuating higher freq.	Plate 1 Plate 2	trace interval used was 2 X's actual receiver interval (10m); velocity used was 3050 m/s; 500 ms half sample interval
Depth conversion		Plate 3 Plate 4	used to correlate between P- and S-wave data sets and with well log

Table 1. P-wave data processing information

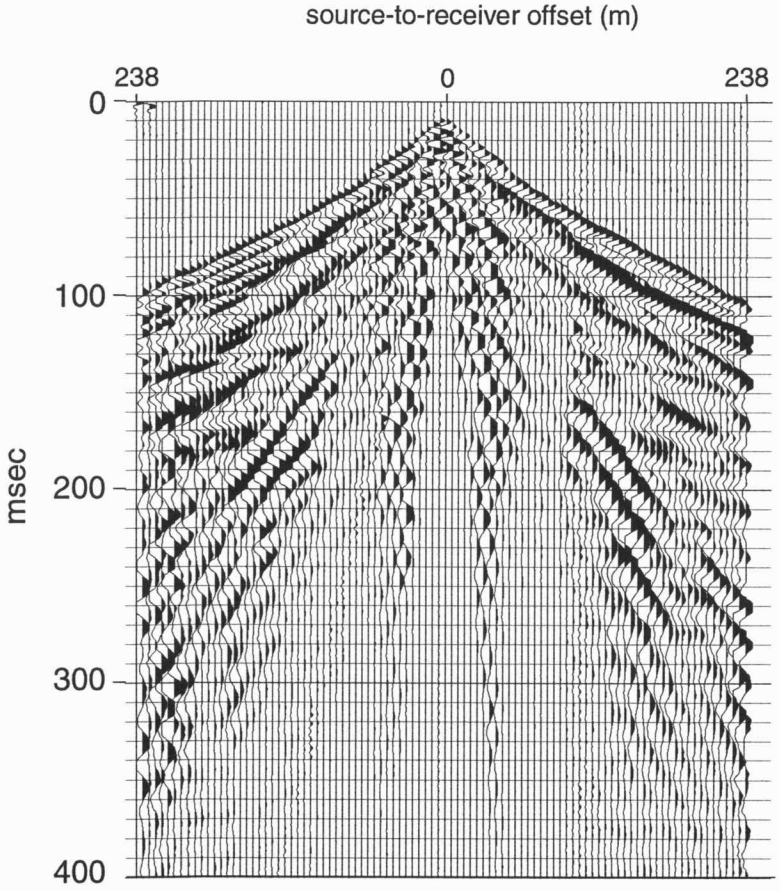


Figure 20a. 96-channel shotgather at CMP station 1130, nearest to the KGS Pitts #1 well. Three shots at each shotpoint have been vertically stacked to produce this raw shotgather.

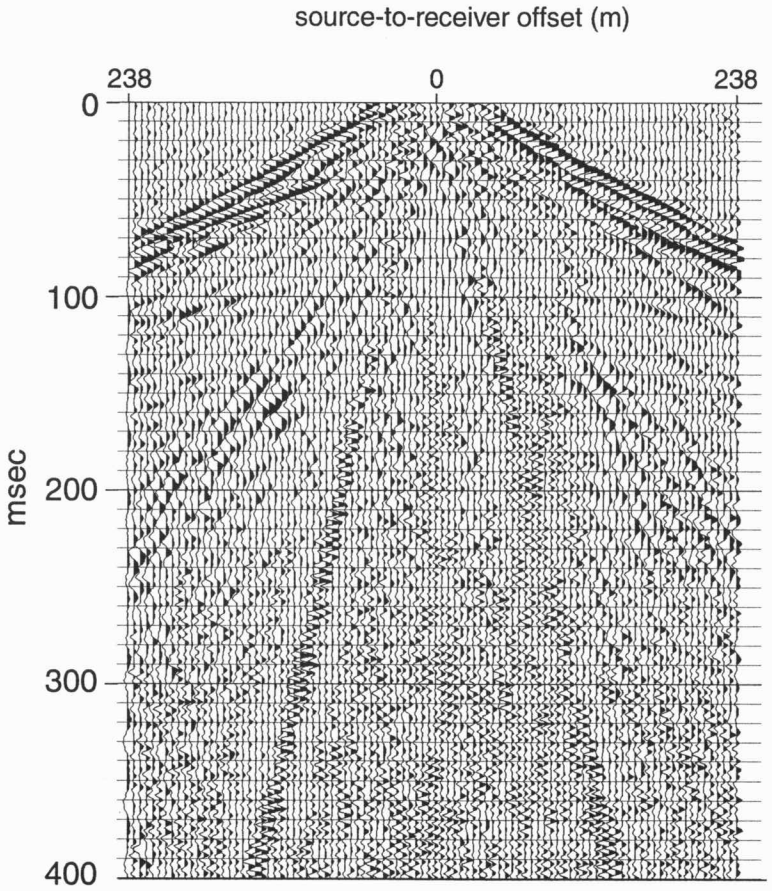


Figure 20b. 96-channel shotgather at CMP station 1130, nearest to the KGS Pitts #1 well. A bandpass filter, AGC window, and elevation statics have been applied.

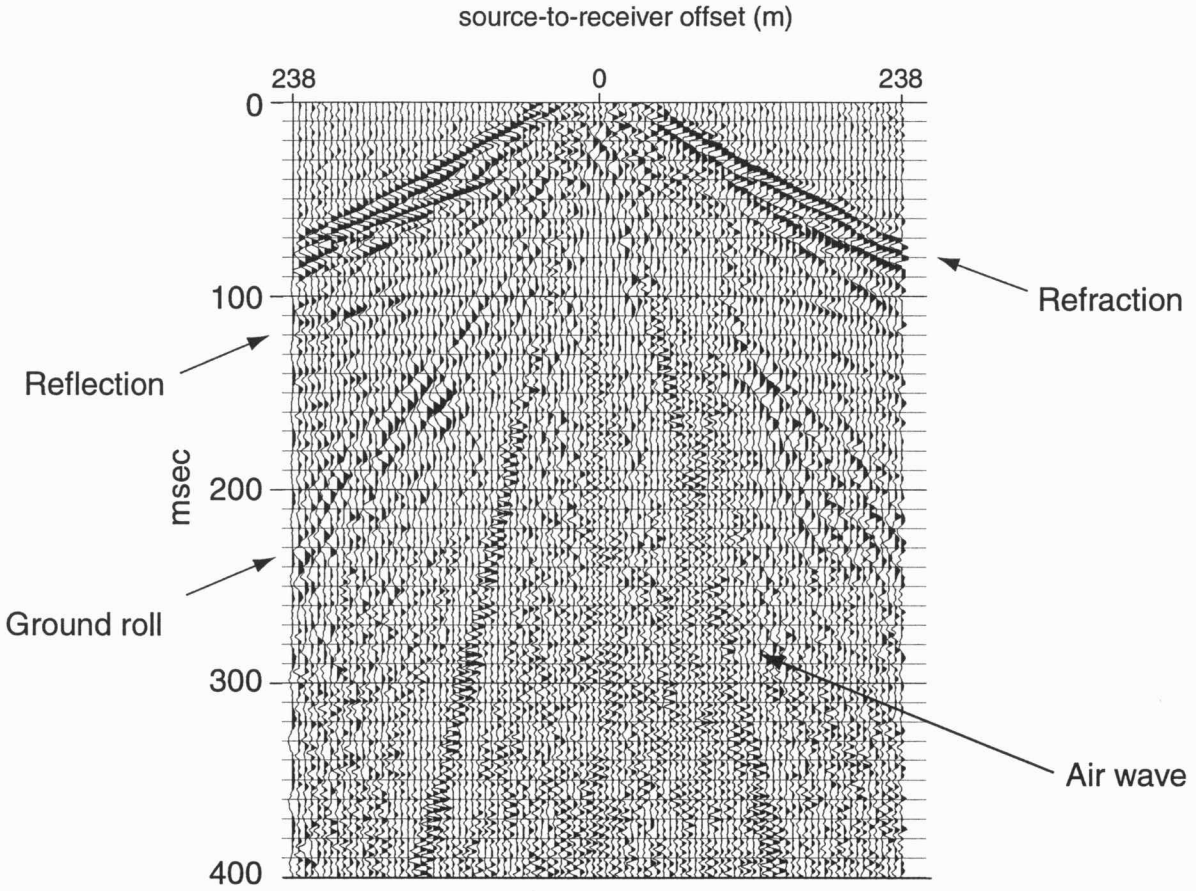


Figure 20c. 96-channel shotgather at CMP station 1130 shows the different types of energy oftern found in shallow reflection data.

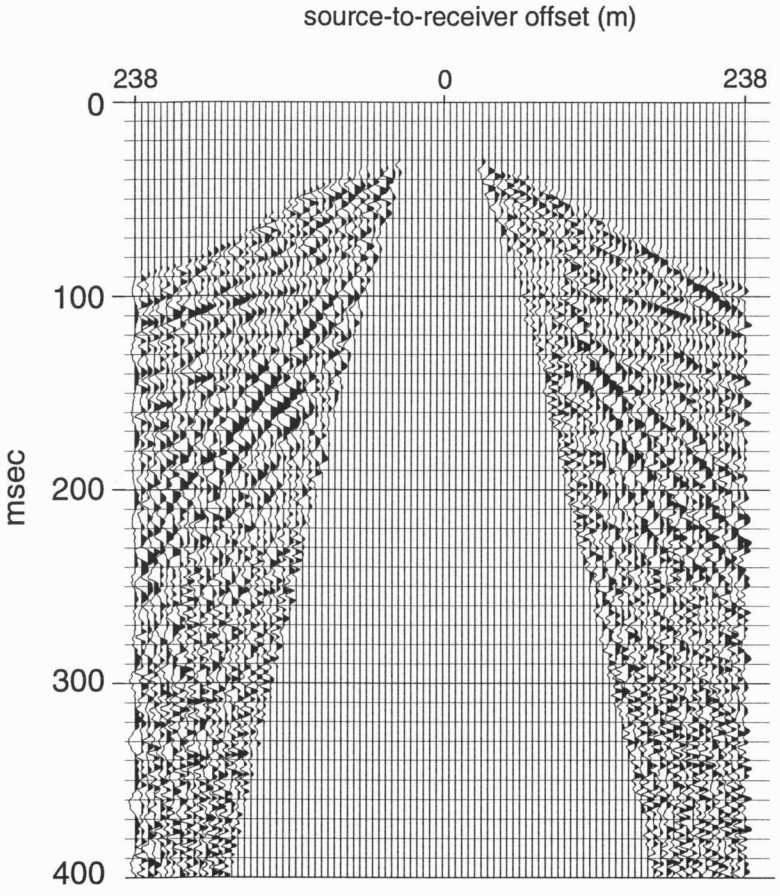


Figure 20d. 96-channel shotgather at CMP station 1130, nearest to the KGS Pitts #1 well. First arrival and surgical muting have been applied.

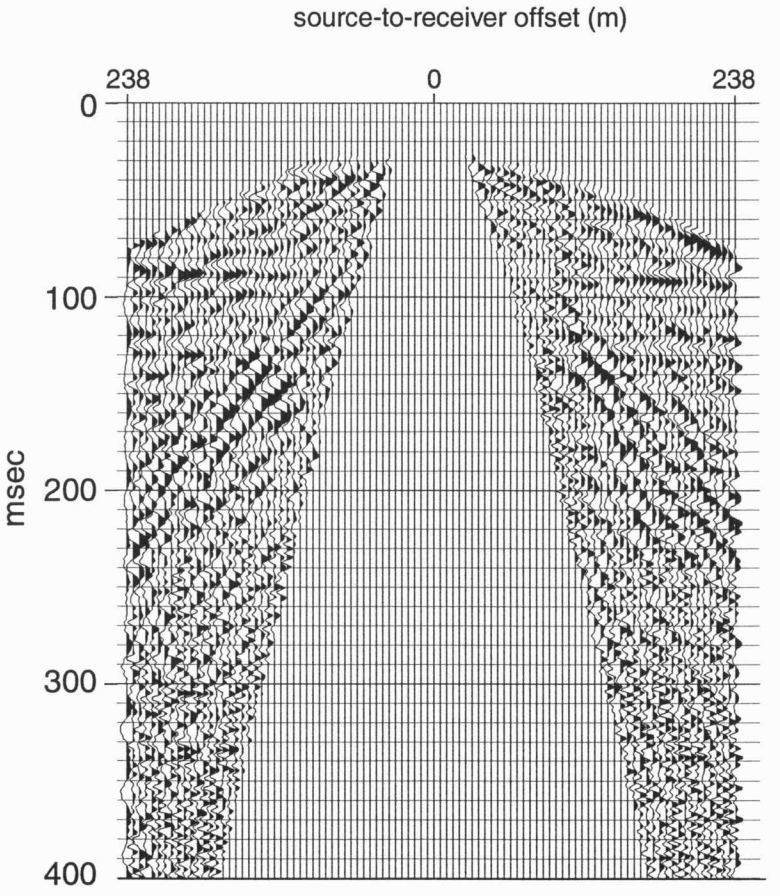


Figure 20e. 96-channel shotgather at CMP station 1130, nearest to the KGS Pitts #1 well. A normal moveout function has been applied.

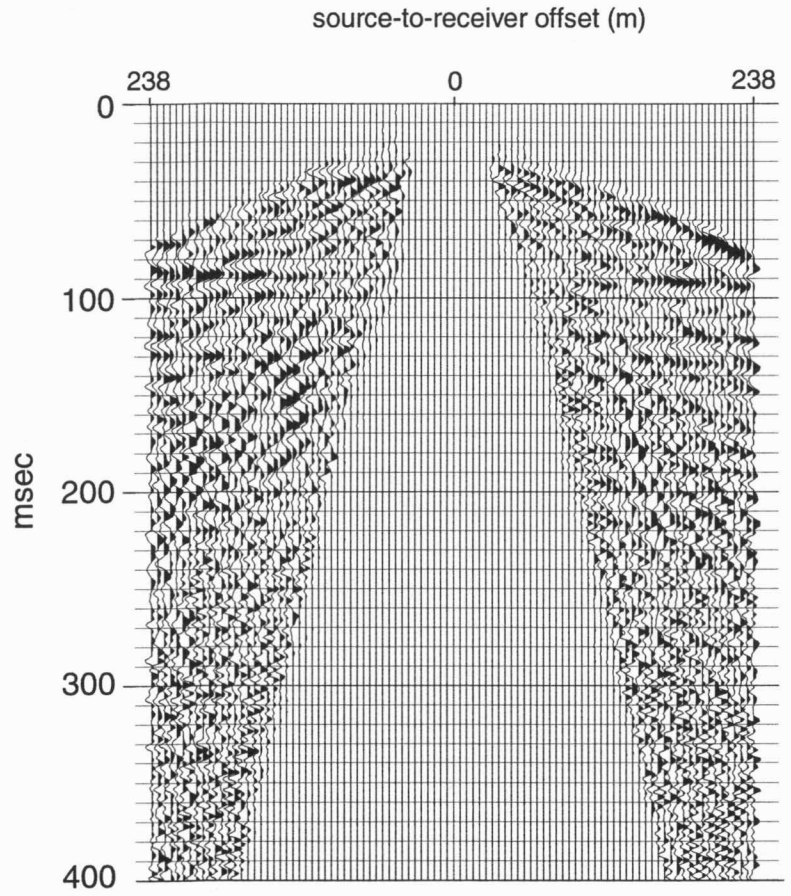


Figure 20f. 96-channel shotgather at CMP station 1130, nearest to the KGS Pitts #1 well. An f-k filter has been applied to suppress some of the ground roll in the data.

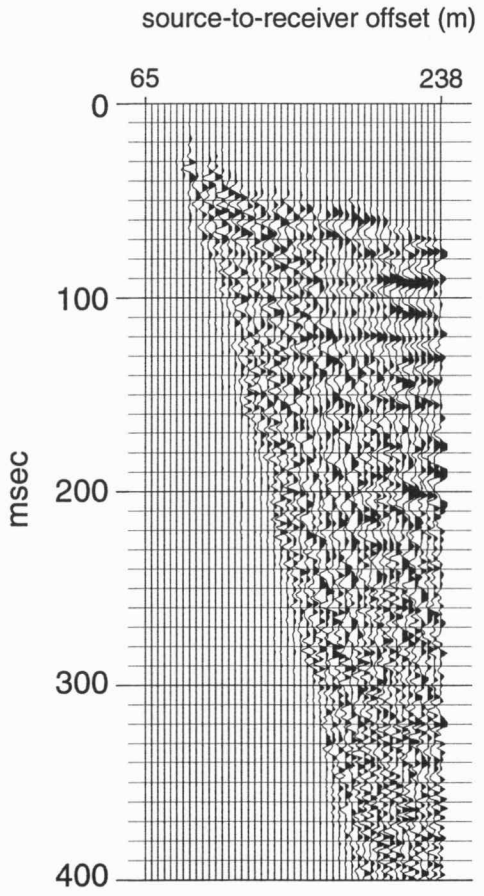


Figure 20g. Normally moved out CMP gather at CMP station 1130 for the 96-channel data.

P-wave (96-channels) non-AGC data

Given the importance of using amplitude versus offset (AVO) analysis in confirming the presence of a gas sand, the P-wave data were subject to processing steps that involved no amplitude balancing, specifically no AGC window (Figure 21; Table 2) (Castagna, 1993). Amplitude adjustments were based on a geometric spreading correction that was applied to the data after the geometry was assigned.

The geometric spreading correction is important in gain recovery when working with true amplitudes. As the wavefront propagates through the subsurface, energy decreases in strength (Sheriff and Geldart, 1982). Various factors are responsible for this decrease in energy. These factors include geometric spreading, absorption, wave scattering, reflection coefficient, source strength, geophone sensitivity and other factors (Sheriff and Geldart, 1982). Amplitude recovery factors other than geometric spreading are not approached here.

Following the application of spherical divergence, the data were subjected to the processing flow outlined in Table 2. The results of various steps of the processing flow are shown in Figure 22a, b, c, d, and e. The final stacked section for the 96-channel data shows a very distinct amplitude anomaly at 90 msec (Figure 23). This anomaly is also imaged on the 240-channel stacked section (Figure 24). With the absence of using an AGC scaling window and correcting for geometric spreading, these data could be considered to display true amplitude.

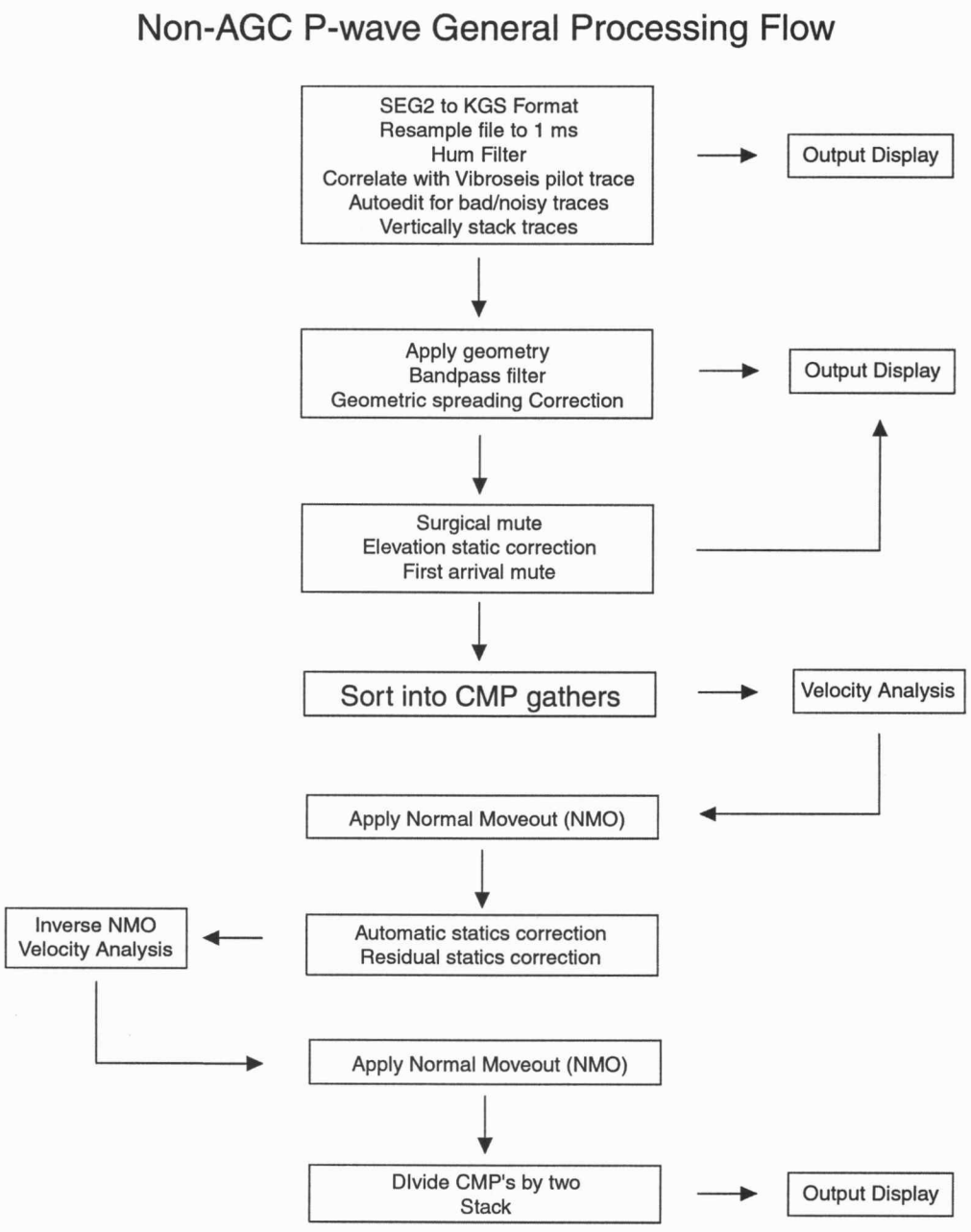


Figure 21. General processing flow used in processing the non-AGC P- wave data set. Care was taken to maintain the amplitude of the reflections.

Processing Steps	Purpose	Figure	Additional information
Resampled the data	different sampling rates		mid acquisition, sampling rate was changed (96-channel only)
Power line noise filter			at frequencies 60, 120, 180 Hz
Deconvolve data with ground force	correlate data with vibroseis		
Trace editing	kill noise/dead traces		
Vertical stacking	enhance S/N	22a	stacked three files at each shotpoint
Geometry			
Bandpass filter	no spectral balancing	22b	BP filter 30 60 225 275 (96-channel); 30 60 150 225 (240-channel)
Spherical divergence	geometric spreading cor.	22b	used 20 dB/sec
F-k filter	filter linear events	22f	conducted in the shot domain
First arrival mute	mute noise	22c/d	mute direct arrivals, refractions, correlation noise
Surgical mute	mute within the air wave cone incl. ground roll	22c 22d	also mute most of ground roll (noise)
Elevation static correction	correct data for changes in elevation	22b	
Velocity analysis	determine stacking vel.		used constant velocity scans at every 100 CDPs
Normal Moveout (NMO)	produce normal incident data	22e	
Automatic and Residual static corrections	correct for slight diff. In arrival times		7 ms static limit; 320 ms window centered at 240 ms; 21 CDP's x-cor 3 ms static limit; 300 ms window centered at 240 ms; 9 CDP x-cor.
Divide CMP's by 2	equal trace spacing	22g	amplitude increase with offset at 90 msec (class 2 gas sand)
Stack		23/24	the 90 msec reflection shows a bright spot

Table 2. True amplitude P-wave data processing information

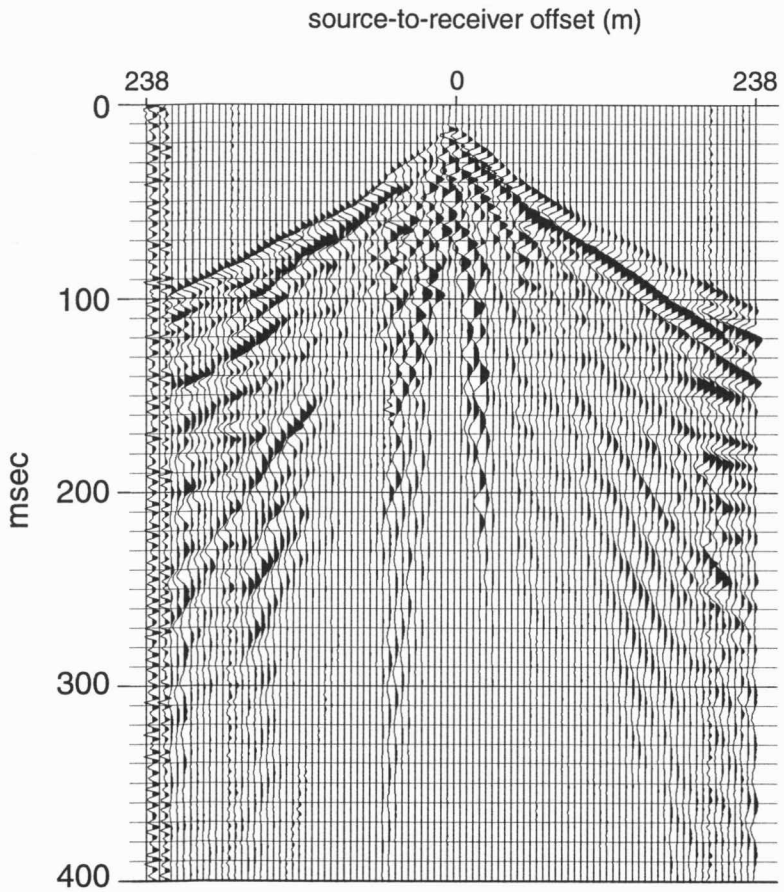


Figure 22a. 96-channel shotgather at CMP station 1140, close to the KGS Pitts #1 well. Three shots at each shotpoint have been vertically stacked to produce this raw shotgather.

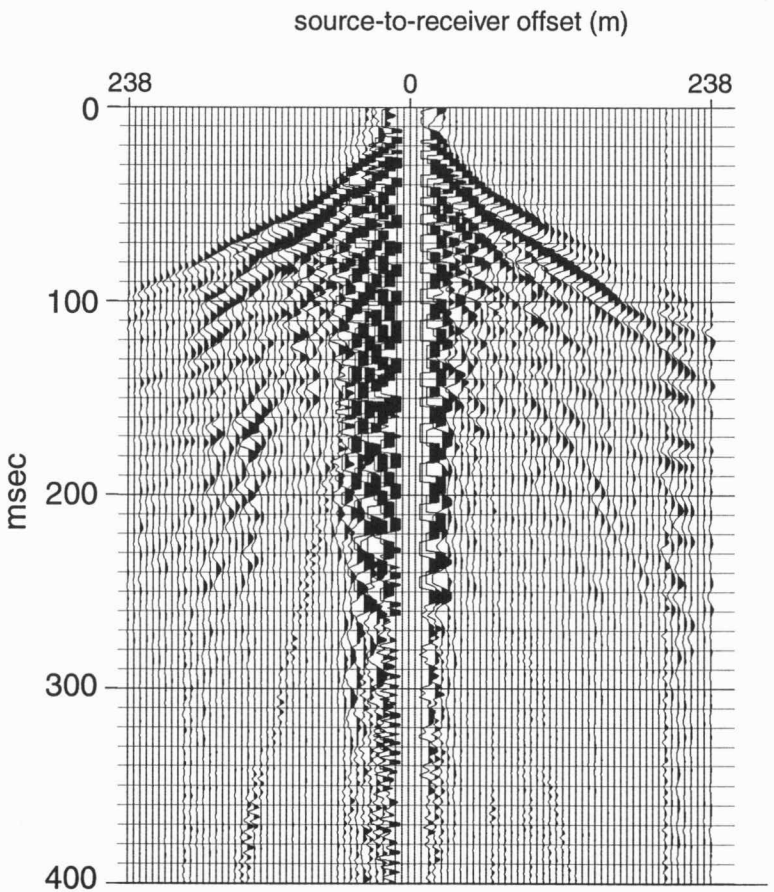


Figure 22b. 96-channel shotgather at CMP station 1140. A bandpass filter and geometric spreading correction have been applied. Spectral balancing and AGC have not been applied.

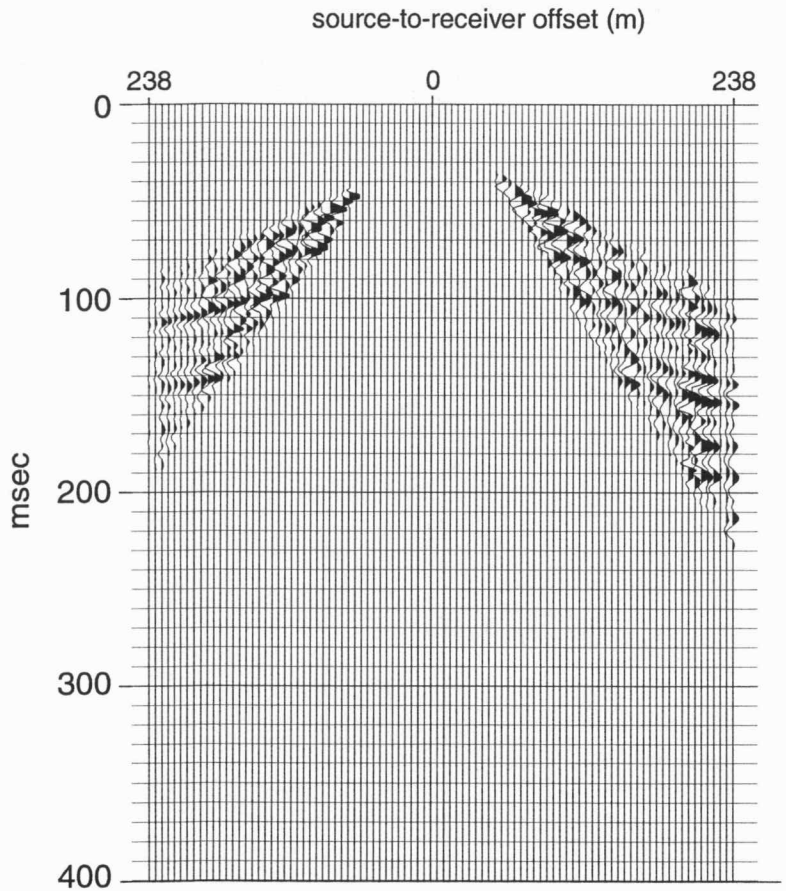


Figure 22c. 96-channel shotgather at CMP station 1140, close to the KGS Pitts #1 well. An f-k filter, severe surgical mute (for the low frequency ground roll), elevation static correction, and first arrival mute have been applied.

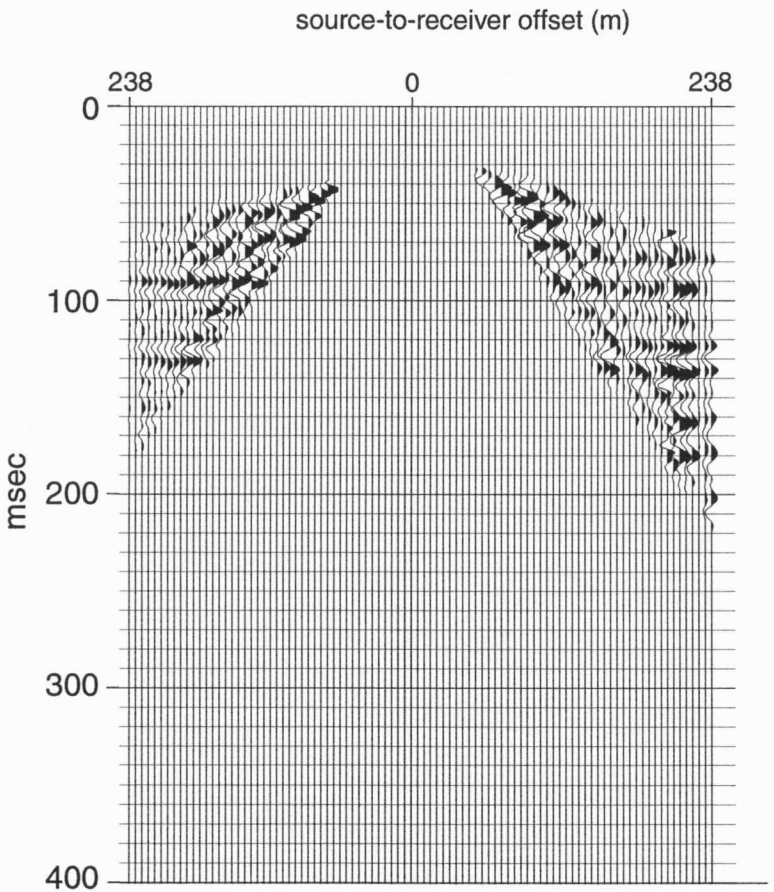


Figure 22d. 96-channel shotgather at CMP station 1140, close to the KGS Pitts #1 well. A normal moveout function has been applied.

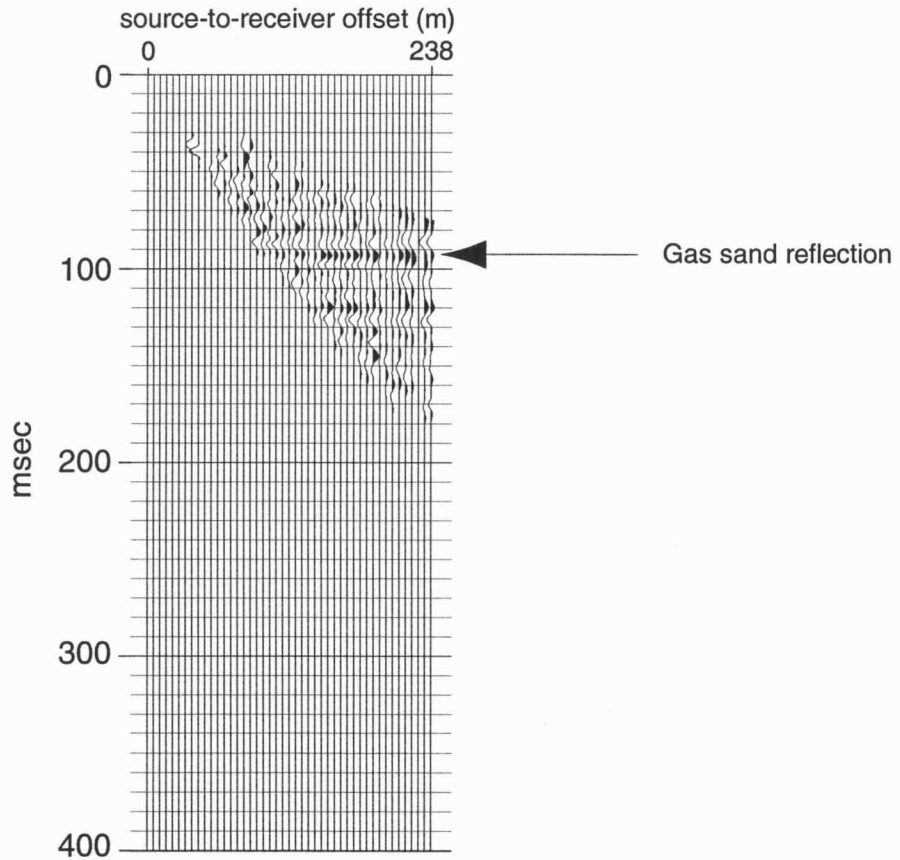


Figure 22e. 96-channel CMP gather at CMP station 1140, close to the KGS Pitts #1 well.

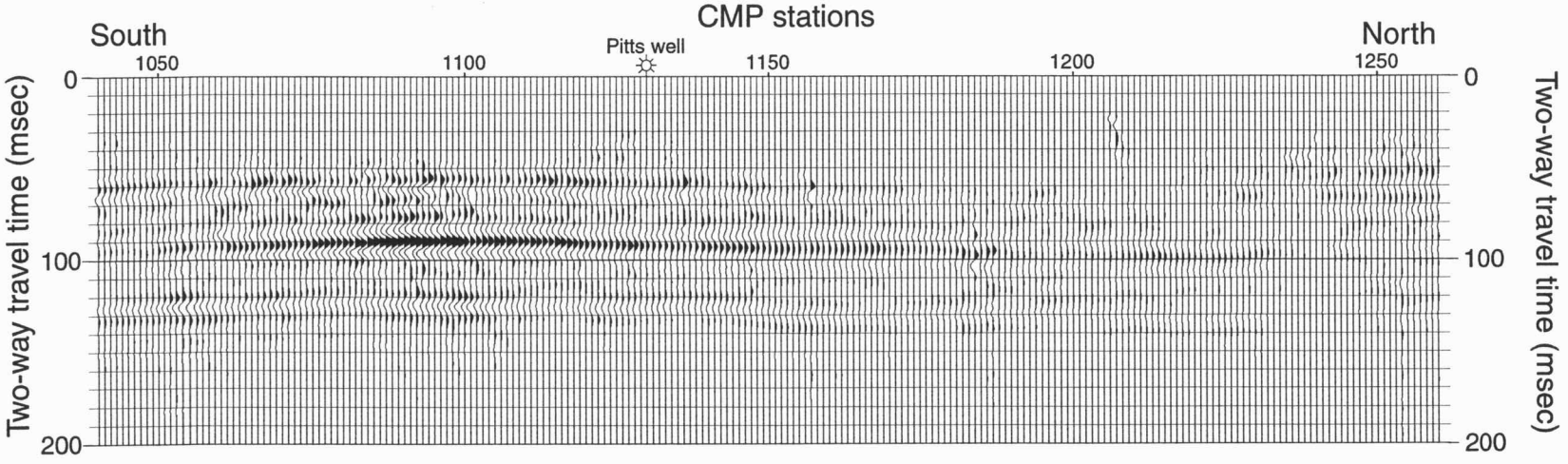


Figure 23. CMP time stacked section with geometric spreading correction applied, P-wave Trip1(96-channels). The Pitts well is 100 m offline west of the seismic line.

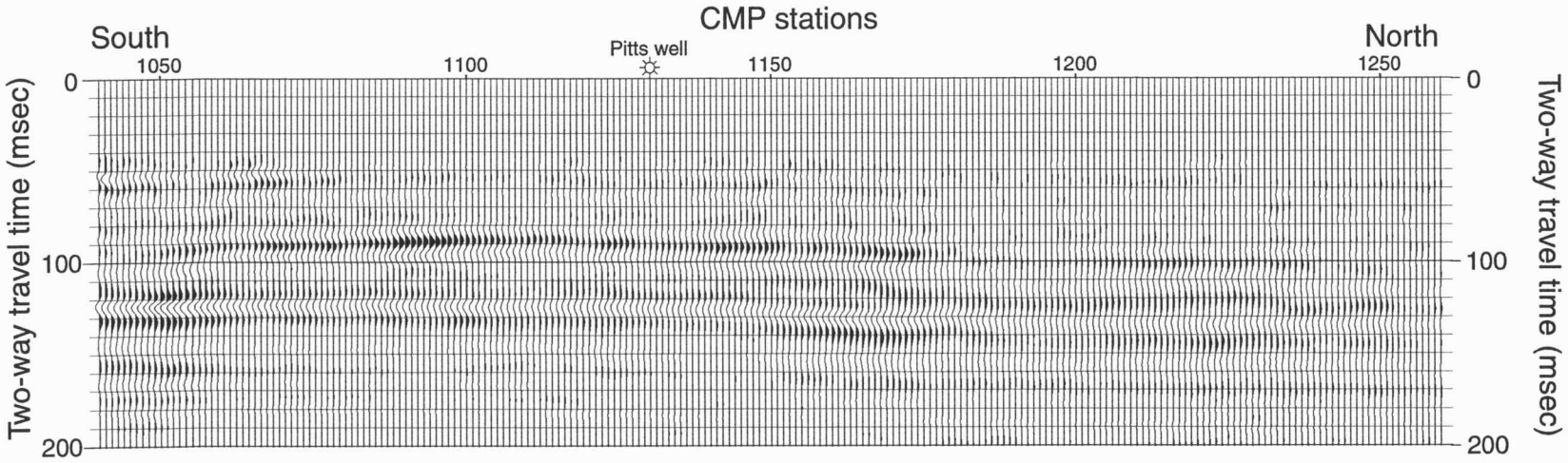


Figure 24. CMP time stacked section with geometric spreading correction applied, P-wave Trip2 (240-channels). The Pitts well is 100 m offline west of the seismic line.

S-wave data

The S-wave data were processed using a sequence similar to that used for the P-wave (Figure 17). This processing flow along with significant parameters is presented in Table 3. The results of certain portions of the flow are shown in Figure 25a, b, c, and d. As with the P-wave data, the shear-wave data were deconvolved with the ground force. After muting and filtering the data for noise, an iterative velocity analysis was conducted using constant-velocity scans. Residual static corrections, with a maximum of a 7 msec static shift, were applied to the data.

The data were then stacked with a 200 msec AGC window applied to the stacked section. A migration filter is applied to the stacked section to attenuate the high frequency noise in the data (Plate 5). The shear-wave time stacked section was subjected to depth conversion using the stacking velocities to generate a depth stacked section (Plate 6).

Processing Steps	Purpose	Figure	Additional information
Deconvolve data with ground force	correlate data with vibroseis		
Trace editing	kill noise/dead traces		
Vertical stacking	enhance S/N	25a	stacked three files at each shotpoint
Geometry			
F-k filter	filter linear events	25f	conducted in the shot domain
Elevation static correction	correct data for changes in elevation	25b	
Bandpass filter		25b	BP filter 15 30 60 90
Automatic Gain Control	enhance deep reflections	25b	200 msec scaling window
First arrival mute	mute noise	25c/d	mute direct arrivals, refractions, correlation noise
Velocity analysis	determine stacking vel.		used constant velocity scans at every 100 CDPs
Normal Moveout (NMO)	produce normal incident data	25e	
Automatic and Residual static corrections	correct for slight diff. In arrival times		7 ms static limit; 300 ms window centered at 450 ms; 21 CDP's x-cor 9 ms static limit; 300 ms window centered at 450 ms; 11 CDP x-cor.
Divide CMP's by 2	equal trace spacing	25g	
Stack and apply AGC	enhance deep reflections		200 msec scaling window
Migration filter	attenuating higher freq.	Plate 5	trace interval used was 2 X's actual receiver interval (10m); velocity used was 1500 m/s; 500 ms half sample interval
Depth conversion		Plate 6	used to correlate between P- and S-wave data sets and with well log

Table 3. S-wave data processing information

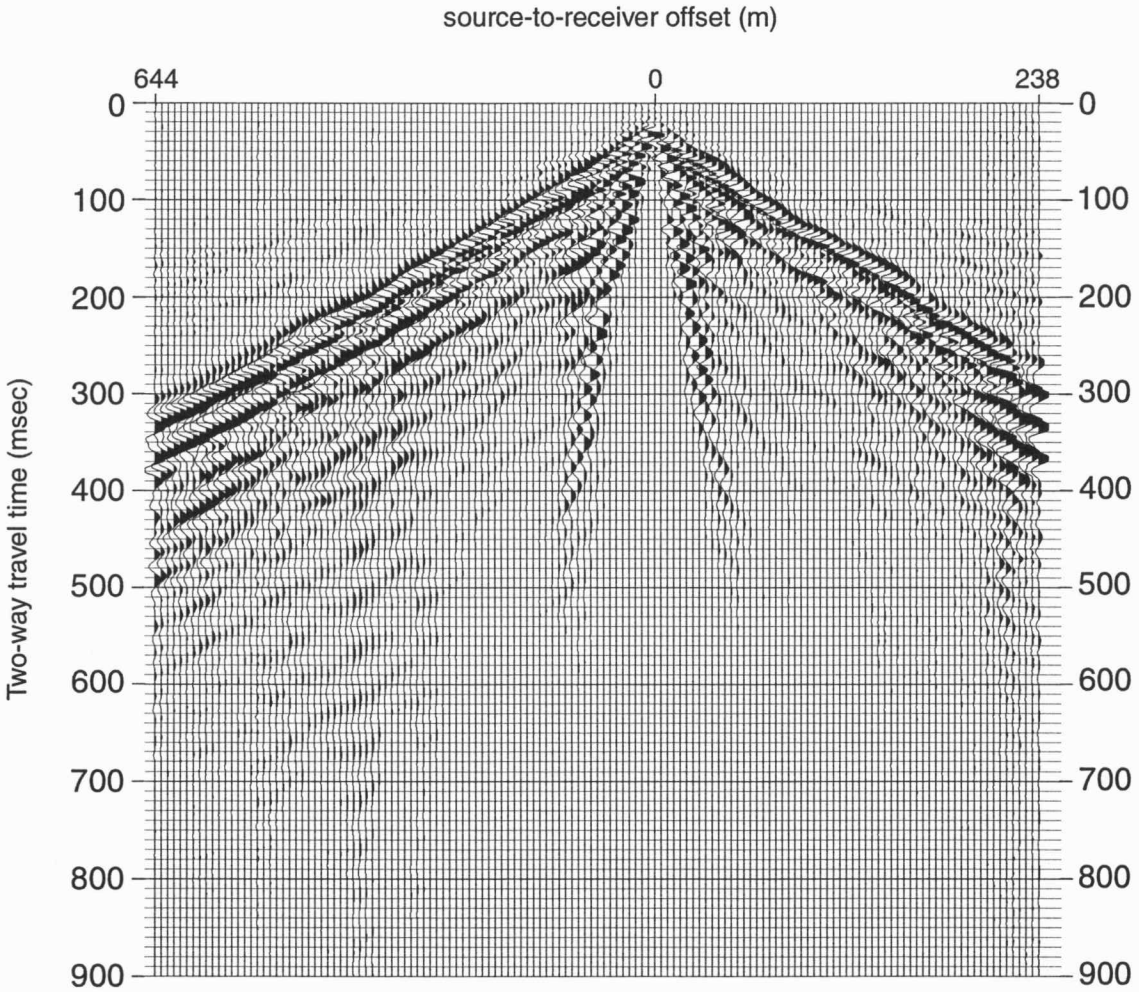


Figure 25a. Raw Shear-wave shotgather at CMP station 1119, south of the KGS Pitts #1 well at station 1130.

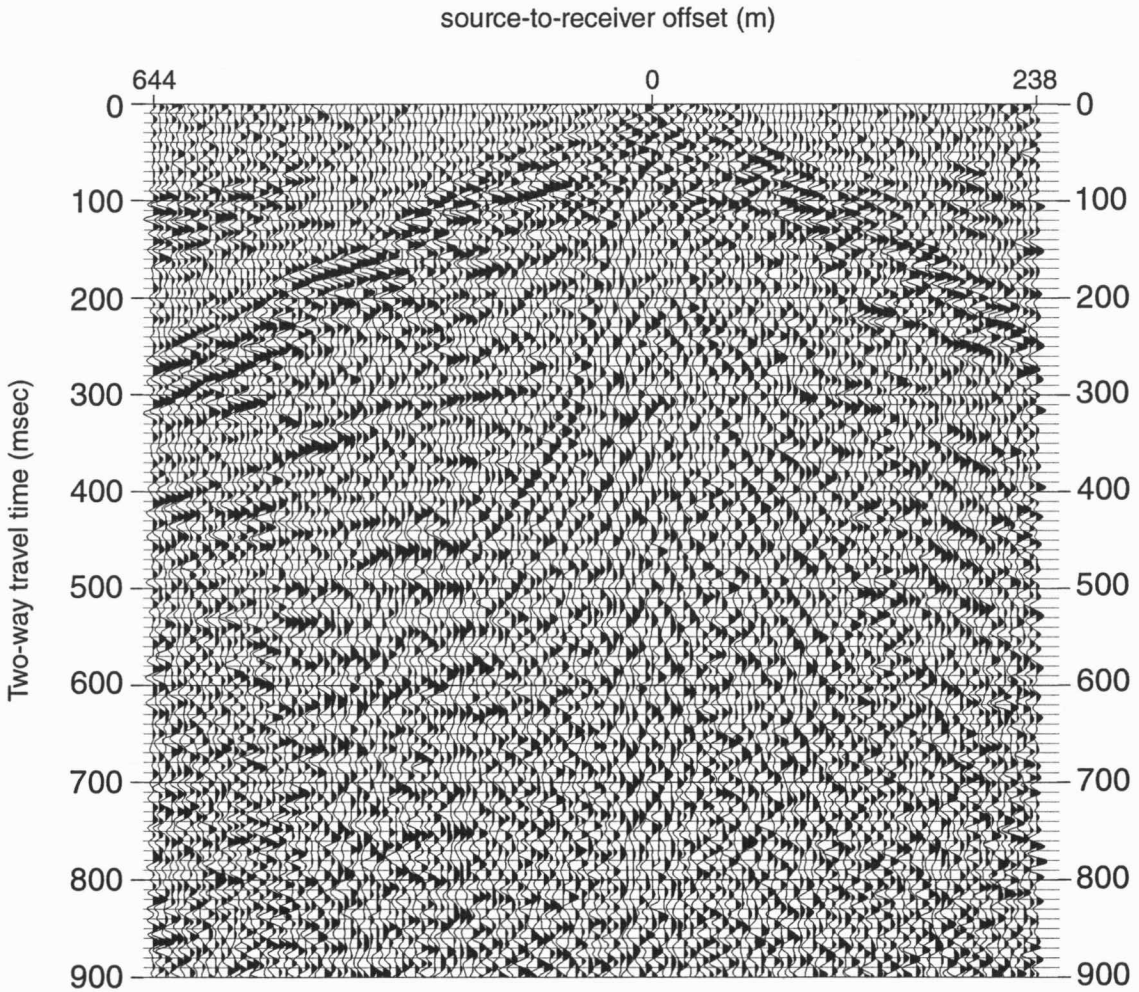


Figure 25b. S-wave shotgather at CMP station 1119. A bandpass filter, AGC window, and elevation statics have been applied.

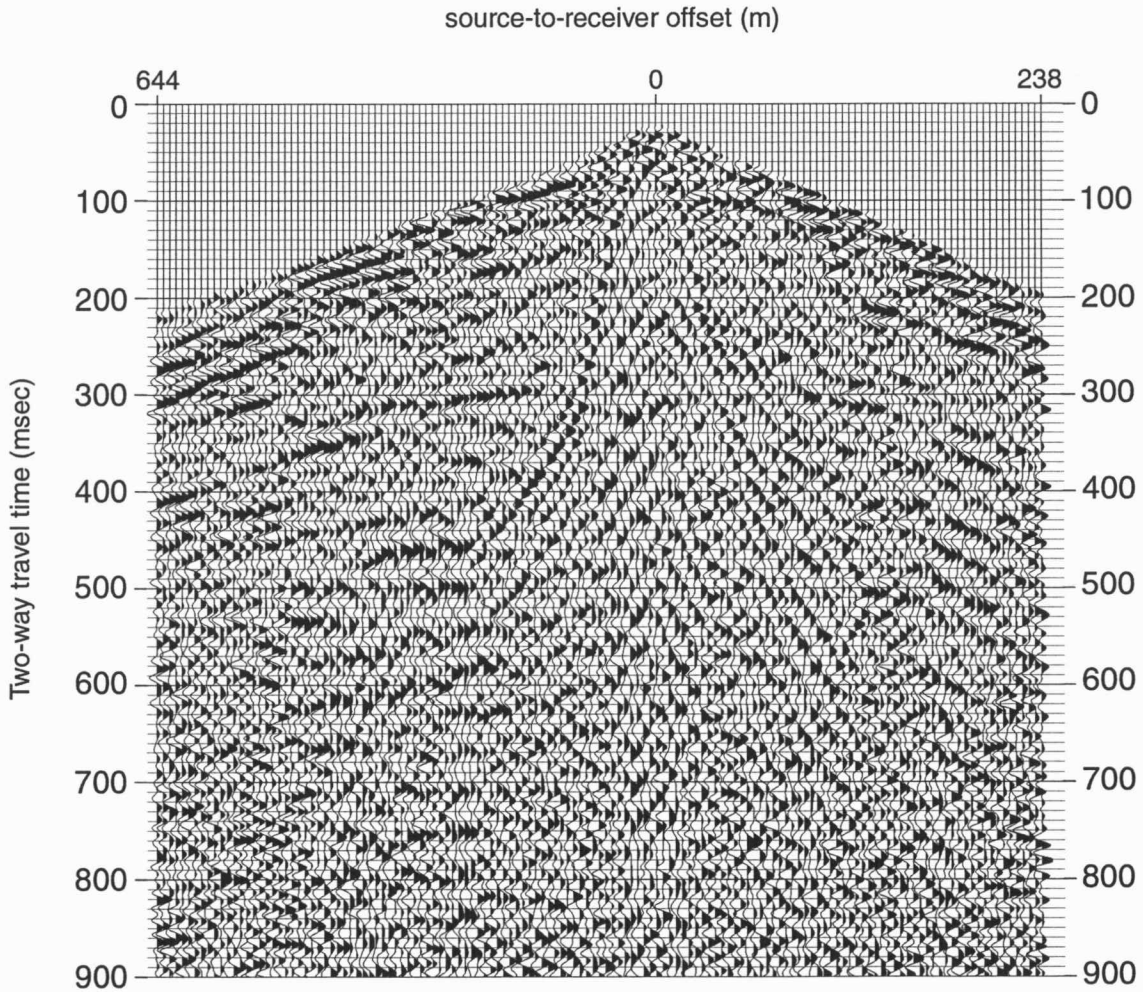


Figure 25c. S-wave shotgather at CMP station 1119. FIrst arrival muting has been applied.

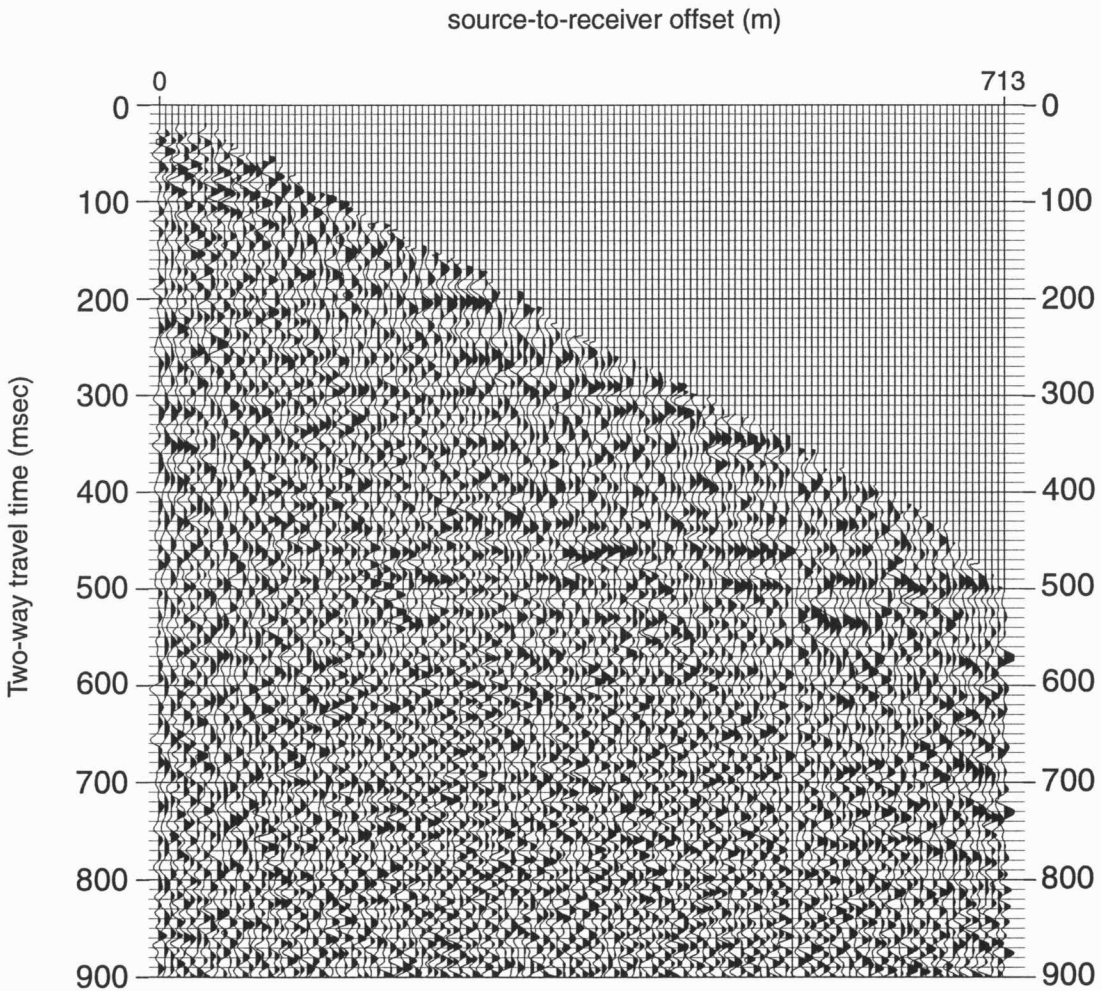


Figure 25d. S-wave normally moved-out CMP gather at station 1119.

Vertical Seismic Profile (VSP) data

The VSP data were filtered, static corrected for two-way travel time, noise muted, and stacked (Figure 18). These steps including parameters are detailed in Table 4. Applying an f-k filter to all offsets, 6.1 m, 30.5 m, and 60.1 m, helped determine which offset provided the better reflections (Figure 26). In viewing the data, the 60.1 m offset imaged deeper reflections when compared to the other two offsets. The results of the processing flow used for the VSP data is shown in figure 27a, b, c, d, e, f, g, and h. The 3-component data that were acquired were separated into P- and S-wave data followed by the application of the geometry.

An important step in processing VSP data is applying an f-k filter to filter out the downgoing (noise) events (Figure 27c). The downgoing and upgoing waves have different dips; therefore they will map in different regions in the f-k space domain (Yilmaz, 1987). Once the filter was applied to the downgoing waves, reflection events can be seen. The next step involves flattening the reflection events so that they may coincide with events on a CMP stacked section. The flattening of reflections involve datuming the receivers in the well bore to the surface. This was accomplished by using static corrections (Figure 27d). After the data were muted and stacked, this was correlated with the final CMP stacked sections for the P- and S-wave data (Plate 13, 14, and 15).

Processing Steps	Purpose	Figure	Additional information
Cross correlate data with ground force	correlate data with vibroseis		
Vertical stacking	enhance S/N	27a	stacked three files at each shotpoint
S-wave component rotation	to generate on direction		rotated S1 and S2 directions so that they are perpen. to each other
Geometry			
Automatic Gain Control	enhance deep reflections	27b	200 msec scaling window
F-k filter	filter linear events	27c	filter out downgoing events
Borehole elevation correc.	correct borehole depths to surface	27d	used to generate two-way travel time to correlate with CMP stack section
First arrival and surgical mute	mute noise	27e/f	to mute f-k filtering wrap around artifacts
Stack		27g	
Multiply stacked trace by 5	for visual effect	27h	
Correlation with the CMP stacked sections		Plate 16, 17, 18	data had to be shifted; P-wave shifted 21 ms for datum corr. only S-wave shifted 41 ms for datum corr. only

Table 4. VSP data processing information for both P- and S-components

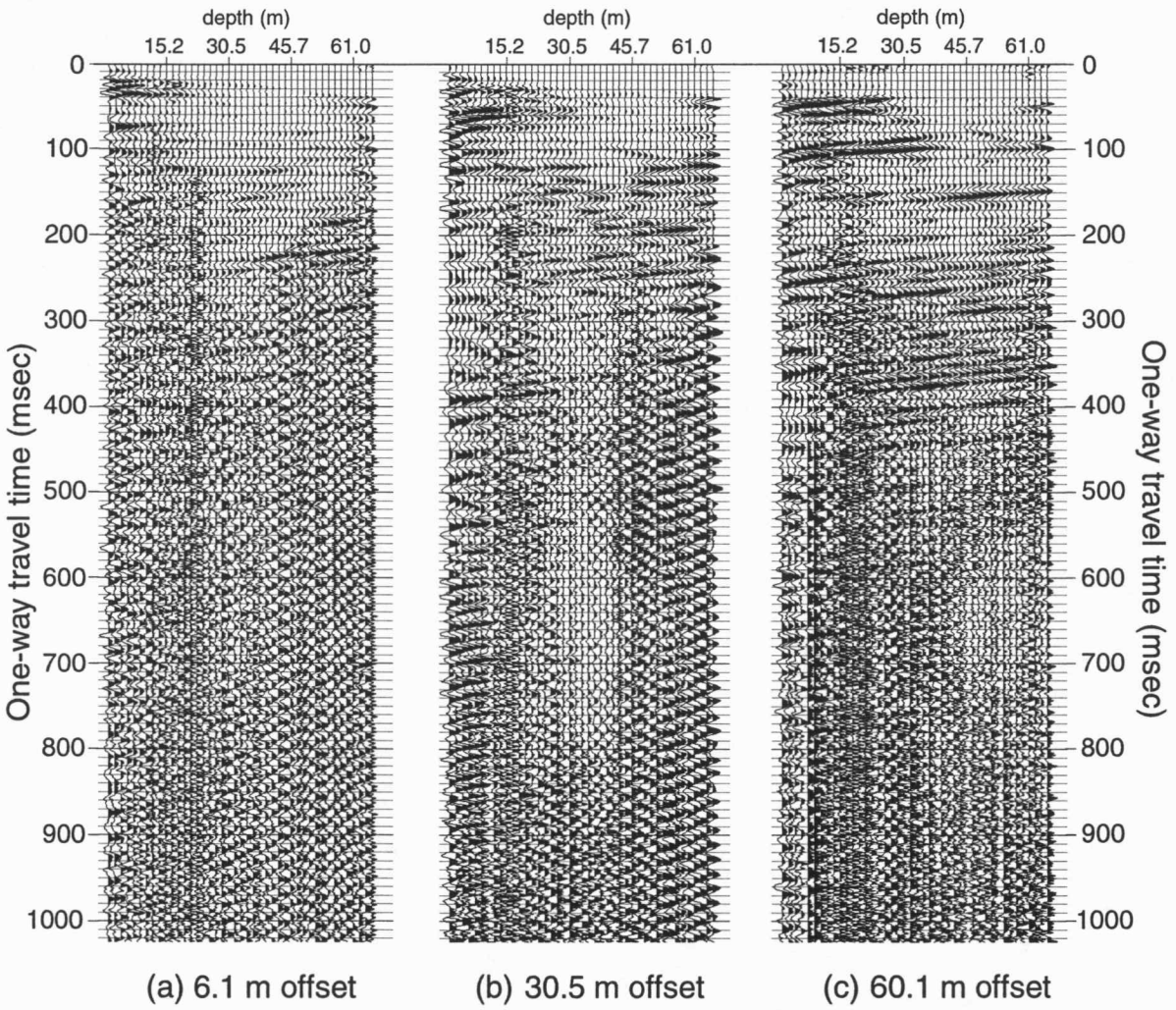


Figure 26. P-wave uphole survey for the various offsets recorded at the Pitts #1 well near station 1130. The 60.1 offset provided the best reflections.

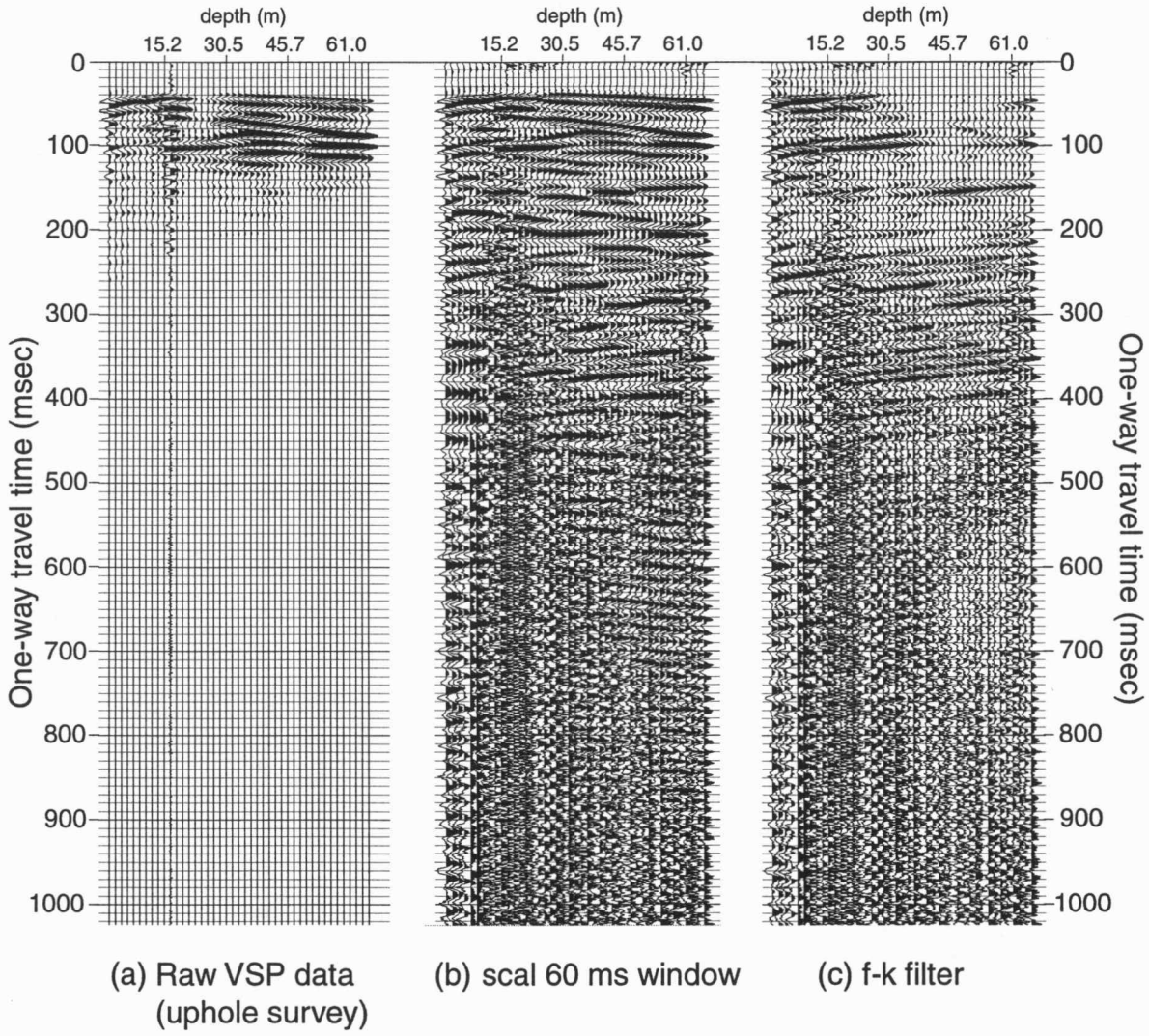


Figure 27. VSP processing steps used to produce a P-wave stacked trace in the Pitts well for the 60.1 offset.

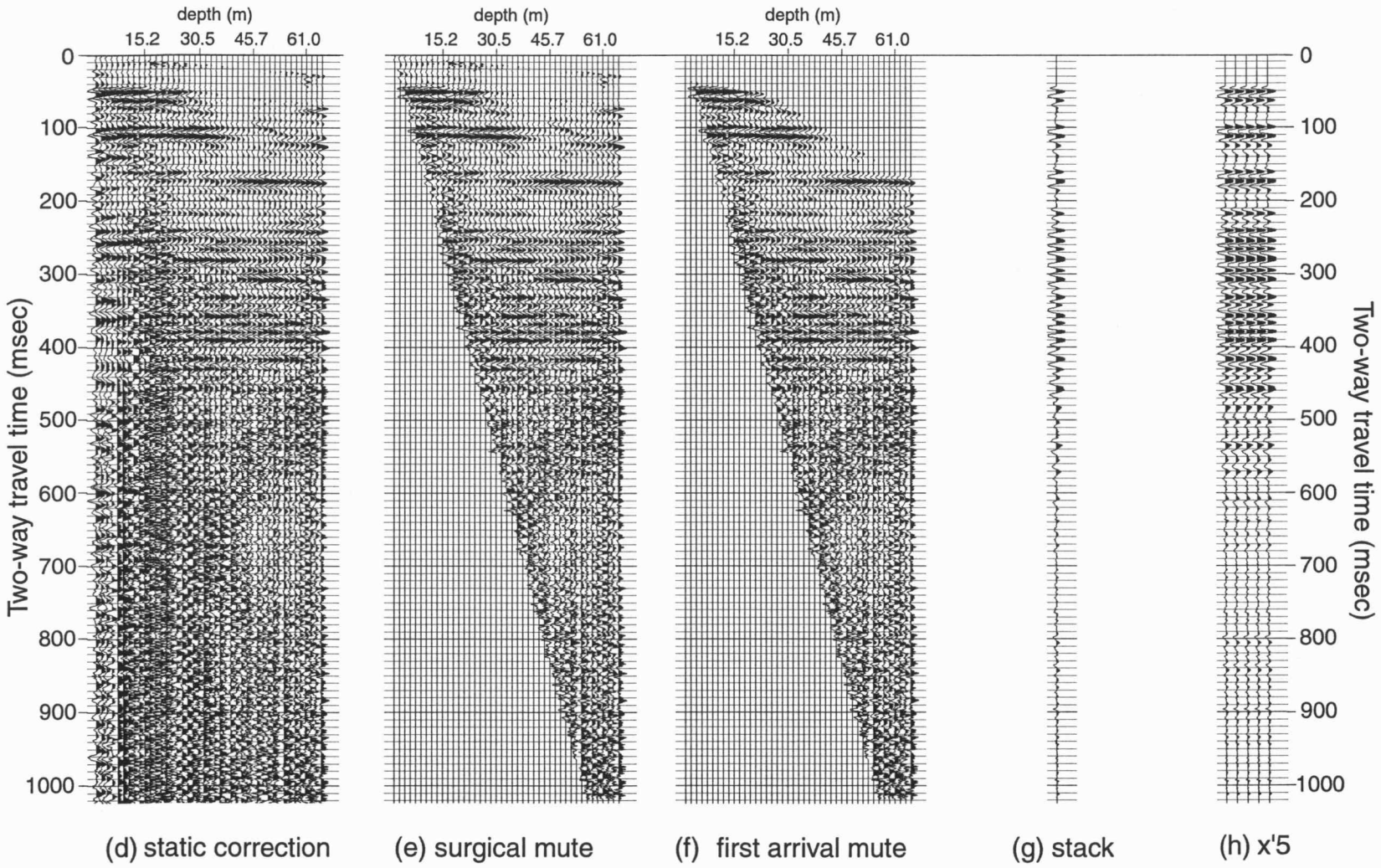


Figure 27. Continuation of the VSP processing steps used to produce a P-wave stacked trace in the Pitts well for the 60.1 offset.

Seismic Data Analysis

On the stacked sections, interpretable reflections from depths of less than about 650 m can be seen on all data sets. These reflections correlate with confidence to the core interpretations and well log curves from the Pitts well (Figure 28; Plate 13, 14, and 15). However, the sonic log has a gap in the data between 95 to 152 m due to instrument recording attributed to the presence of the gas in the drilling mud. Unfortunately, the depth of the gas is interpreted to be within the data gap at 150 m.

Reflections from about 60 ms to more than 350 ms are imaged on both P-wave stacked sections (Plate 1 and 2). They can also be interpreted on the S-wave stacked section from about 100 msec to over 800 msec (Plate 5). The 96-channel P-wave stacked section possess a nominal 24-fold, whereas, the 240-channel P-wave data have a nominal 60-fold. The true fold of the 96-channel data is dominantly between 40 and 50 (Plate 10). The 240-channel true fold varies between 110 and 120 (Plate 11). The S-wave data have a nominal 60-fold with a dominant true fold of about 100 (Plate 12). Time-to-depth conversion for the P- and S-wave data was accomplished using stacking velocities obtained through careful analysis of constant-velocity scans.

The 96-channel data had stacking velocities determined from constant-velocity scans that ranged from about 3000 m/sec at 60 ms to over 3700 m/sec at about 340 ms (Plate 7). The stacking velocities of the 240-channel data set were

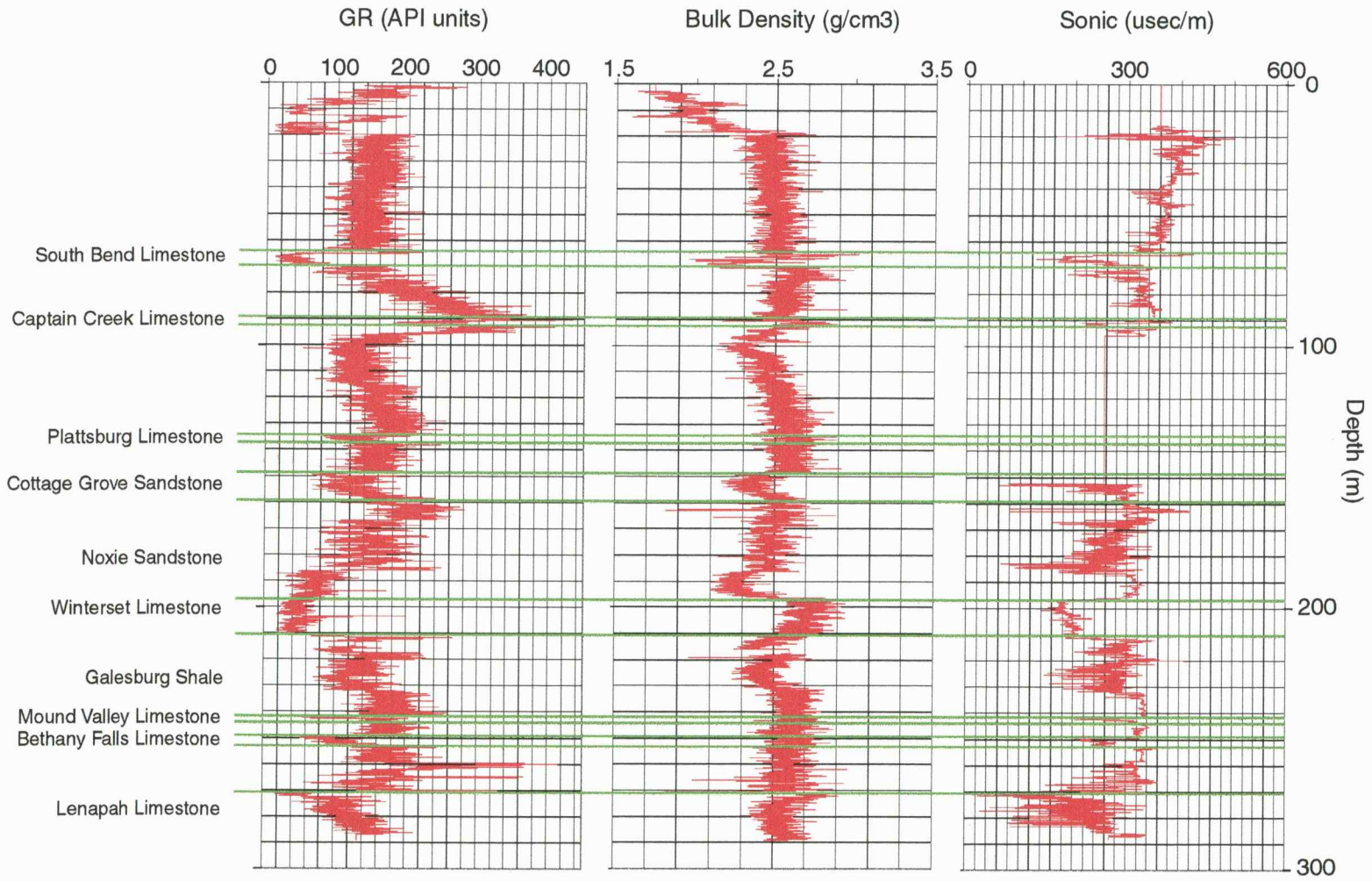


Figure 28. Interpreted Pitts #1 edited well data. Cottage Grove Sandstone (host rock for gas) is at depth 150m.

comparable to the 96-channel data (Plate 8). Stacking velocities used in the S-wave data set ranged from about 1400 m/sec at 80 msec to 2200 m/sec at 750 msec (Plate 9). This range of velocities is consistent with the consolidated limestone/shale sequences overlain by a 0 to 1 m veneer of weathered shale present at this site.

Between CMPs 1050 and 1250 on both P-wave stacked sections, a high-amplitude reflection at a time of 90 ms is more prominent than at any other location on the line (Plate 1 and 2). Continuous core acquired 100 m offline and adjacent to station 1130 (Pitts well) encountered a thick sand sequence and free gas at a depth of around 150 m (Figure 31, Plate 3, and Plate 4). This depth is equivalent to the 90 msec reflection on the P-wave stacked section.

Reflections on the P-wave stacked sections that can be correlated to this potential gas reservoir in this apparent class 1 environment should be characterized by amplitude dimming. This class 1 expectation is based on the general geology that includes limestone/shale interbedded with sandstone cyclic sequences. This sharp contrast in acoustic impedance between these moderate to highly compacted units should provide a high impedance contrast, indicative of a class 1 sand. However, reflections from at or within the gas reservoir produce a "bright spot" on the stacked sections, inconsistent with a class 1 model. There were sufficient offsets acquired at the time/depth of interest to observe a phase reversal if present as would be expected for high impedance gas reservoirs.

P-wave shot gathers over the gas-rich portion of the sand possess AVO effects consistent with a near-zero impedance gas sand reservoir (class 2) (Figure 20e or 20g). Near-zero impedance reservoirs are characterized by gradational upper contacts, usually in moderately consolidated environments. This was not expected in this setting, which, based on the local geology alone, should be considered a mature highly compacted sand (class 1 sand). However in examining the well log and seismic data, the upper boundary of this sand is described as a gradational contact between sand and shale. Interpretations from the core describe the upper contact as grading from a sand to a siltstone then a silty shale to a shale. High amplitude reflections associated with this 150 m deep reflector, located at 90 ms, become quite pronounced at offsets greater than 200 m. This observation is completely consistent with the geologic interpretations made from the core and log data from the Pitts well drilled near CMP station 1130. As a result of these interpretations and the lack of a "dim out" on the stacked section, this gas sand is characterized as a class 2 sand.

To further support the presence of the gas sand at a depth of 150 m, the data were subjected to a processing flow that involved a geometric spreading correction and no other amplitude adjustments; therefore, this data can be considered to have true amplitude. An amplitude anomaly is prominent on this data set at 90 msec with the higher amplitude portion located at CMP station 1105. This gas sand appears to be capped by an impermeable shale layer based on well logs. Core interpretations

above the sand indicate a silty shale unit may serve as the reservoir seal. In addition to this trap, the northern and southern ends of the anomaly appear to pinch out into the surrounding shale rather abruptly. This stratigraphic pinch out may also serve as a trap for the gas.

The shear-wave stacked data do not image the amplitude anomaly at 150 m, the depth of the gas sand. S-wave velocities are not sensitive to gas or liquid saturation due to the lack of a distinct change in velocity as the wave propagates through the medium. This lack of an amplitude anomaly on the S-wave stacked section confirms the presence of gas within the pore space of this sandstone (Plate 15).

A reflection at 260 ms on the shear wave stacked section translates to a depth of 221 m using a stacking velocity calculated to be 1700 m/sec (Plate 5, 6, and 7). This reflection directly correlates to the 120 ms reflection on the P-wave sections (Plate 1 and 2). This P-wave reflection, identified as the Winterset Limestone, has a stacking velocity of about 3200 m/sec. This approximately 2 to 1 velocity ratio is consistent for this general geologic setting (Plate 13, 14, 15) (Carmichael, 1989).

The VSP data correlated with confidence to the P- and S-wave stacked sections (Plate 16, 17, and 18). The P-wave VSP corridor stack was subject to a shift of 40 msec when compared to the CMP stacked section. Before the VSP corridor

stack could be correlated to the CMP stacked section, it was corrected for statics. This was accomplished by determining the difference in elevation between the well head and the datum used in processing the data. A total shift of 21 msec was determined using a difference in elevation of 30 m and a velocity of about 2900 m/s.

An additional shift was required to correlate the VSP data with the CMP stacked data. Given the dominant frequency of the P-wave stacked section to be about 80 Hz, the VSP corridor stack was subject to a maximum shift of less than one wavelength (cycle). Using the 2 to 1 velocity ratio between the P- and S-wave data, a static shift for the S-wave VSP corridor stack is 41 msec. Correlating the S-wave VSP to the CMP stacked section required an additional shift in the data. As with the P-wave VSP corridor stack, the S-wave VSP data were shifted less than one wavelength.

When processing the S-wave data, an excellent observation occurred when conducting time-depth conversions. In viewing the time stacked section for the S-wave data, there appears to be an anticlinal-shaped structure along the entire length of the seismic line (Plate 5). However, when the data were subjected to depth conversion, the appearance of this antiform disappears (Plate 6). The depth stacked section shows the flat, horizontal layering that describes the true geology of this area. The P-wave depth stacked section further provides evidence of this horizontal

geology. As a result of this observation, the true structure should only be interpreted from the S-wave depth stacked section.

Resolution of the strata is dependent on the dominant frequency, velocity, and depth to the reflector of interest. Utilizing the Fresnel zone as an indication of the horizontal resolution, a dominant frequency for the 96-channel data set is equal to 90 Hz. Using a velocity of 3100 m/s and a frequency of 90 Hz, the wavelength computed for the gas sand is 34.4 m. Applying the one-quarter wavelength principle as the threshold for vertical resolution, the gas sand is resolvable to about 8 m for both data sets (Yilmaz, 1987). The 8 m wavelength and a depth of 150 m translates to a radius of the first Fresnel zone to be 50m. For comparison, the 240-channel P-wave data set has a Fresnel radius of 48 m. With receiver spacing for the P-wave data to be 5m, the gas sand is considered to be well-sampled (Knapp and Steeples, 1986).

Conclusions

Coincident P- and S-wave data associated with VSP data were collected to provide information in confirming the presence of a shallow gas sand. Based on core and well log information, this gas sand is interpreted as the Cottage Grove Sandstone member of the Upper Pennsylvanian Chanute Shale. The preliminary identification of this amplitude anomaly was evident on the 96-channel P-wave data. As a result, more data were collected in this region to test the ability to confidently image a shallow gas reservoir using seismic data along with geologic information.

Generally, this mature, consolidated geologic setting would provide amplitude versus offset characteristics consistent with a class 1, high impedence reservoir. The data presented here support a near-zero impedence classification. In response to an amplitude anomaly on the P-wave stacked sections, shear-wave data were collected and processed to produce a comparable depth section with the P-wave data. The shear-wave data did not exhibit an amplitude anomaly at the depth of the gas.

The presence of gas is supported by an anomaly on the P-wave stacked sections. As expected for gas-filled reservoirs, a reflection due to the presence of gas within pore spaces would not show up on an S-wave stacked section. During the drilling of the Pitts well, free gas was encountered in the well. According to well log information, the gas is at a depth of 150 m. This is equivalent to the depth of the gas on both the P- and S-wave stacked sections. To study this gas sand further, a non-

AGC data set was processed using both P-wave data sets. After the data were corrected for geometric spreading, the resulting stacked sections showed a clear amplitude anomaly. A peculiar observation of the S-wave time stacked section showed structure not actually present in this geologic setting. The P-wave data collected here confirms this lack of structure. When converting the S-wave time section to a depth section, the anticlinal structure disappeared. This observation proves the importance of interpreting true structure from depth sections not from time sections.

High- resolution seismic reflection surveys have the potential to image shallow gas reservoirs in southeastern Kansas and adjacent parts of Oklahoma. P-wave data was successful in drawing attention to this particular sand body. Determining whether this amplitude anomaly is due to the presence of gas became the modified objective of this study. Utilizing both seismic and geologic data helped confirm gas saturation within the Cottage Grove Sandstone.

References

Baars, D.L., W.L. Watney, D.W. Steeples, E.A. Brostuen, 1989, Petroleum: a primer for Kansas, Educational Series 7, Kansas Geological Survey, The University of Kansas, 40 p.

Baker, G.S., D.W. Steeples, and M. Drake, 1998, Muting the noise cone in near-surface reflection data: An example from southeastern Kansas: *Geophysics*, v. 63, p. 1332-1338.

Bass, N.W., 1936, Origin of the shoestring sands of Greenwood and Butler counties, Kansas: Kansas Geological Survey, Bulletin no. 23, 135 p.

Carmichael, R.S., 1989, Practical Handbook of Physical Properties of Rocks and Minerals: CRC Press, Inc.

Castagna, J.P., 1993, AVO analysis – Tutorial and review, in J.P. Castagna and M.M. Backus, *eds.*, Offset Dependent Reflectivity – Theory and practice of AVO analysis: Soc. Expl. Geophys., p. 3-36.

Doll, W.E., R.D. Miller, and J. Xia, 1996, Enhancement of swept source near-surface seismic reflection data at a hazardous waste site: 66th Annual Internat. Mtg., Soc. Expl. Geophys., Expanded Abstracts, p. 877-879.

Doll, W.E., R.D. Miller, and J. Xia, 1998, A noninvasive shallow seismic source comparison on the Oak Ridge Reservation, Tennessee: *Geophysics*, v. 63, p. 1318-1331.

Domenico, S.N., and S.H. Danbom, 1987, Shear-wave technology in Petroleum Exploration – Past, Current, and Future, *in* S.H. Danbom and S.N. Domenico, *eds.*, Shear-wave Exploration, Geophys. Dev. No. 1: Soc. Expl. Geophys., p. 3-18.

Fernandez, S. I., 1993, Stratigraphy, Petrology, Diagenesis, and Depositional Environments of the Pennsylvanian (Missourian) Chanute Shale, Southeastern Kansas, Northeastern Oklahoma: M.S. Thesis, University of Iowa, 222 p.

Gerlach, P, 1999, Kansas Oil and Gas Exploration; 10 year history and future strategies: Kansas Geological Survey Open File Report 1999-55.

Heckel, P.H., 1979, Field guide to Pennsylvanian cyclic deposits in Kansas and Nebraska, Ninth International Congress of Carboniferous Stratigraphy and Geology, Field trip No. 10, Pennsylvanian Cyclic Platform Deposits of Kansas and Nebraska, Guidebook Series 4, Kansas Geological Survey, The University of Kansas, p. 14.

Heckel, P.H., 1980, Paleogeography of eustatic model for deposition of midcontinent Upper Pennsylvanian cyclothems *in* Fouch, T.D., and Magathan, E.R., eds., Paleogeography of west-central United States: SEPM, Rocky Mountain Paleogeograpy Symposium 1, p. 197-215.

Helbig, K., 1987, Shear-waves – What they are and how they can be used, *in* S.H. Danbom and S.N. Domenico, *eds.*, Shear-wave Exploration, Geophys. Dev. No. 1: Soc. Expl. Geophys., p. 19-36.

Jenden, P.D., K.D. Newell, I.R., Kaplan, and W.L. Watney, 1988, Composition and stable-isotope geochemistry of natural gases from Kansas, Midcontinent, U.S.A. in M. Schoell (Guest-Editor, Origins of Methane in the Earth. Chem. Geol., 71, p. 117-147.

Jewett, J.M., 1954, Oil and Gas in Eastern Kansas, Kansas Geological Survey Bulletin 104, 391 p.

Jewett, J.M., C.K. Bayne, E.D. Goebel, H.G. O'Conner, A. Swineford, and D. E. Zeller, 1968, The stratigraphic succession in Kansas, Kansas Geological Survey Bulletin 189, p. 27-34.

Jongerius, P., and K. Helbig, 1988, Onshore high-resolution seismic profiling applied to sedimentology: *Geophysics*, v. 53, p. 1276-1283.

Kansas Geological Survey website, 2001, Oil and Gas Production in Kansas; http://www.kgs.ukans.edu/PRS/petro/interactive.html (accessed January 18, 2001).

Khattri, K., R. Mithal, and V. Gaur, 1979, Pattern space of seismic anomalies associated with hydrocarbon deposits: *Geophysical Prospecting*, v. 27, p. 339-359.

Knapp, R.W., N.L. Anderson, and J. Youle, 1995, Cherokee Sandstone Reservoir, Southeastern Kansas, Geophysical Atlas of Selected Oil and Gas Fields in Kansas, Kansas Geological Survey Bulletin 237, p. 158-161.

Knapp, R.W. and D.W. Steeples, 1986, High-resolution common-depth-point reflection profiling: Field acquisition parameter design: *Geophysics*, v. 51, p. 283-294.

McCormack, M.D. and R.H. Tatham, 1986, Shear-wave Exploration Seismology Course Notes: Soc. Explor. Geophys. Continuing Education Program,.

Miller, R.D., D.W. Steeples, and M. Brannan, 1989, Mapping a bedrock surface under dry alluvium with shallow seismic reflections: *Geophysics*, v. 54, p. 1528-1534.

Miller, R.D., 1992, Normal moveout stretch mute on shallow-reflection data: *Geophysics*, v. 57, p. 1502-1507.

Miller, R.D., N.L. Anderson, H.R. Feldman, and E.K. Franseen, 1995, Vertical resolution of a seismic survey in stratigraphic sequences less than 100 m deep in Southeastern Kansas: *Geophysics*, v. 60, p. 423-430.

Mitchell, J.C., 1981, Stratigraphy and Depositional History of the Iola Limestone Upper Pennsylvanian (Missourian), Northern Midcontinent, U.S.: Ph.D. dissertation, University of Iowa, 364 p.

Newell, K. D., 1995, Overview of Petroleum Geology and Production in Kansas, Geophysical Atlas of Selected Oil and Gas Fields in Kansas, Kansas Geological Survey Bulletin 237, p. 2–6.

Ostrander, W.J., 1982, Plane-wave reflection coefficients for gas sands at nonnormal angles-of-incidence: *Geophysics*, v. 49, p. 1637-1648.

Parham, K.D., 1993, Introduction to Permian Plays, In, Bebout, D.G., White, W.A., Hentz, T.F., and Grasmick, M.K., (eds.); Atlas of major Midcontinent gas reservoirs: The University of Texas at Austin, Bureau of Economic Geology, p. 6-7.

Peddy, C.P., M.K. Sengupta, and T.L. Fasnacht, 1995, AVO analysis in high impedance sandstone reservoirs: the Leading Edge, v. 14, p. 871-877.

Pullan, S.E., and J.A. Hunter, 1990, Delineation of buried bedrock valleys using the optimum offset shallow seismic reflection technique: Soc. Explor. Geophys. Investigations in Geophysics no. 5, S.H. Ward, ed., *Volume 3: Geotechnical*, p. 75-87.

Pullan, S.E., J.A. Hunter, H.M. Jol, M.C. Roberts, R.A. Burns, and J.B. Harris, 1998, Seismostratigraphic investigations of the southern Fraser River delta: *In Geology and Natural Hazards of the Fraser River Delta, British Columbia*, ed. J.J. Clague, J.L. Luternauer, and D.C. Mosher. Geological Survey of Canada, Bulletin 525, p. 91-122.

Rascoe, B. Jr., and F.J. Adler, 1983, Permo-carboniferous hydrocarbon accumulations, Mid-Continent, U.S.A.: *American Association of Petroleum Geologists Bulletin*, v. 67, no. 6, p. 979-1001.

Ross, C.P, and D.L. Kinman, 1995, Nonbright spot AVO: Two examples: *Geophysics*, v. 60, p. 1398-1408.

Rutherford, S.R., and R.H. Williams, 1989, Amplitude-versus-offset variations in gas sands: *Geophysics*, v. 54, p. 680-688.

Sheriff, R.E. and L.P. Geldart, 1982, Exploration Seismology, Cambridge University Press, 595 p.

Shtivelman, V., U. Frieslander, E. Zilberman, and R. Amit, 1998, Mapping shallow faults at the Evrona playa site using high-resolution reflection method: *Geophysics*, v. 63, p. 1257-1264.

Steeples, D.W., and R.D. Miller, 1990, Seismic reflection methods applied to engineering, environmental, and groundwater problems: Soc. Explor. Geophys. Investigations in Geophysics no. 5, Stan H. Ward, ed., *Volume 1: Review and Tutorial*, p. 1-30.

Watney, W.L., J.A. French, and E.K. Franseen, 1989, Sequence Stratigraphic Interpretations and Modeling of Cyclothems in the Upper Pennsylvanian (Missourian), Lansing and Kansas City Groups in Eastern Kansas, Field guide 41st Annual Field Trip Kansas Geological Society, Kansas Geological Survey, The University of Kansas.

Xia, J. and R.D. Miller, 1998, Hum filter: Power-Line Noise Eliminator for Shallow Seismic Data: Symp. on the Applications of Geophys. to Eng. and Environ. Problems, Proceedings, p. 1043-1052.

Yilmaz, O., 1987, Seismic data processing, in S.M. Doherty, ed., E.B. Neitzel, series ed., Series: *Investigations in geophysics no. 2*: Soc. Expl. Geophys.

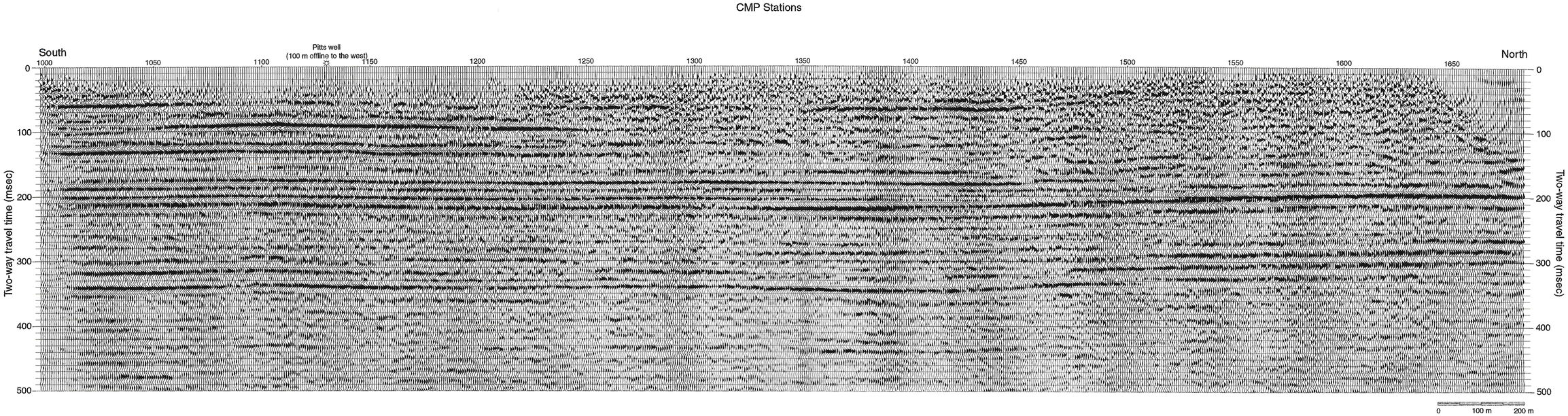


Plate 1. CMP time stacked section, P-wave Trip 1(96-channels)

2001-73

CMP Stations

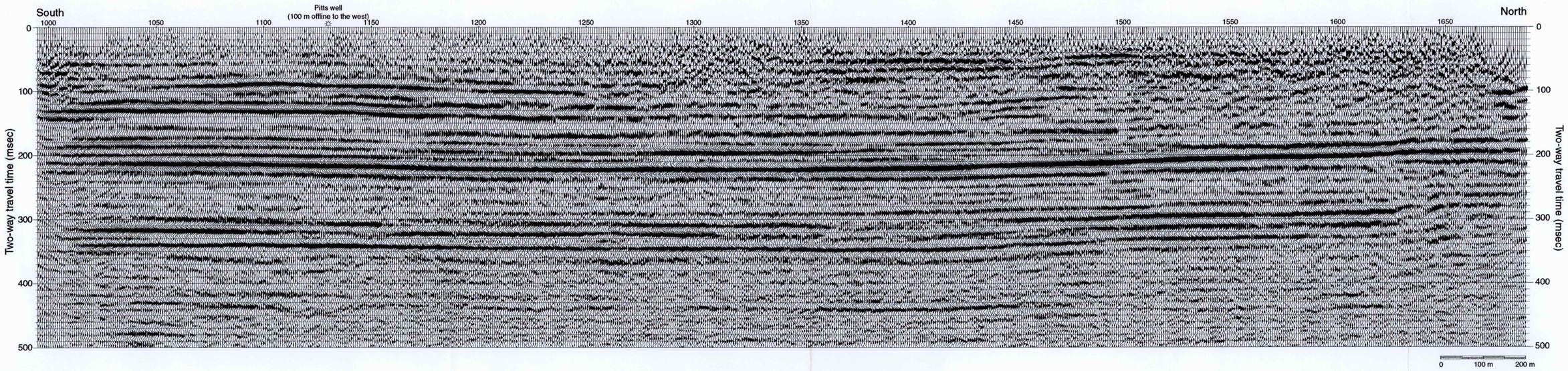


Plate 2. CMP time stacked section, P-wave Trip 2(240-channels)

2001-73

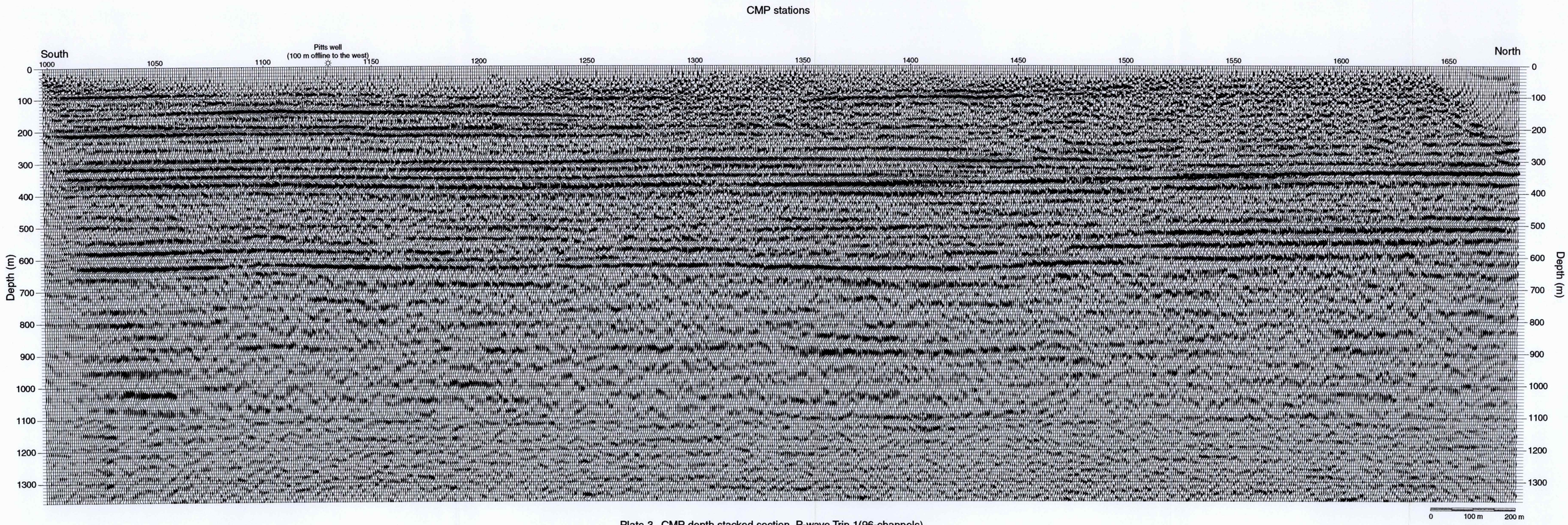


Plate 3. CMP depth stacked section, P-wave Trip 1(96-channels)

2001-73

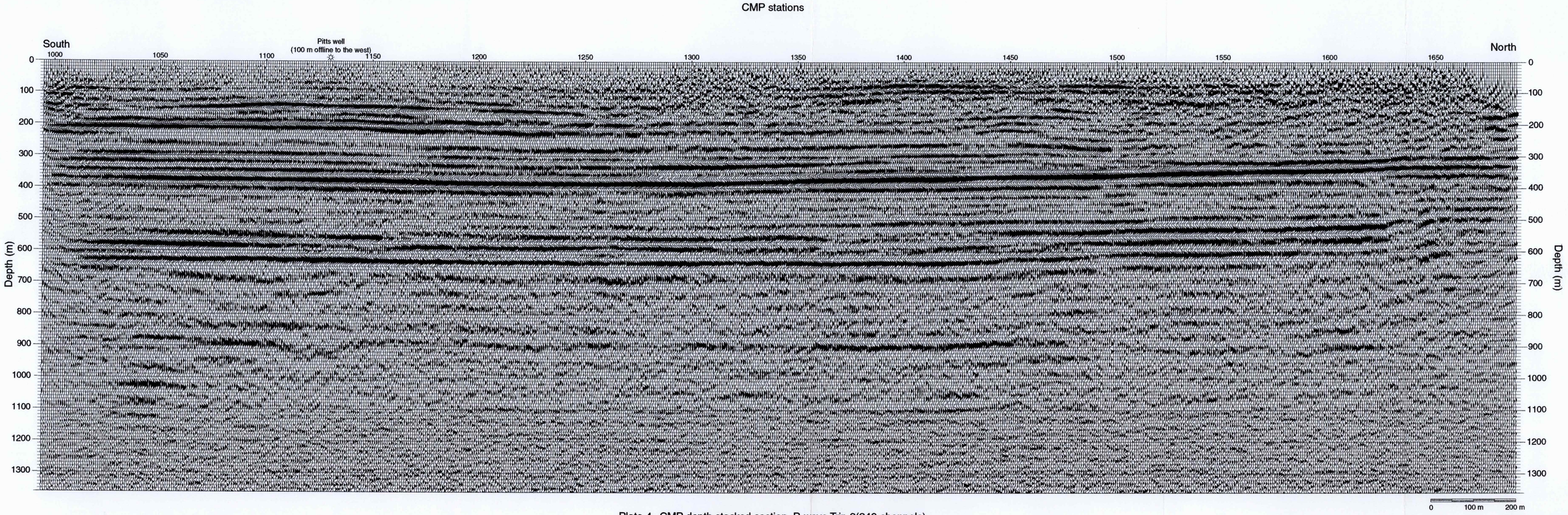


Plate 4. CMP depth stacked section, P-wave Trip 2(240-channels)

2001-73

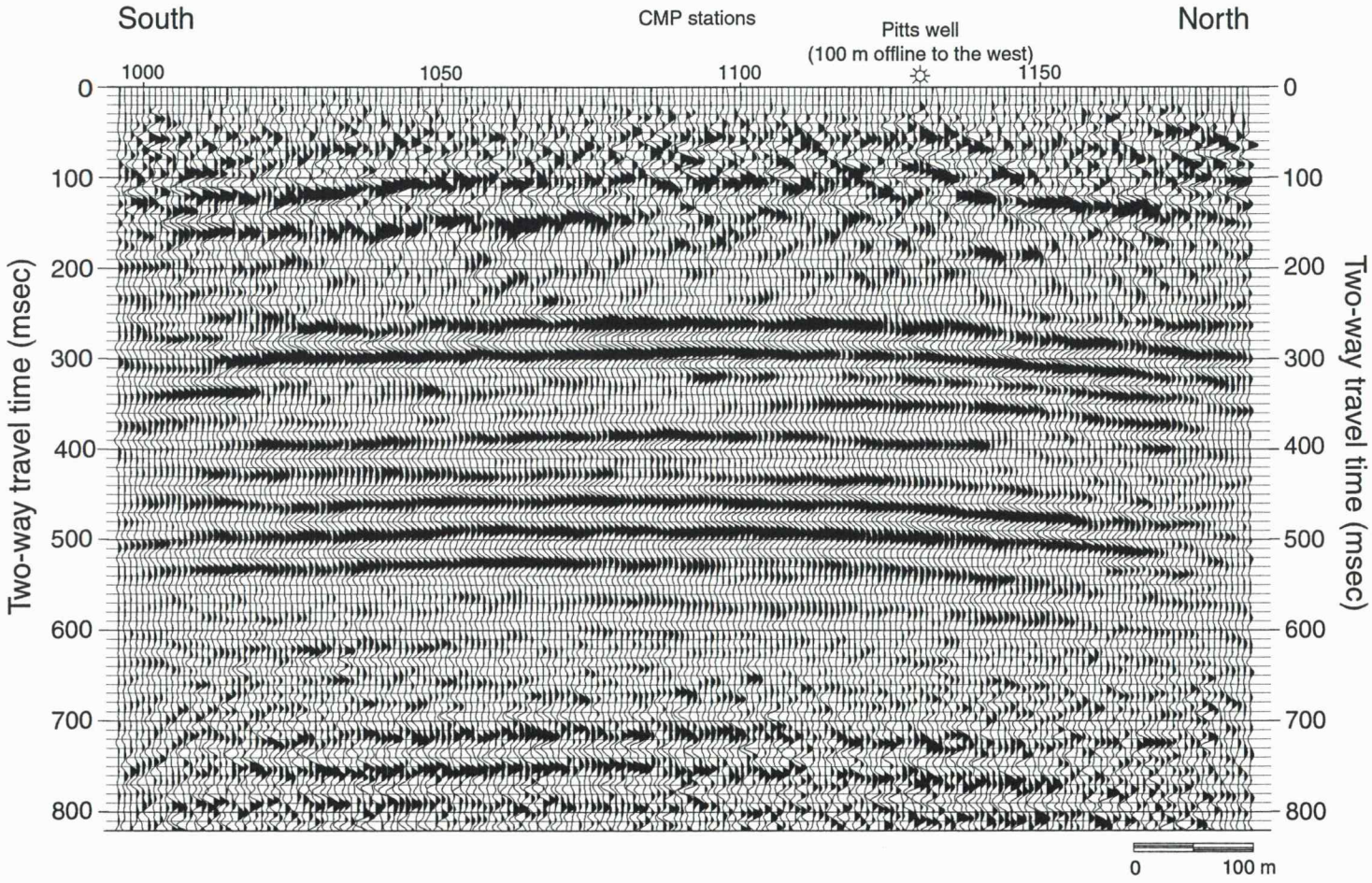


Plate 5. Shear-wave CMP time stacked section.

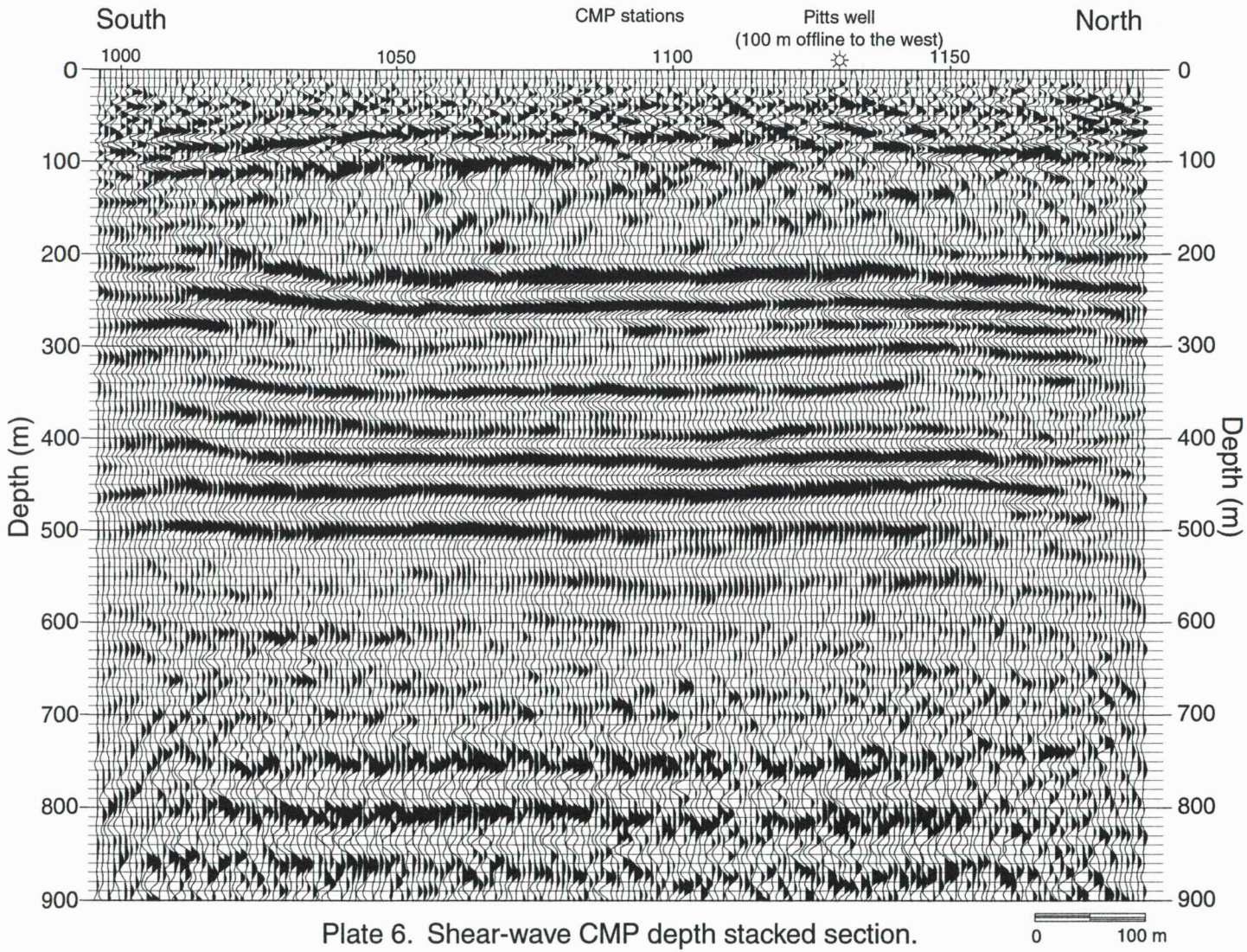


Plate 6. Shear-wave CMP depth stacked section.

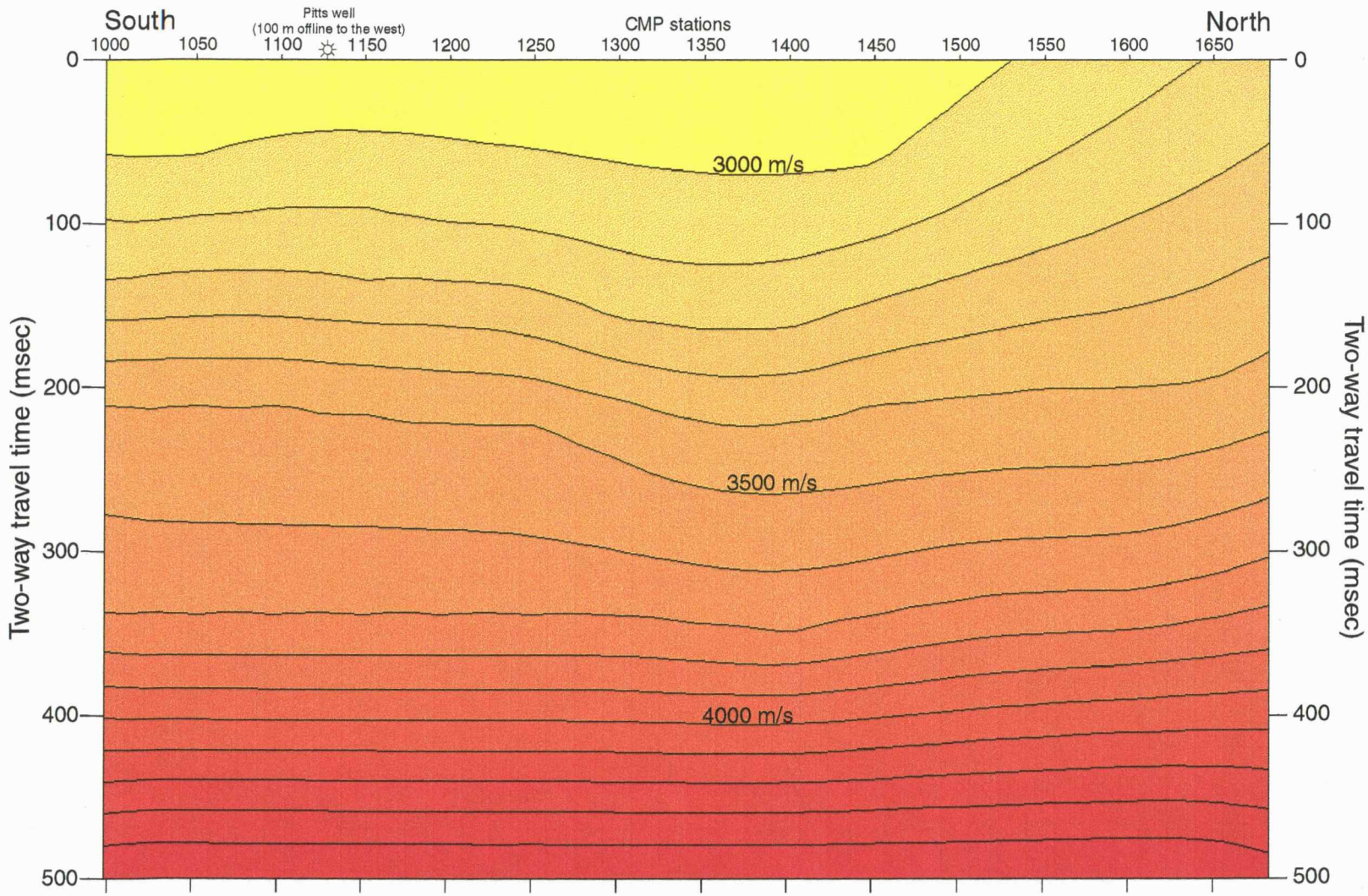


Plate 7. P-wave Trip1(96-channels) Stacking Velocity Field

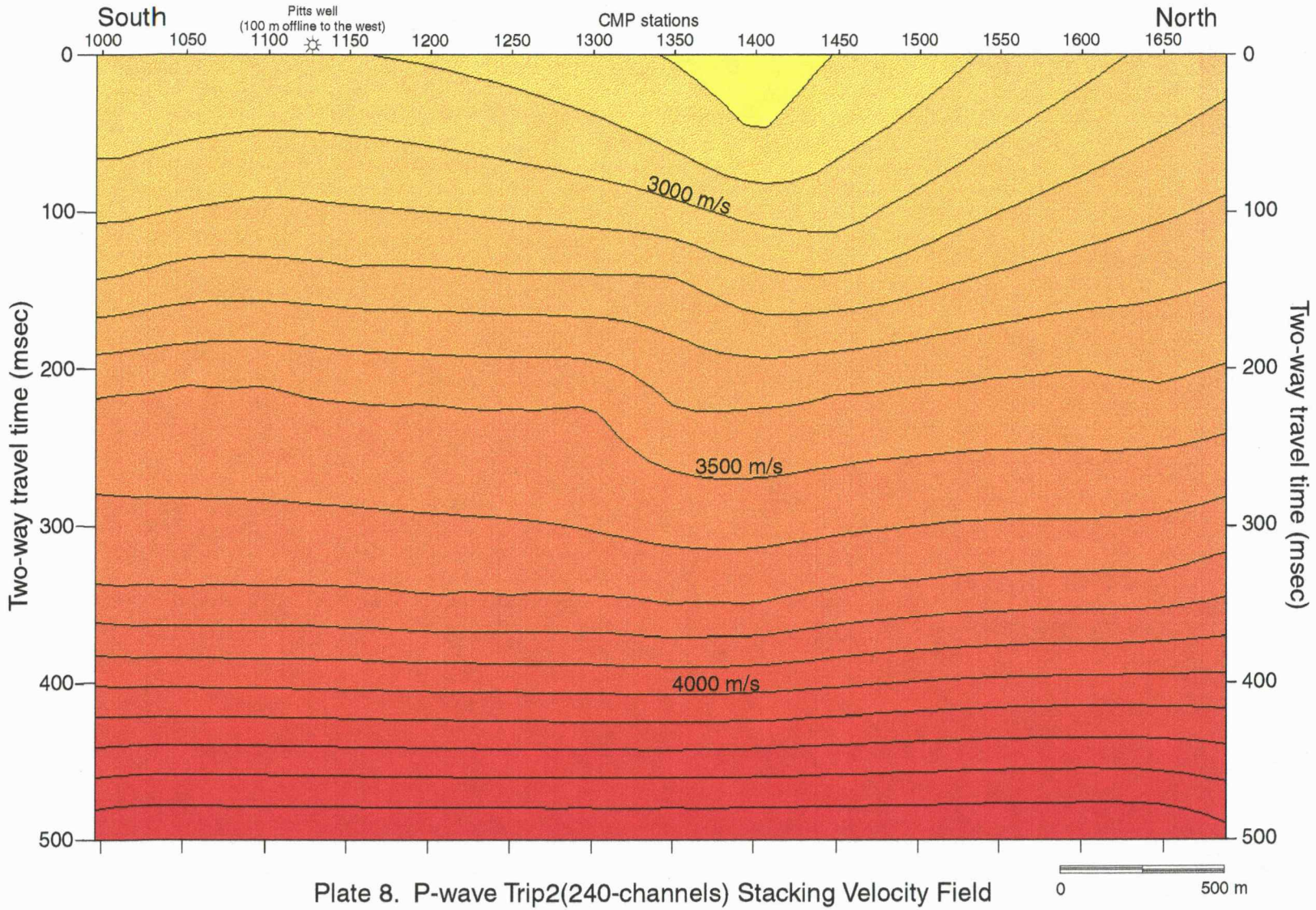


Plate 8. P-wave Trip2(240-channels) Stacking Velocity Field

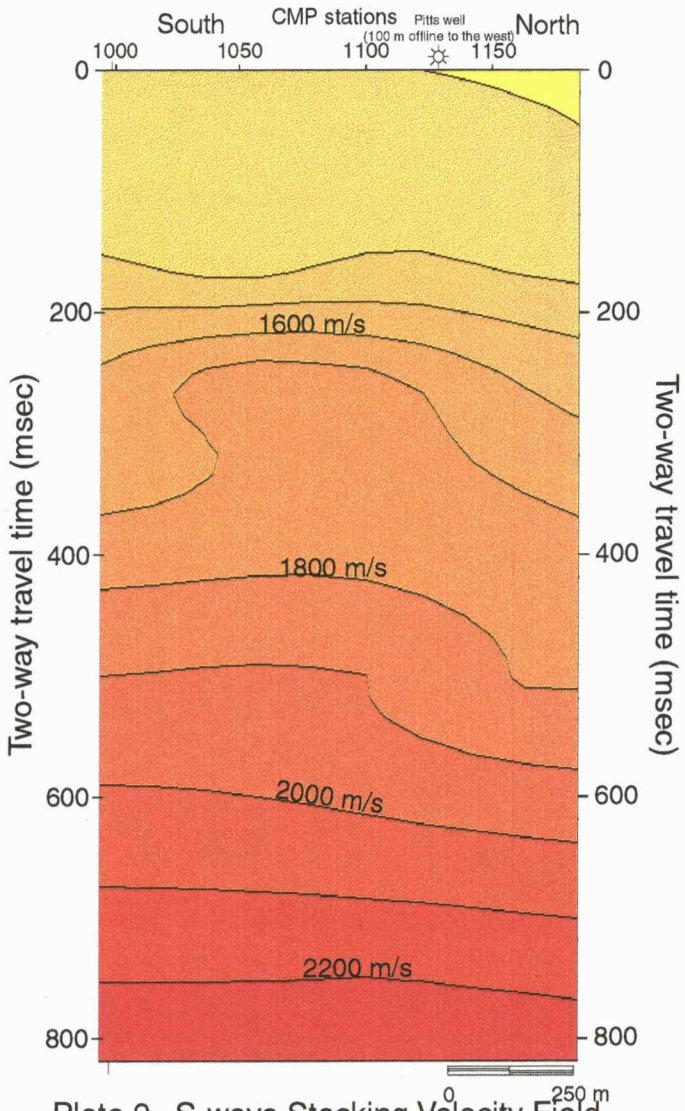


Plate 9. S-wave Stacking Velocity Field

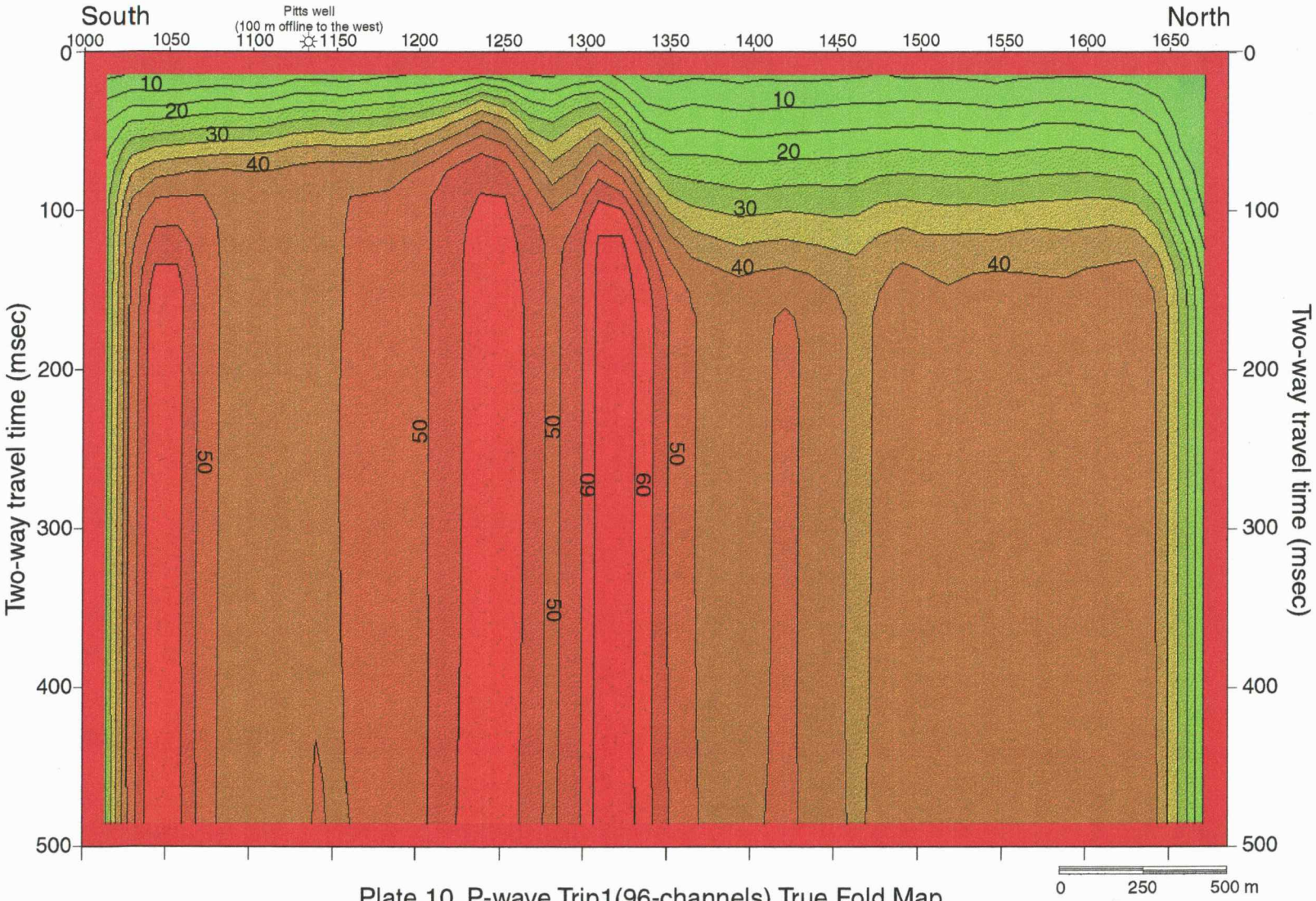


Plate 10. P-wave Trip1(96-channels) True Fold Map

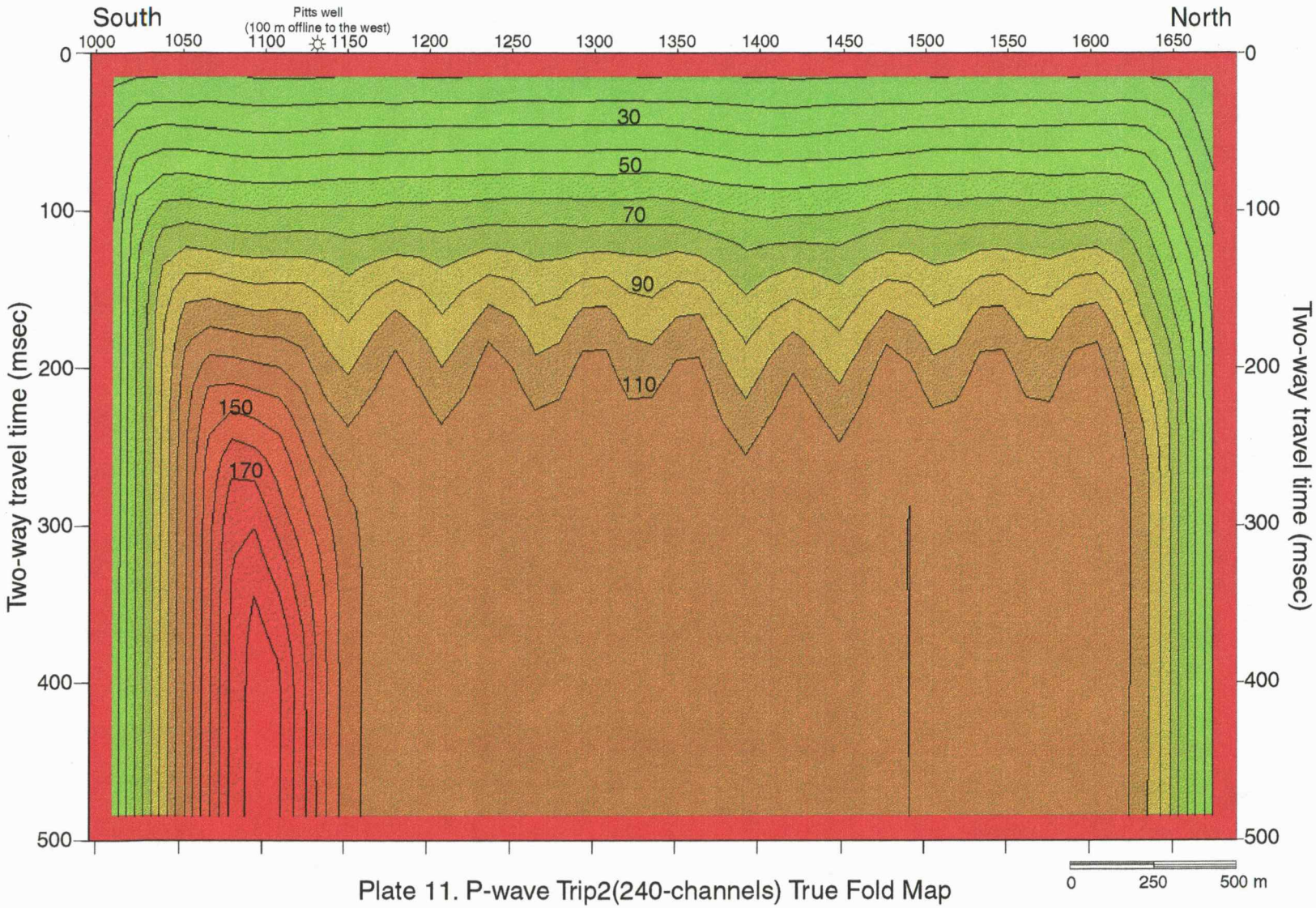


Plate 11. P-wave Trip2(240-channels) True Fold Map

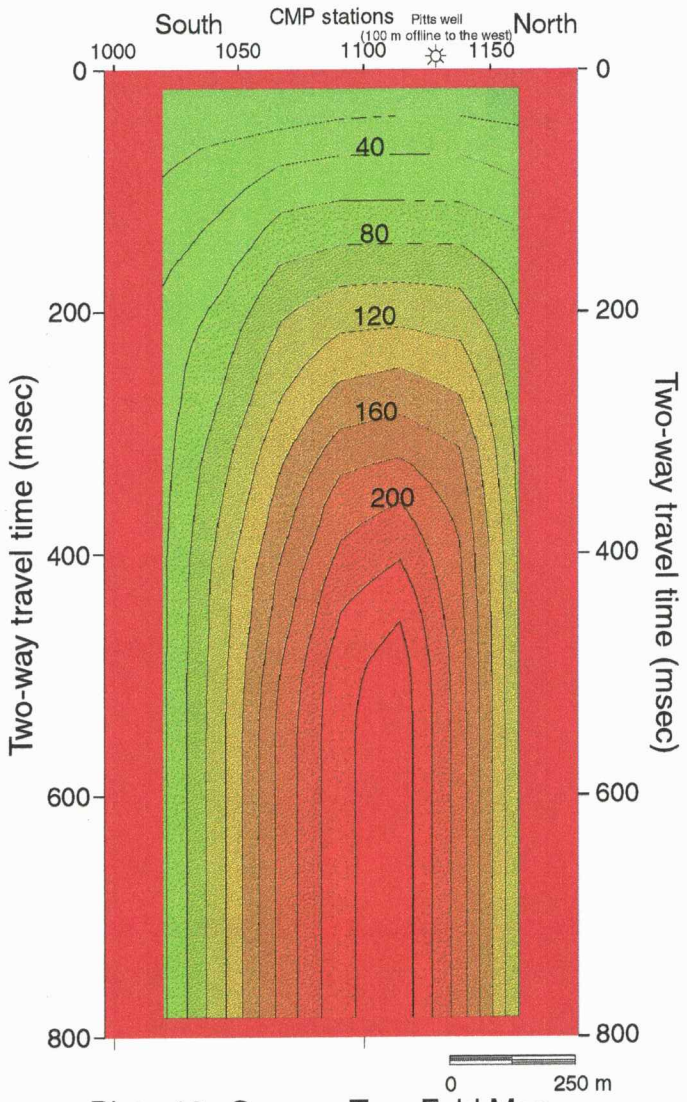


Plate 12. S-wave True Fold Map

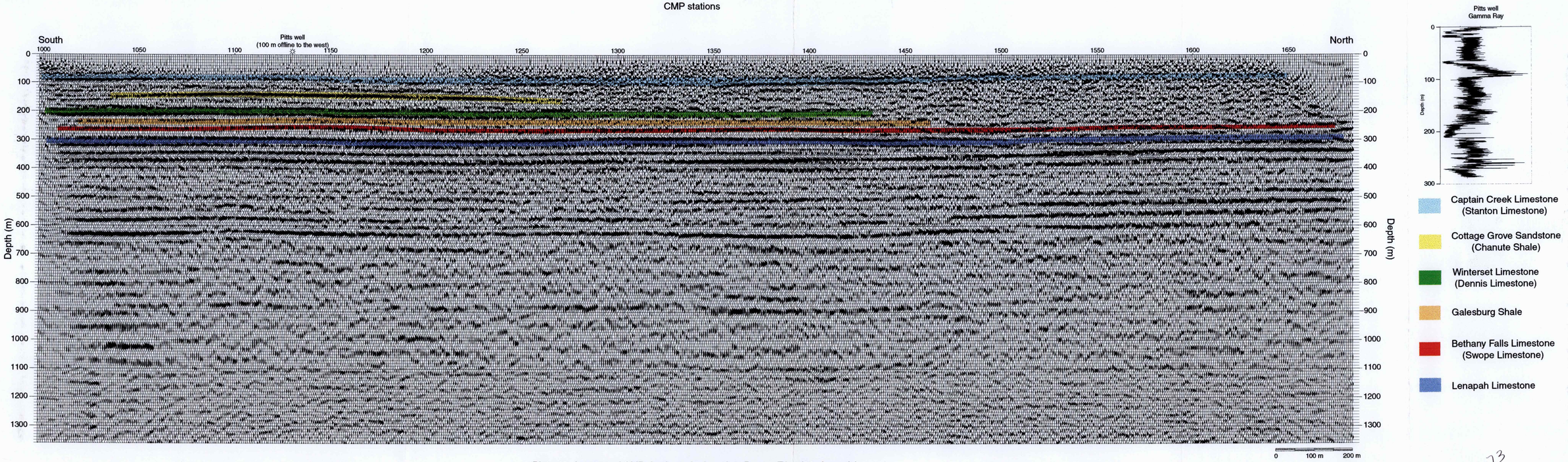


Plate 13. Interpreted CMP depth stacked section, P-wave Trip 1(96-channels)

2001-73

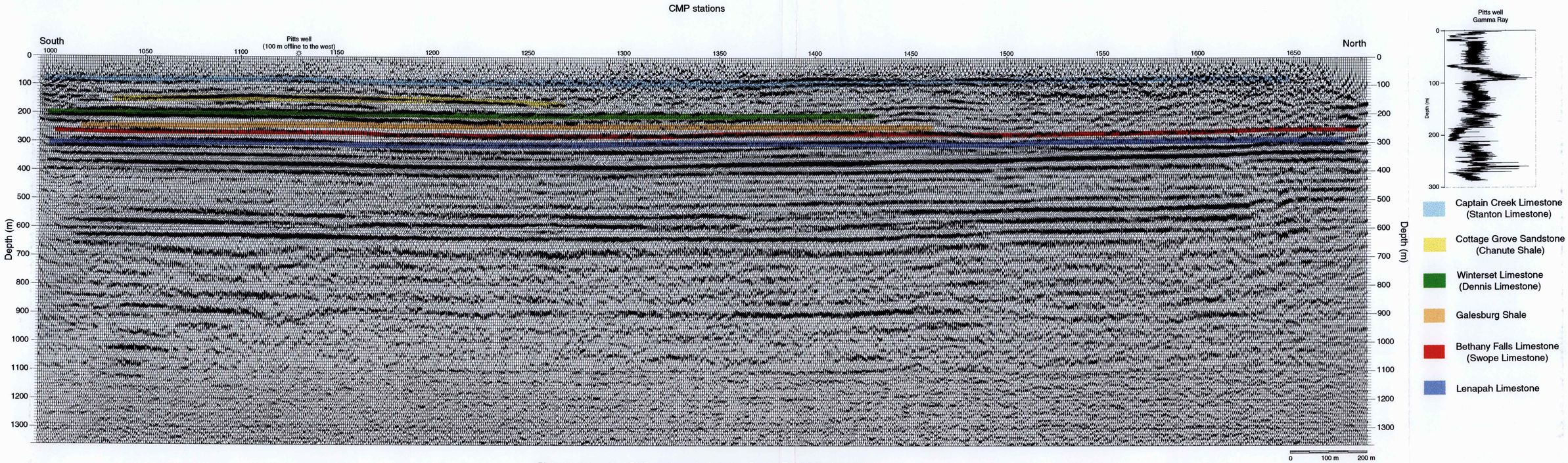


Plate 14. Interpreted CMP depth stacked section, P-wave Trip 2(240-channels)

2001-73

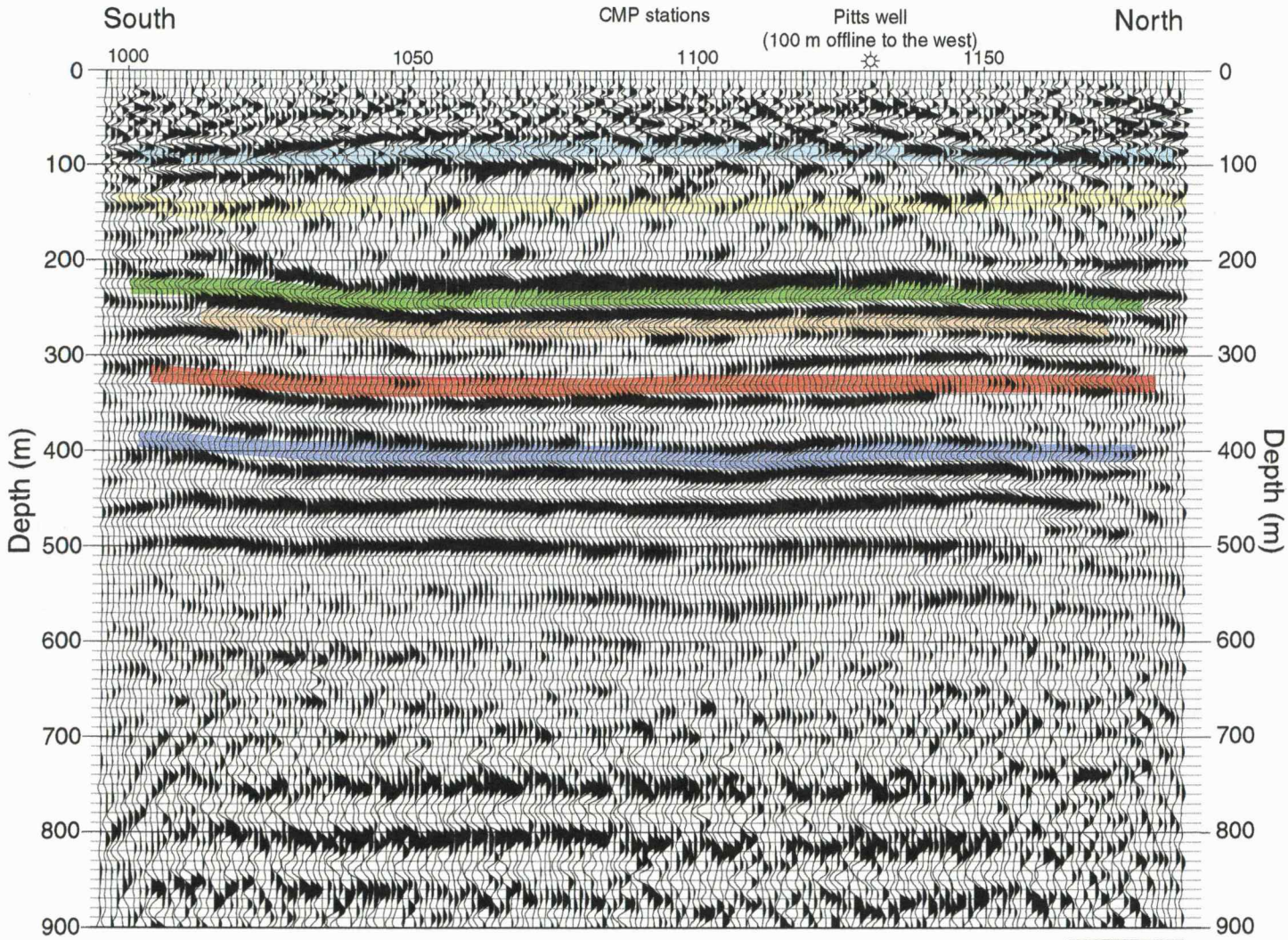


Plate 15. Interpreted shear-wave CMP depth stacked section. Colors are defined in Plate 13 and 14.

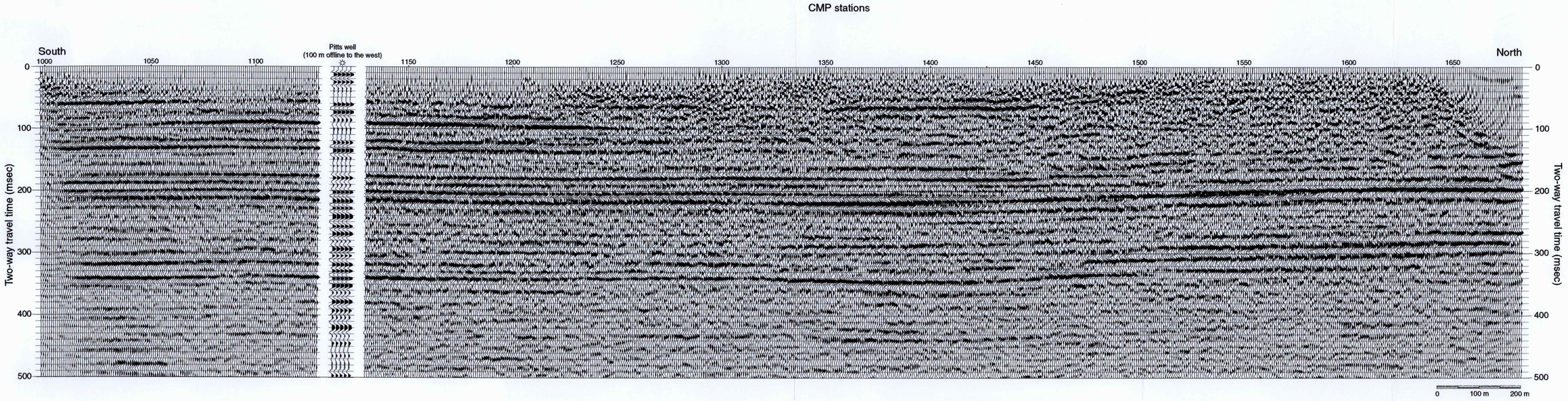


Plate 16. CMP time stacked section with corridor VSP stack , P-wave Trip 1(96-channels)

2001-73

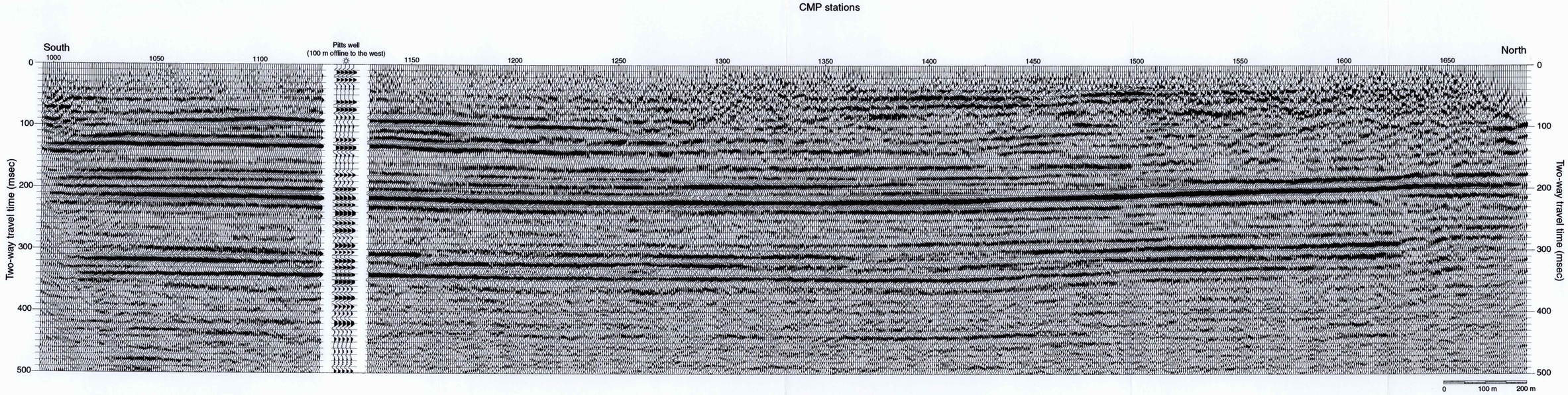


Plate 17. CMP time stacked section with corridor VSP stack , P-wave Trip 2(240-channels)

2001-73

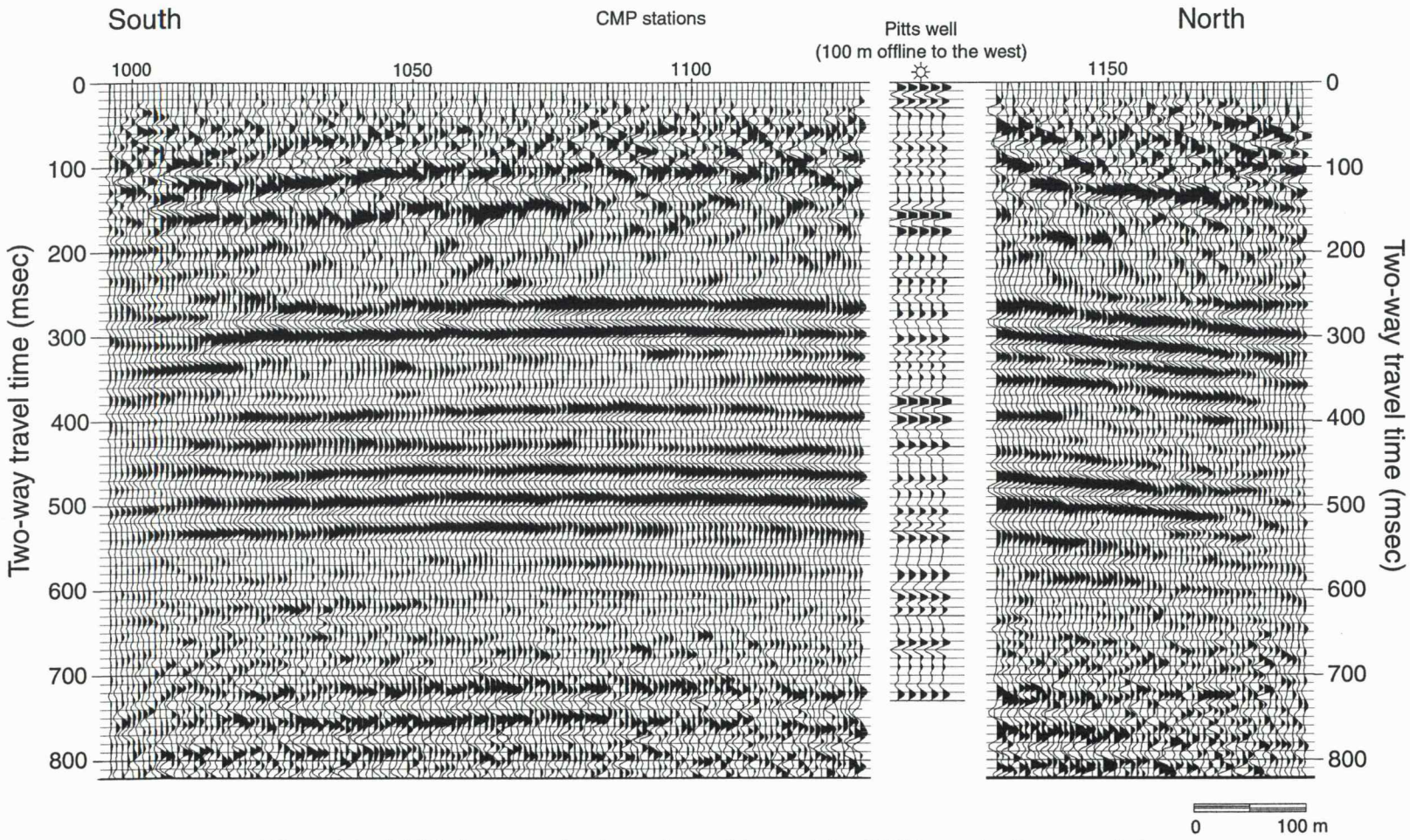


Plate 18. CMP time stacked section with corridor VSP stack, S-wave data.